Barometers behaving badly: Assessing the influence of analytical and experimental uncertainty on clinopyroxene thermobarometry calculations at crustal conditions

Key Words: Clinopyroxene, Thermobarometry, Analytical uncertainty, Experimental uncertainty, Monte Carlo

Penny E. Wieser[1*, 2], Adam J.R. Kent[2], Christy B. Till[3], John Donovan[4], David A. Neave[5], Dawnika L. Blatter[6], Michael J. Krawczynski[7]

Affiliations

1. **Corresponding author**: Penny_wieser@berkeley.edu, 541–908–4572. Department of Earth and Planetary Sciences, McCone Hall, UC Berkeley, 94720, USA

2. College of Earth, Ocean and Atmospheric Sciences, Oregon State University, 97331, USA

3. School of Earth and Space Exploration, Arizona State University, Tempe, AZ 85281, USA

4. Department of Earth Sciences, University of Oregon, 97403, USA.

5. Department of Earth and Environmental Sciences, The University of Manchester, Oxford Road, Manchester M13 9PL, UK

6. U.S. Geological Survey, California Volcano Observatory, 345 Middlefeld Road, Menlo Park, CA 94025, USA

7. Department of Earth and Planetary Sciences, Washington University in St. Louis, 1 Brookings Drive, St. Louis, MO 63130, USA

Barometers behaving badly: Assessing the influence of analytical and experimental uncertainty on clinopyroxene thermobarometry calculations at crustal conditions

Running Title: Barometers behaving badly

Key Words: Clinopyroxene, Thermobarometry, Analytical uncertainty, Experimental uncertainty, Monte Carlo

Penny E. Wieser[1*, 2], Adam J.R. Kent[2], Christy B. Till[3], John Donovan[4], David A. Neave[5], Dawnika L. Blatter[6], Michael J. Krawczynski[7]

Affiliations

1. **Corresponding author**: Penny_wieser@berkeley.edu, 541–908–4572. Department of Earth and Planetary Sciences, McCone Hall, UC Berkeley, 94720, USA

2. College of Earth, Ocean and Atmospheric Sciences, Oregon State University, 97331, USA

3. School of Earth and Space Exploration, Arizona State University, Tempe, AZ 85281, USA

4. Department of Earth Sciences, University of Oregon, 97403, USA.

5. Department of Earth and Environmental Sciences, The University of Manchester, Oxford Road, Manchester M13 9PL, UK

6. U.S. Geological Survey, California Volcano Observatory, 345 Middlefeld Road, Menlo Park, CA 94025, USA

7. Department of Earth and Planetary Sciences, Washington University in St. Louis, 1 Brookings Drive, St. Louis, MO 63130, USA

Abstract

The composition of clinopyroxene and Clinopyroxene-Liquid (Cpx-Liq) pairs are frequently used to calculate crystallization/equilibration pressures in igneous systems. While canonical uncertainties are often assigned to calculated pressures based on fits to calibration or test datasets, the sources of these uncertainties (and thus ways to reduce them) have not been rigorously assessed. We show that considerable uncertainties in calculated pressures arise from analytical error associated with Electron Probe Microanalyser (EPMA) measurements of Cpx. Specifically, low X-ray counts during analysis of elements with concentrations <1 wt% resulting from insufficient count times and/or low beam currents yield highly imprecise measurements (1σ errors of 10–40% for Na_2O).

Low analytical precision propagates into the calculation of pressure-sensitive mineral components such as jadeite. Using Monte Carlo approaches, we demonstrate that elemental variation resulting from analytical precision alone generates pressures spanning ~4 kbar (~15 km) for a single Cpx and ~6 kbar for a single Cpx-Liq pair using popular barometry expressions. In addition, analytical uncertainties in mineral compositions produce highly correlated arrays between pressure and temperature that have been previously attributed to transcrustal magma storage. Before invoking such geological interpretations, the more mundane origin from analytical imprecision must be ruled out. Most importantly, low analytical precision does not just affect the application of barometers to natural systems; it has also affected characterization of Cpx in experimental products used to calibrate and test barometers. The impact of poor precision on each individual measurement is also often magnified by the small number of measurements made within experimental charges, meaning that low analytical precision and true variability in mineral compositions have not been sufficiently mediated by averaging multiple EPMA analyses. We compile the number

of Cpx measurements performed in N=295 experiments used to calibrate existing barometers, and N=459 new experiments, finding ~40% of experiment charges were characterized by ≤5 individual Cpx analyses. Insufficient characterization of the true composition of experimental phases likely accounts for the fact that all Cpx-based barometers exhibit large errors (± 3 kbar) when tested using global experimental datasets.

We suggest specific changes to analytical and experimental protocols, such as increased count times and/or higher beam currents when measuring low concentration elements in relatively beam resistant Cpx in experiments and natural samples. We also advocate for increasing the number of analyses per experimental charge, resolving interlaboratory analytical offsets and improving data reporting. Implementing these changes is essential to produce a more robust dataset to calibrate and test the next generation of more precise and accurate Cpx-based barometers. In turn, this will enable more rigorous investigation of magma storage geometries in a variety of tectonic settings (e.g., distinguishing true transcrustal storage vs. storage in discrete reservoirs).

1. INTRODUCTION

Constraining the conditions under which magma is stored and transported within the crust is of critical importance to understanding volcanic systems (e.g., McGuire et al., 2017). It has long been recognised, based on thermodynamic principles and from chemical characterization of experimental products, that the composition of igneous minerals and co-existing liquids can be used to place constraints on the pressures, temperatures, and water concentrations at which these phases grew and equilibrated (e.g., Bacon and Carmichael, 1973; Brown and Parsons, 1981; Lindsley and Andersen, 1983; Putirka, 1999, 1997, 2008). Many of the most commonly used mineral-based igneous thermobarometers revolve around clinopyroxene (Cpx), perhaps because this phase is relatively abundant in a wide variety of different volcanic systems and tectonic settings (e.g., mid-oceanic ridges, oceanic islands, and volcanic arcs), and in a wide

range of lava compositions (basalts to rhyolites). Cpx-based equilibria are sensitive to pressure because there is a large change in volume associated with the exchange of Na and Al (the jadeite component, $NaAlSi_2O_6$) between liquid (Liq) and Cpx. There are also relatively large volume changes between different Cpx components (e.g., jadeite and diopside-hedenbergite, $CaMgSi_2O_6$–$CaFeSi_2O_6$, Putirka, 2016; Putirka et al., 1996). The exchange of jadeite and diopside-hedenbergite between clinopyroxene and liquid is also sensitive to temperature, so the abundance of these components can be used as a thermometer (e.g., Putirka, 1999).

By parameterizing the relationship between phase composition and intensive parameters in experiments, measurements of natural crystals and co-existing equilibrium liquids can be used to calculate pressures and temperatures (e.g., Neave and Putirka, 2017; Petrelli et al., 2020; Putirka, 1999, 2008; Wang et al., 2021). The vast majority of published calibrations have a structure rooted in thermodynamics, both in terms of the form of the expression, and the compositional components included (e.g., jadeite in Cpx).

For example, both the Putirka (1996) eqP1 and Putirka (2008) eq30 models for Cpx-Liq barometry have the same general form informed by thermodynamics:

$$P = a + \frac{bT}{10^4} + \frac{cT}{10^4}\ln\left(\mathrm{Jd}^{\mathrm{Cpx-Liq}}\right) + \cdots \qquad \text{[Equation 1]}$$

Additional empirical composition terms are added to improve regression statistics (Neave and Putirka, 2017), although sometimes these terms can also be approximately tied to thermodynamic reasoning. For example, the $X_{Na}^{Liq}\ X_{Al}^{Liq}$term in Putirka (1996) eqP1 implies identical activity coefficients for Na and Al in the liquid. In general, an increasing number of empirical terms have been added to barometry equations to improve the fit between calculated and experimental pressures in calibration datasets as more experimental data have become available. For example, while both eqP1 (P1996) and eq30 (P2008) have additional empirically derived terms for the sum of the cation fraction of Na and Al, eq30 has additional terms for the

liquid Mg#, the diopside-hedenbergite component in the Cpx, and the log of liquid Fe, Mg and K cation fractions.

More recently, machine learning algorithms have been calibrated for equilibria involving Cpx (Higgins et al., 2022; Jorgenson et al., 2022; Petrelli et al., 2020). Instead of creating equations with specific terms informed by thermodynamics (as in Equation 1), these machine learning techniques simply input selected oxide data from a training dataset into the machine learning algorithm, along with the predictor variable (e.g., pressure or temperature; Petrelli et al., 2020).

When discussing errors and uncertainties associated with different thermobarometers in this manuscript, we follow the National Physics Laboratory terminology guidelines (Bell, 2001). Error is taken as the difference between the measured value and the true value; if a barometer calculates a pressure of 3 kbar but the experiment was performed at 2 kbar, the error is +1 kbar. Uncertainty quantifies the doubt about the measurement result, so an error with an unknown magnitude is referred to as an uncertainty. A random uncertainty or error means that if the measurement is repeated, a different value is obtained each time, but averaging of sufficient measurements converges on the true value. Random uncertainties may follow a normal or Poisson distribution (or other unskewed distribution). However, the central limit theorem states that as the sample size grows, a distribution of sample means approximates a normal distribution (even if the data aren't normally distributed). Systematic uncertainties or errors cause the measurement to be offset from the true value, so additional measurements do not help to converge on the correct answer, meaning that more measurements produce a more precise, but inaccurate result.

The success of a given barometer or thermometer is normally assessed by comparing predicted pressures and temperatures with experimentally determined pressures and temperatures. The goodness of fit is typically assessed using R^2 values, estimates of the standard error estimate

(SEE) or the root-mean-square error (RMSE). In general, Cpx and Cpx-Liq thermometers have high R^2 values (>0.8) and relatively low SEE (e.g., ±20–100 K, e.g., Putirka, 2008, Petrelli et al., 2020). These SEEs represents only a 2-10% error considering the temperatures of most magmatic systems (~1000–1400 K). In contrast, barometers commonly have SEE of 1.4-5 kbar (~±6–19 km, using ρ=2700 kg/m^3 throughout this paper), which corresponds to very large percentage errors given the depths of interest in many volcanic systems. For example, these large SEEs span the entire crustal column in many tectonic settings (e.g., 5–8.5 km in MORB, White et al., 1992, 14–24 km in Hawai'i, Leahy et al., 2010). This means that pressures calculated on individual Cpx analyses do not have sufficient precision/resolution to reliably identify upper, mid or lower crustal storage, or distinguish storage in distinct magma reservoirs separated by ~1–2 km (unlike melt inclusion saturation pressures, which can achieve such precision at relatively low pressures, Lerner et al., 2021; Wieser et al., 2022; Wieser et al., 2021). Even in arcs with Moho pressures of 8±3 kbar (based on ~30±12 km from Profeta et al., 2016), these SEE estimates can only just distinguish between upper, mid and lower crustal storage. As many of the uncertainties associated with thermobarometers are random uncertainties, averaging multiple experiments (or natural Cpx analyses) can result in significant improvements. For example, Putirka et al. (1996) showed that the SEE on individual experiments using their eqP1 is 1.36 kbar, but can be reduced to 0.32 kbar if they average experiments conducted at the same pressure. The importance of such averaging is discussed in detail in Section 2.3.1.

In general, more recent calibrations of mineral-only and mineral-melt barometers state smaller SEEs (e.g., ±1.4 kbar for Cpx-Liq from Neave et al., 2017, ±1.66 kbar for Cpx-only from Wang et al., 2021, vs. ±3.6 kbar for equation 30 and ±5 kbar for eq32c of Putirka, 2008). However, statistics quoted by different studies are not directly comparable. For example, the ±1.4 kbar SEE commonly stated by petrological studies using the Neave and Putirka (2017) barometer

describes the model fit to the calibration dataset of 113 experiments. When this thermobarometer is applied to their global compilation of experimental data that span a wider compositional range than was used in the calibration, the error is ±3.6–3.8 kbar. When applied to test data with compositions more similar to the calibration dataset (i.e., tholeiitic basalts), the Neave and Putirka (2017) barometer return errors similar to the quoted error of 1.4 kbar. The ±1.66 kbar error from Wang et al. (2021) describes the overall fit to 100 random splits into training and validation of the calibration dataset. However, when applied to global datasets (including data not used at any point during model tuning), this barometer has a SEE of ±3.68 kbar. Finally, the Cpx-only and Cpx-Liq machine-learning barometer of Petrelli et al. (2020) have SEEs of ±3.1 kbar and ±3.2 kbar, respectively, when applied to a subset of N=119 experiments not used for calibration. The "global" statistics for newer barometers are more similar to the larger quoted errors of Putirka (2008), who calculate statistics using a global calibration dataset.

It is also important to recognise that the quoted SEE describes the overall fit across the range of pressures or temperatures being considered. Close to the edges of the distribution (e.g., very shallow or very deep pressures), the error can be larger than the SEE, and towards the centre of the distribution, the error can be smaller. Additionally, the SEE estimated from a barometer between 0–40 kbar (e.g., Putirka, 1996) is not directly comparable to one estimated between 0–20 kbar (e.g., Petrelli et al., 2020), which can also make comparison of statistics from different barometers challenging.

Despite the fact that it is difficult to directly compare statistics, we can say in general that the majority of Cpx-based barometers show large SEE (±2–5 kbar, 7.6–19 km) when applied to global datasets. Given that significantly greater precision in crustal barometry is needed to address many of the key issues in igneous petrology (McGuire et al., 2017), we try to reconcile

the source of these large errors, to identify ways in which to improve Cpx-based barometric methods in future.

1.1. A new test dataset – ArcPL

The majority of Cpx-based barometers were calibrated using experiments present in the LEPR dataset compiled in 2008 (Library of Experimental Phase Relationships; Hirschmann et al., 2008, e.g., N=850 experiments in Petrelli et al., 2020). For clarity, in this paper the word experiment is used to represent a single experimental run/capsule/charge. In addition to using experimental data within LEPR, we also compile Cpx-bearing experiments on variably hydrous compositions ranging from basalt to rhyolite at crustal conditions (<15 kbar) that were not included in LEPR. Most of the studies represented in this new dataset were published after LEPR, and have not been added to it yet (Almeev et al., 2013; Alonso-Perez et al., 2009; Andújar et al., 2015; Blatter et al., 2013, 2017; Bogaerts et al., 2006; Cadoux et al., 2014; Costa, 2004; Erdmann and Koepke, 2016; Erdmann et al., 2016; Feig et al., 2010; Firth et al., 2019; Hamada and Fujii, 2008; Husen et al., 2016; Krawczynski et al., 2012; Mandler et al., 2014; Melekhova et al., 2015; Mercer and Johnston, 2008; Nandedkar et al., 2014; Neave et al., 2019; Parat et al., 2014; Parman et al., 2011; Pichavant and Macdonald, 2007; Rader and Larsen, 2013; Riker et al., 2015; Ulmer et al., 2018; Waters et al., 2021). We also include a small number of pre-2008 experiments which were not included in LEPR (Berndt, 2004; Rutherford et al., 1985; Sisson et al., 2005). We call our new dataset ArcPL (Arc post-LEPR, N=469). One advantage of ArcPL is that many of the experiments were conducted relatively recently, meaning that it was easier to obtain additional analytical information from the authors, and more information on analytical conditions was generally presented in the text and supporting information. We use these two datasets of experiments (LEPR and ArcPL) to place quantitative constraints on sources of uncertainty when calibrating and testing Cpx-based barometers.

1.2. Sources of uncertainty

Thermobarometer calibrations based on experimental products are subject to three main sources of uncertainty:

1) Uncertainties relating to the regression method used to calibrate thermobarometry equations and models (e.g., extrapolation, overfitting, incomplete data, Fig. 1a).

2) Analytical uncertainties associated with measurements of minerals and glasses, normally by electron probe microanalyser (EPMA, e.g., insufficient counts, heterogeneity in primary standards within a single chip and between chips, beam damage, instrument miscalibration, Fig. 1b).

3) Experimental errors (e.g., crystallization under disequilibrium conditions, uncertainty in the pressure in a piston-cylinder, Fig. 1c), as well as additional issues associated with analysing small experimental products (Fig. 1d).

Each of these are discussed in detail below.

1.2.1 Model formulation and calibration

One unavoidable reason why barometers have higher percentage errors than thermometers relates to thermodynamics; namely, major and minor element variations in available igneous phases are simply more sensitive to temperature than pressure, because relevant reactions have larger changes in entropy (relating to T) than volume (relating to P). This is in contrast to subsolidus metamorphic systems where a relatively large number of very P-sensitive phase transitions and chemical reactions are available (Powell and Holland, 2008). The paucity of P-sensitive reactions between solid mineral phases and silicate melts reflects the ability of liquid-rich igneous systems to absorb changes in volume (and to a lesser extent temperature and composition) without drastically changing the composition of the coprecipitating phases (Putirka, 2008). Thus, it is expected that regressions of experimental Cpx compositions against

pressure will have relatively poor predictive power (Fig. 1a), as many variables other than pressure have more influence on the reaction (e.g., temperature, water content, melt composition).

However, there are a number of sources of uncertainty that can be introduced during the calibration of barometric models which decrease the accuracy and precision of barometers beyond some theoretical limit determined by the thermodynamics of each reaction. Identifying these is vital to produce the best possible barometers for igneous systems.

Firstly, the calibration dataset may span a restricted compositional, pressure or temperature range, and empirical fits developed on this dataset may return poor results when extrapolated outside this range (Fig. 1a). For example, Neave and Putirka (2017) cautioned users about the limited applicability of their model in highly oxidised and alkaline systems, as it was predominantly calibrated using tholeiites. Similarly, Wang et al. (2021) attributed the poorer performance of their barometer at pressures >12 kbar to the lack of high-pressure experiments in their calibration dataset. Models can also be overfitted to calibration data. This is a particular problem for certain machine-learning algorithms such as extra tree regressors which can perfectly fit the training data, but produce erratic results on test data (see section 2.2).

A second source of uncertainty relates to the fact that not all experimental studies report the concentrations of all the major and minor elements in Cpx and Liq used when performing thermobarometry calibrations. This is problematic for several reasons. Firstly, missing elements from the quantification routine during EPMA analysis can affect the concentration of elements which are measured. For example, EPMA analyses calculating water by difference without a subsequent iterative matrix correction produce water estimates that are low by as much as 1 to 2 wt% absolute (Roman et al., 2006). This is equally true for other unanalyzed elements (Fournelle et al., 2020). Missing elements also cause issues during regression

analysis. It is generally considered that up to 5% missing data on each attribute (i.e., a single oxide) are manageable during regression, 5–15% requires use of more sophisticated approaches, and >15% can severely impact the prediction accuracy of the model on unseen data (Pyle, 1999; Twala, 2009). Unfortunately, the percentage of missing data in experimental compilations used to calibrate barometers is well within the severe category. For example, in the LEPR dataset used by Petrelli et al. (2020) and Putirka (2008), 66% of experiments don't report H_2O contents in the glass phase and 44% do not report Cr_2O_3 in the Cpx. Yet, both these elements feature heavily in parameterizations of Cpx-only and Cpx-Liq barometry, and the presence/absence of Cr actually affects phase stability (discussed in detail below, Voigt et al., 2017).

There is abundant literature, but little consensus, about how to deal with missing values during regression analysis (Emmanuel et al., 2021). The simplest way is list-wise deletion, where experiments with any missing values for any oxides are simply removed from the calibration dataset. However, in the experimental datasets used to calibrate thermobarometers, which have large amounts of missing data, list-wise deletion can result in a dramatic reduction in the number of observations used for calibration. For example, 54% of experiments in the calibration dataset of Petrelli et al. (2020) do not report P_2O_5 in glass, 56% do not report Cr_2O_3 in glass, and 69% do not report K_2O in Cpx. List-wise deletion would leave only 31/850 experiments, which is far too small a calibration dataset. The software JMP used by Putirka (2008, and previous papers) uses list-wise deletion by default; the shrinking dataset issue was mitigated by excluding elements from the calibration which result in lots of rows being deleted, but likely do not have a major influence on the equilibria of interest (e.g., MnO in liquid, K_2O in Cpx).

List-wise deletion can be very problematic if missing values reflect an underlying bias in the measurement procedure (termed "missing not at random" by Rubin, 1976). For example, it is

far more likely that H_2O-poor or nominally anhydrous experiments do not report H_2O in experimental glasses compared with very water-rich experiments. Removing experiments with no reported water could easily bias the remaining dataset towards compositions and phase assemblages found in more hydrous magmas, meaning the resulting model would be poorly calibrated for relatively anhydrous melts. For H_2O-poor experiments, it is far better to enter H_2O=0 into the dataset than to remove the experiment. Missing H_2O data has been dealt with in several ways. Petrelli et al. (2020) fill all missing values for H_2O (and any other elements) with zeros.

Alternatively, missing values can be imputed (i.e., estimated). For example, Putirka (2008) replaced missing H_2O data with 100 minus the sum of major element totals (i.e., volatiles by difference). While this method is associated with large uncertainty unless calibrated using hydrous standards (Hughes et al., 2019), it is likely better than replacing missing values with the mean or median of the dataset (which can create issues when data are not missing at random, as discussed above for H_2O; Twala, 2009).

The presence/absence of reported Cr_2O_3 (or Cr) data in Cpx demonstrates one challenge associated with imputation for experimental datasets. In many cases, experiments on synthetic starting materials do not report Cr concentrations in Cpx or Liq because no Cr was added (e.g, Hamada and Fujii, 2008), whereas in other studies, Cr was likely present but not reported. For example, Parat et al. (2014) use a natural starting material with ~187 ppm Cr, but report no Cr_2O_3 data in Cpx or glasses. Using an approximate partition coefficient (~10, Hart and Dunn, 1993), their Cpx could contain ~0.1–0.2 wt% Cr_2O_3. Finally, there are experiments where it is unclear whether Cr is present or not. For example, the natural starting materials of Cadoux et al. (2014) are sufficiently evolved (67–71 wt% SiO_2) that it is unlikely there is very much Cr left, but the actual Cr content of the starting material (and experimental Cpx) are not reported.

The paucity of Cr data (resulting from Cr-free starting materials and the lack of Cr measurements in Cr-bearing starting materials) has been discussed in detail in the context of MORB differentiation and liquid-barometry by Voigt et al. (2017). Voigt et al. (2017) showed that Cr-containing experiments stabilize Cpx at higher temperatures than Cr-free experiments. Pressures calculated using their melt geobarometer for Cr=0 versus true Cr contents in MORBs differ by up to 1.5 kbar. Thus, replacing missing values with the mean of the dataset, or any other prediction, would fail to capture the fact that there truly was no Cr, which has likely influenced Cpx stability. We quantitatively evaluate the effect of missing Cr data on the Cpx-only and Cpx-Liq thermobarometers in Section 2.

1.2.2 Analytical Uncertainty

In addition to thermodynamic considerations (larger changes in entropy compared with volume), the larger percentage errors associated with barometers compared with thermometers may result from the lower concentration of elements that are important in barometery compared with thermometry, meaning analytical errors are larger (e.g., Na in Cpx for pressure vs. Mg-Fe for temperature). A number of random and systematic uncertainties can arise during EPMA analyses. Each wavelength dispersive spectrometer (WDS) is calibrated for a specific element using the relationship between the peak-background ratio and the concentration of that element in a primary standard material. In turn, this relationship is used to predict the element concentration in an unknown material based on the measured peak-background ratio. A matrix correction is applied to account for the influence of the specific material analysed on the intensity of measured X-rays (e.g., atomic number effects, absorption, and fluorescence).

The generation of X-rays from a sample excited by an electron beam is a random process (like radioactive decay), meaning that the emission of any given X-ray cannot be predicted. However, if X-ray arrivals are collected over a long enough time interval, the average number of X-ray arrivals per unit time is a function of the rate of X-ray production. X-ray production

is determined by the specific element and electron shell ionization efficiencies, element concentration, beam current, beam voltage and detector take off angle. The instrumental efficiency of X-ray detection is controlled by the WDS crystal size/geometric efficiency and detector efficiency (as well as the vacuum). X-ray intensities are then normalized to beam current, yielding counts per second per nA. Instrumental specific effects are accounted for when converting counts into concentration by performing the X-ray measurements using the same beam energy and spectrometer on both the primary standard and the unknown material to produce a k-ratio, which should be identical within measurement error for all instruments using the same element, X-ray emission line, beam energy and takeoff angle (assuming the high voltage calibration and effective take off angle of the spectrometers are sufficiently similar).

The precision of an EPMA measurement is determined by the total accumulated number of X-rays counted by the WDS detector at the peak and background positions. Errors directly resulting from the fundamentally random process of X-ray generation and detection are termed counting statistics. When averaged over sufficient time period, X-ray counts follow a Poisson distribution which approximates a normal distribution at sufficiently high counting rates (i.e., the central limit theorem). Errors resulting from counting statistics can be estimated using two main methods.

Equation 2 can be used to predict the relative error (100*standard deviation (σ)/concentration) for a given element in an unknown sample using information from count rates in the primary standard (Weill et al., 2013), the relative concentration of the element in the primary standard and sample, and the time spent counting:

$$\text{Error (\%)} = 100 \times \sqrt{\frac{\frac{X_{sample}\,(P_{std}-B_{std})}{X_{std}} + 2B_{std}}{\left(\frac{X_{sample}\,(P_{std}-B_{std})}{X_{std}}\right)^2 t}} \qquad \textbf{(Equation 2)}$$

where P_{std} and B_{std} are the counts per second (cps) of the peak and background for the element in the primary standard, X_{std} is the element concentration in the primary standard (wt%), X_{sample} is the concentration in the unknown sample (wt%), and t is the count time on the unknown sample (s).

Equation 2 assumes that the total count times on the peak and background are the same and does not account for the different matrices of the primary standard and the sample. It can be made more versatile by including a factor for the probe current (I), substituting counts per second on the primary standard with counts per second per nA ($P_{I,\,Std}$ and $B_{I,\,Std}$):

$$\text{Error (\%)} = 100 \times \sqrt{\frac{\frac{X_{sample}\left(I\,P_{I,std} - I\,B_{I,std}\right)}{X_{std}} + 2\,I\,B_{I,std}}{\left(\frac{X_{sample}\left(I\,P_{I,std,} - I\,B_{I,std}\right)}{X_{std}}\right)^2 t}} \qquad \textbf{(Equation 3)}$$

When the measured total counts ($P_{Tot,sample}$) on the peak and background ($B_{Tot,sample}$) are known, A more precise way of calculating the relative error for a specific element is given by:

$$Error\ (\%) = 100 \times \frac{\sqrt{\frac{P_{Tot,\ sample}}{t^2} + \frac{B_{Tot,\ sample}}{t^2}}}{\left(\frac{P_{Tot,\ sample}}{t} - \frac{B_{Tot,\ sample}}{t}\right)} \quad \textbf{(Equation 4)}$$

Equations 2–4 yield very similar results (often within ~1%), with slight discrepancies resulting from the fact that Equation 4 accounts for differences in the matrix of the sample and standard, which affects the intensity of generated X-rays, and slight differences in the background count rate on the sample and standard. The main advantage of Equations 2–3 is that they can be used predictively to assess the approximate precision on an unknown using count rates from primary standards on a given spectrometer and crystal. Equation 4 is best applied after an analysis has been conducted, and is what most commercial EPMA software uses to output 1 sigma errors for a specific analysis.

Uncertainties resulting from counting are almost always random (i.e., following a Poisson distribution), whereas instrument calibration can introduce systematic errors. Historically, because the accuracy of the physical models used for performing matrix corrections were limited (though today that is generally no longer the case), EPMA analyses of geological materials have tended to use primary standards with similar matrices to the target analytes (e.g., Na in Albite for analysis of Na in feldspar, Na in jadeite for analysis of Na in pyroxene). The most common primary standards are from the Smithsonian National Museum of Natural History (NMNH) collections (Jarosewich, 2002; Jarosewich et al., 1980). However, it is well documented that different chips of the same natural NMNH standard may differ from published compositions determined by wet chemistry, and that heterogeneity can also exist within a single chip (Fournelle, 2012; Jarosewich et al., 1980; Rose et al., 2008). As each EPMA laboratory has its own set of primary standards, for any given named standard (e.g. San Carlos olivine), heterogeneity between the different chips in different laboratories can result in systematic offsets between measurements made in these laboratories. Different laboratories also rely on different primary standards to calibrate a specific element, increasing the variability. Some laboratories also utilize “home grown” materials obtained from their mineral collections or synthetically produced “in-house” standards, and some commercially available standard materials may not be what are advertised. For example, some commercial “San Carlos olivine” has not been split from the Smithsonian mineral collection, but rather was merely collected from the same geographical vicinity.

The resulting systematic offsets in instrument calibration can be identified using round-robins, where the same material is analysed as an unknown in different laboratories using their routine calibration strategy. Hunt et al. (1998) distributed a Lipari Obsidian sample to five laboratories, and Kuehn et al. (2011) distributed 3 different glass compositions (rhyolite, phonolite, basalt) to 27 laboratories. The Kuehn round-robin identified a number of outlier laboratories with

large systematic errors, especially with regards to the correction of time dependent intensity (TDI) effects, sometimes referred to as volatile element or beam damage effects. These changes in emitted intensity are usually due to ion mobility within the interaction volume (Morgan and London, 2005 and Hughes et al., 2019) and are observable on not only highly mobile alkali elements such as Na and K (which can dramatically decrease in intensity during the measurement and therefore must be extrapolated back to their zero time intensities), but also for less mobile elements such as Si and Al, whose apparent intensities increase as the alkali element intensities decrease due to migration towards subsurface charge accumulation. Such TDI corrections can range from under a few percent (relative) to 30–100%. Thus, changes in counts during beam exposure should be carefully inspected for each element in representative samples when performing a study on hydrous/alkaline melt compositions and used to inform decisions about which elements to perform TDI corrections for. As many Cpx-Liq thermobarometers are parameterized in terms of Na and K (and Si and Al) in the liquid (e.g., Neave and Putirka, 2017, eq30–31 of Putirka, 2008), different TDI correction routines used to measure different experiments could add significant scatter to an experimental dataset compiled from many different laboratories.

At various points over the last few decades, authors have used smaller round-robins to identify systematic offsets in glass measurements and have corrected data compiled from these different laboratories to produce a more consistent calibration dataset. For example, Yang et al. (1996) performed corrections to glass data collected at both Massachusetts Institute of Technology (MIT) and the Smithsonian prior to performing modelling and thermobarometric calculations. Most recently, Gale et al. (2013) performed a round-robin using VG2 to obtain correction factors for MORB glasses relative to EPMA analyses from Lamont Doherty Earth Observatory (hereafter, Lamont; Fig. 2). To our knowledge, no such reconciliation has been performed for

datasets used to calibrate Cpx-based barometers (or any other mineral barometers), so we quantify the possible effects of interlaboratory offsets in Section 2.1.

Additional systematic and random analytical uncertainty during EPMA analyses can result from problems relating to beam damage/charging of materials under the electron beam, poor sample preparation (e.g., bad polishing, sample tilt) and drift of the instrument (e.g., stage Z height, changes in the temperature and pressure in the room; Fig. 1b). It should also be mentioned that other sources of systematic analytical inaccuracy can be introduced from improperly calibrated instruments, for example assumed dead time constants and picoammeter readings from poorly maintained instruments. However, these are almost impossible to quantify retrospectively from published data, so are not discussed further.

1.2.3 Experimental scatter

Analysis of the experimental products used to calibrate thermobarometers are subject to the analytical uncertainty discussed above, along with several other sources of uncertainty (Fig. 1c). Firstly, experimental phases may be heterogeneous because of zoning resulting from changing P-T-fO_2-H_2O conditions during the run, remnant seed crystals, or kinetic effects during growth and sample quench. Capsules may also experience Fe and H^+ exchange with samples and assemblies (Botcharnikov et al., 2005; Gaetani and Grove, 1998), resulting in poor redox buffering. Relict crystals from the starting material may be present if the starting material was not fully melted (Mutch et al., 2016). The relatively small size of experimental products also enhances EPMA uncertainty relative to natural crystals, because the interaction volume of the electron beam may directly enter other phases, and neighbouring phases may influence the measurement through secondary fluorescence (Llovet and Galan, 2003, Fig. 1d).

There are also a number of sources of uncertainty that can arise from the experimental set up. Experiments conducted at <~5–7 kbar were mostly performed using TMZ/MHZ vessels

(Sisson and Grove, 1993a, 1993b) and internally heated pressure vessels (IHPV, e.g., Cadoux et al., 2014; Di Carlo, 2006; Hamada and Fujii, 2008; Parat et al., 2014). Pressure in IHPV experiments is monitored with strain gauge manometers, Heise Bourdon tube gauges, or digital pressure transducers, which have a precision of ~ 0.01–0.04 kbar (1–4 MPa, Koepke et al., 2018; Pichavant, 2002). Pressure variations during experiments are mostly within ~0.05 kbar (e.g., Parat et al., 2014). Because pressure is transmitted via a gas to the capsule, excluding calibration offsets in gauges/manometers/transducers, an experimental pressure recorded in one lab is likely to be similar to that in another lab.

In contrast, most experiments conducted at > 5 kbar were performed in piston cylinders (Baker and Eggler, 1987; Gaetani and Grove, 1998; Mercer and Johnston, 2008), where a solid-medium transmits pressure to an enclosed capsule. Pressure in the piston cylinder apparatus is commonly monitored using a Heise gauge, and maintained to within ±0.5 kbar (Hamada and Fujii, 2008). In solid-medium experiments the pressure experienced by the experimental capsule can differ from the pressure applied to the hydraulic piston (measured with the Heise gauge), with the correction between the two often referred to as a friction correction (Condamine et al., 2022; Tamayama and Eyring, 1967). This friction/pressure correction can be evaluated for each experimental set up by running experiments for reactions which are well constrained in P-T space, and applying a shift to account for any offsets between the observed and predicted transition.

However, different laboratories investigating Cpx equilibria correct for friction in different ways, which could easily introduce bias to an experimental dataset compiled from many different studies. For example, Mercer and Johnston (2008) and Draper and Johnston (1992) do not include a friction correction. Likewise, Bartels et al. (1991) do not apply a correction, because their offsets calculated from the melting point of Au are only 0–1 kbar, which is within the uncertainty of the Au calibration (Akella and Kennedy, 1971). Grove et al. (2003) corrected

for the offset using the reaction between anorthite+gehlenite+corundum → Ca-tshermakite (now kushiroite, Hays, 1966), and although they do not give the magnitude of the offset, they stated that after this correction pressures are accurate to ±0.5 kbar. Gaetani and Grove (1998) used this Ca-tshermakite/kushiroite reaction in addition to the melting point of Au, resulting in a friction correction of 300 MPa. In contrast to this constant offset applied to 12, 16 and 20 kbar experiments, Hamada and Fuji (2008) apply a -10% correction for their 4 kbar experiments, and a -15% correction for their 7 kbar experiments based on a calibration using the water solubility of albite melt (Behrens et al., 2001). Ulmer et al. (2018) stated that they follow the experimental approach of Villiger (2004), who applied a correction of -3% calibrated against the quartz-coesite transition at 3.07 GPa and 1000°C (Bose and Ganguly, 1995) and fayalite+qtz→ orthoferrosilite reaction at 1.41 GPa and 1000°C (Bohlen et al., 1980). Finally, Blatter et al. (2013, 2017) calibrated at each pressure by bracketing the CsCl melting curve (Bohlen and Boettcher, 1982).

The wide variation in the reactions chosen for calibration (and the variation in the pressures and temperatures of these calibration reactions) means that it is perfectly plausible that systematic offsets still exist between different laboratories, up to the magnitude of the corrections applied (e.g. ~10–15%, or a few kbar). For example, Johannes et al. (1971) showed that measurements of the pressure of the albite→ jadeite+quartz reaction at 600°C using the same starting material in six different laboratories varied from 15.7 kbar to 16.8 kbar Additionally, Condamine et al. (2022) showed that friction can decrease during a run (from 29% in 6 hr runs to 21% in 24 hr runs), which means that the true pressure experienced by the capsule may also be influenced by the length of the experimental run, which varies greatly between studies. Johannes et al. (1971) also pointed out that the friction correction can also vary between runs conducted with identical protocols, because of a softer than average batch of the solid-medium material, or more efficient wall lubrication. This means that a piston

cylinder experiment reported at 10 kbar in one laboratory may not have experienced the same pressures as an experiment performed at 10 kbar in another laboratory, and variations may exist even within experiments run at 10 kbar in a single laboratory. Uncertainties in the true pressure experienced by the charge explains why experimentalists tend to space out their piston-cylinder pressures within a single study, to ensure that trends are at least coherent. However, when all these data are compiled to calibrate a barometer, offsets on the order of 0.5–1 kbar will increase scatter, and could create systematic uncertainties based on different laboratories investigating different regions of PT space.

Temperature variations in piston cylinders are generally measured with thermocouples (e.g., Pt-Rh, Baker and Eggler, 1987, W-Re, Mercer and Johnston, 2008), although the exact geometry varies in different laboratories. Although thermocouples are reasonably precise and accurate (±10°C), the larger source of error results from thermal gradients within the piston cylinder, requiring a correction to be made to account for the higher temperatures in the hotspot where the experimental capsule is placed versus the position of the thermocouple tip. These corrections depend on the capsule geometry and assembly, but can easily reach 20–40°C (Brugman et al., 2021; Grove et al., 2003). Variable thermal gradients between the capsule and thermocouple could result in systematic differences between runs and laboratories, and thermal gradients within capsules themselves (Harlow, 1997) can cause crystals grown in different parts of the capsule to show different compositions (increasing the compositional scatter seen in experiments). Putirka et al. (1996) stated that the most consistent pyroxene analyses are when rim compositions are analysed along with the neighbouring liquid interface, perhaps helping to mitigate the effect of thermal gradients (and thus compositional variations throughout the capsule).

2.1. Quantifying the effect of interlaboratory EPMA analysis offsets

The dataset of experiments from LEPR used by Putirka (2008) and Petrelli et al. (2020) to calibrate their Cpx ± Liq thermobarometers lists 45 unique experimental laboratories, with a relatively small number of laboratories performing a large proportion of experiments (MIT=25%, Penn State=7%, Lamont=6.4%, Hannover and University of Oregon=4%). If all laboratories investigated the same P-T-X conditions, and interlaboratory offsets were normally distributed about the nominally correct value, inter-laboratory EPMA offsets would simply add random uncertainty to calibration and test datasets. However, as different experimental laboratories, which mostly use a specific EPMA instrument, tend to target different research questions, the occurrence of these analytical offsets in the experimental dataset is not uniformly distributed, and could thus lead to systematic uncertainty. For example, in the LEPR dataset, at pressures >10 kbar, experiments performed at Australia National University (ANU) tend to focus on higher SiO_2 liquids than experiments performed at MIT or University of Tasmania (Supporting Fig. 1–2). Thus, interlaboratory offsets mean the calibration could be skewed as a function of liquid composition.

Interlaboratory offsets can also affect the statistics determined from a test dataset if a specific laboratory has an offset relative to the average offset of the LEPR dataset (or even the average value in a specific P-T-X region of calibration dataset). It is noteworthy that the relative contribution of different laboratories at crustal pressures (0–13 kbar) has changed dramatically between our newly compiled ArcPL dataset and LEPR. For example, experiments conducted at Hannover account for 40% of the ArcPL, but just 1% of the LEPR dataset, while MIT comprises 10.4% of the LEPR dataset and 10.5% of the ArcPL dataset. If, say the EPMA lab at Hannover (or any other laboratory which has greater output since LEPR was compiled) had an offset from one of the dominant EPMAs in the LEPR dataset used for calibration, this could

help to account for the fact that new experimental data are predicted poorly by existing barometry calibrations.

In general, interlaboratory analytical differences from glass round-robins are <10% (Gale et al., 2013; Hunt et al., 1998; Kuehn et al., 2011), although occasionally it is noted that one or more laboratories produce discrepancies >10% (their identity is kept anonymous in Hunt et al., 1998). Compared to other analytical techniques, relatively little attention has been paid to interlaboratory EPMA offsets in petrology, with most studies being conducted on silicate glasses by the tephrochronology community (Hunt et al., 1998; Kuehn et al., 2011). To our knowledge, no round-robins have been conducted on pyroxene or other silicate minerals. As many of the EPMAs used to measure the pre-2008 experiments in the LEPR dataset have been decommissioned, we conclude that we will never be able to fully determine the exact value of offsets for Cpx. In the absence of other data, we assume that the interlaboratory offsets for VG2 glass reported by Gale et al. (2013; Fig. 2a-b) are a first-order estimate of the interlaboratory differences that may have occurred during Cpx analysis. The round-robin conducted by Gale et al. (2013) is particularly useful because it targeted a number of laboratories which have analysed experimental charges used to calibrate and test various thermobarometers.

To assess whether 0–10% offsets between different EPMA laboratories could adversely affect thermobarometric calibrations and assessment using test datasets, we consider the average reported Cpx and glass compositions from experiments from Krawczynski et al. (2012) analysed on the MIT EPMA. We multiply these measured compositions by the correction factors from Gale et al. (2013) to obtain the compositions that would have been measured on the Lamont EPMA. Using the interlaboratory comparisons to Lamont from Gale et al. (2013), we also estimate the composition that would have been measured at a number of other EPMA labs. We then calculate pressures and temperatures for these corrected compositions by

iterating eq32d (T) and eq32b (P) for Cpx-only thermobarometry, and eq33 (T) and eq31 (P) for Cpx-Liq thermobarometry (equations from Putirka 2008).

The range of calculated pressures resulting from these laboratory offsets is significant (Fig. 2c-f), and varies greatly between different experiments and different thermobarometry expressions (Fig. 2, Supporting Figs. 3–5). Cpx-Liq pressures that would have been calculated from mineral compositions measured in different laboratories show offsets from one another of ~0.5 to 6 kbar (Fig. 2d, f, Supporting Figures 3–5), while Cpx-only pressures show offsets of ~3 to 5 kbar (Fig. 2c, e, Supporting Figures 3–5). Interlaboratory offsets also impact calculated temperatures (~10 to 50 K), but to a lesser extent. These interlaboratory offsets likely contribute to the overall scatter between calculated versus experimental pressures in calibration and test datasets. In fact, it is noteworthy that our calculated offsets are similar in magnitude to quoted SEEs on barometers. These offsets also affect natural samples which barometry equations are applied to; it is highly concerning that calculated pressures may vary by 3–5 kbar based solely on the EPMA laboratory used to perform analyses.

2.2. Variability in treatment of Chromium

As discussed in the introduction, many experiments in the calibration dataset do not report Cr data, yet the Cpx-only thermobarometers of Wang et al. (2021, eq1, 2, 32dH), Putirka (2008, eq32b, 32d) and Petrelli et al. (2020) include a term for the Cr content of the Cpx. For Cpx-Liq thermobarometry, only the model of Petrelli et al. (2020) is parameterized directly in terms of the Cr content of the Cpx and the liquid. However, Cr in the Cpx is used to calculate the CrCaTs component of the Cpx, which is then used to calculate the diopside-hedenbergite (DiHd) component:

$$\mathrm{CrCaTs}=0.5*\mathrm{Cr}_{\mathrm{cat\ frac}}$$

$$\mathrm{DiHd}=\mathrm{Ca}_{\mathrm{cat\ frac}}-\mathrm{CaTs}-\mathrm{CaTi}-\mathrm{CrCaTs}.$$

The DiHd component is included in the Cpx-Liq barometers of Putirka (2008, eq30 and 31), Neave and Putirka (2017), and the Cpx-only barometers of Putirka (2008, eq32a, 32b). Additionally, even Cpx-Liq or Cpx-only barometers which have no compositional term dependent on Cr in Cpx are normally parameterized in terms of Cpx cation fractions, either directly or in terms of components like jadeite which are calculated from cation fractions. If Cr is present in the sample, but not measured, the calculated cation fractions of other elements such as Na (and therefore jadeite) are artificially high. Thus, a wide range of barometers are directly or indirectly sensitive to the Cr content of the Cpx.

The proportion of missing Cr data is very similar in the calibration dataset and ArcPL. Missing Cr data in the calibration dataset may have resulted in the relationship between components dependent on Cr and P and T being incorrectly parameterized (or correctly parameterized, but with the addition of significant noise). Missing Cr data in our test dataset will also cause noise when comparing predicted versus experimental pressures, because if Cr was present but not reported, calculated pressures and temperatures using true Cr contents may differ from those calculated using the Cr=0 wt% (and would perhaps lie closer to the 1:1 line). To investigate the possible offsets caused by not reporting Cr when it is actually present, we calculate pressures and temperatures for all Cpx and Cpx-Liq pairs in the ArcPL dataset with reported Cr data, and compare this to calculations using Cr=0 wt% (Fig. 3).

Different barometers show different sensitivity to Cr. For the Wang et al. (2021) Cpx-only barometer and thermometer, there is a clear correlation between the change in pressure and the Cr content of the Cpx, with the most Cr-rich Cpx showing pressures up to 2.8 kbar too high when Cr is set to 0 wt% (Fig. 3a). The effect on temperature is proportionally smaller (~ 44 K, Fig. 3b). Strong correlations with true Cr content are also seen for pressures calculated using Putirka (2008) eq32d-32b, with max offsets of 2 kbar (and 16 K for temperature). In contrast, the change in pressure using the Petrelli et al. (2020) Cpx-only barometer shows no apparent

relationship to the Cr content of the Cpx, and shows significantly larger variations than the other barometers (max ΔP=4.9 kbar, ΔT=125 K). This unpredictable response reflects the use of decision trees, where the Cr content affects the route taken through the tree.

For Cpx-Liq thermobarometers, iteration of Putirka (2008) eq33 (T) with eq30 (P), or eq33 (T) with Neave and Putirka (2017, P, red triangles) shows very little sensitivity to Cr content (apart from a single Cpx-Liq pair showing a large change for all equations, Fig. 3c). Iteration of various thermometers with eq32c for pressure shows slightly more sensitivity, with offsets of up to ΔP=1 kbar and ΔT=10 K. As for their Cpx-only thermobarometer, the extra-trees regressions for Cpx-Liq of Petrelli et al. (2020) are significantly more sensitive to Cr, with temperatures varying by up to ±100 K simply by changing the Cr content, and no clear correlation between the offset and the actual Cr content of the Cpx. Overall, these comparisons show that the presence/absence of Cr data in both calibration and test datasets can clearly introduce noticeable uncertainty in terms of calculated pressures (>1 kbar).

2.3. Quantifying the effects of analytical versus experimental variability in test and calibration datasets

Variability in measured phase compositions within a single experiment can also affect calibration and test datasets. Analytical uncertainty associated with the random process of X-ray generation can produce variability in measured phase compositions, even if the experimental phases themselves are entirely homogeneous. Because analytical uncertainty resulting from counting statistics is normally distributed and random, if infinite numbers of compositionally homogenous Cpx crystals are analysed from a single experiment, the mean composition will be the same regardless of the precision of each analysis. However, if only a very small number of Cpx are measured, analytical uncertainty can easily yield a reported

average composition that is significantly different from the true composition. In the more likely scenario that experimental Cpx are also chemically heterogeneous (e.g., zoned or sector zoned), large numbers of EPMA analyses are required to correctly characterize the average composition of each experiment, even if each EPMA analysis is highly precise. For example, Neave et al. (2019) noted that their Cpx show highly variable Al and Ca contents, which they attributed to sector zoning. They suggested based on their observations of chemical heterogeneity that at least 20–40 analyses are required to meaningfully characterize the composition of Cpx.

2.3.1. Are we sufficiently averaging experimental and analytical variability?

To address the possible influence of analytical and experimental variability, we compile the number of reported Cpx analyses in the 459 experimental charges from the ArcPL dataset to investigate how many publications approach the Neave et al. (2019) recommendation of 20–40 analyses. We supplement the ArcPL dataset with a compilation of Cpx measurements in 295 experimental charges in the LEPR dataset conducted at 0–13 kbar in arc-like compositions. We note that we do not know for each individual experimental charge whether the number of analyses reported in the associated paper represents measurements of N discrete Cpx crystals, or N analyses, with some Cpx being characterized by more than 1 EPMA spot (e.g., perhaps 10 analyses from 8 Cpx crystals).

In 40 experimental charges (5% of the combined dataset) only a **single** Cpx analysis was performed, 47 (6%) performed just 2 Cpx analyses, 67 (9%) performed 3 Cpx analyses, and 77 (10%) performed 4 Cpx analyses (Fig. 4a-b). Overall, 43% of the compiled experimental runs were characterized by ≤5 Cpx analyses, 25% by ≥10 Cpx analyses, and only 5% by ≥20 Cpx analyses (as recommended by Neave et al., 2019).

Concerningly, the experiments with the lowest number of analyses tend to be concentrated at lower pressures, where Na_2O contents are generally lower and more susceptible to large analytical uncertainties (Fig. 4a). It is notable that the discrepancy between the calculated pressure using the reported Cpx composition and the true experimental pressure increases with decreasing number of Cpx analyses (for the Wang et al. 2021 and Putirka, 2008 Cpx-only barometers, Fig. 4c, d). This indicates that insufficient averaging of analytical variability or true phase variability (e.g., zoning) is affecting the performance of barometers. As the median number of analyses per experiment is 6 for both our new dataset and the subset of LEPR we have compiled the number of analyses for, we assume the statistics given above are representative of the entire LEPR database used for literature thermobarometry calibrations.

Assessing the relative influence of analytical uncertainty and experimental variability in experimental compositions is vital to address how barometry calibrations can be improved. If variability in measured Cpx compositions results from true variation in the composition of that phase (e.g. zoning and other disequilibrium processes), it means we must direct more attention to understanding and identifying disequilibrium in experimental products, measure very large numbers of phases from each experiment (e.g., Neave et al., 2019), and possibly redo experiments that have not sufficiently approached equilibrium (or remove these experiments from the calibration dataset). In contrast, if analytical variability is the primary culprit, it means we need to direct our attention to improving EPMA analyses of experimental products. Hereafter, we refer to true variation in Cpx compositions in experimental charges as “phase variability” and variability resulting from EPMA analyses as “analytical precision.”

2.3.2. Distinguishing analytical and experimental variability

Unfortunately, the information required to quantify the relative influence of phase variability versus analytical precision is largely absent from the information provided in most legacy experimental studies. In-text pdf tables are normally used to report the mean composition and

standard deviation of each phase in each experimental charge. It is very unusual for the individual EPMA analyses from each experiment to be reported, except in the most recent publications (e.g., Erdmann et al., 2016; Neave et al., 2019; Waters et al., 2021). This makes it difficult to assess the true variability in Cpx compositions, because the quoted mean and standard deviation for each phase in each experiment only provide a good description of the underlying data if it is normally distributed, and lacks covariance between oxides. Yet, almost all of the full experimental datasets we have been able to obtain (Blatter et al., 2013; Krawczynski et al., 2012; Melekhova et al., 2015; Neave et al., 2019) do not show normally distributed elemental variations, and exhibit significant correlations amongst different oxides (e.g., Fig. 5a, Supporting Fig. 6–15).

The covariance structure of oxides in each phase gives important clues into the source of variability in experimental products. For example, strong correlations between SiO_2-TiO_2, SiO_2-Al_2O_3, SiO_2-MgO, Al_2O_3-MgO in Cpx are indicative of sector zoning (e.g., Fig. 3b, Neave et al., 2019; Ubide et al., 2019, Supporting Fig. 6–14), whereas elements with variability arising from EPMA counting statistics will be uncorrelated (e.g., MnO-Na_2O, Fig. 5c). Importantly, when the full data are not reported, simulations using the reported mean and standard deviation provide a poor match to the real experimental data when a strong covariance structure is present (e.g., Fig. 5b, simulated Cpx as yellow dots, measured Cpx as red dots from Neave et al., 2019). The poor match of data simulated using just the mean and standard deviation means that it is nearly impossible to simulate the true variability in the LEPR dataset, where individual analyses could not be recovered.

Similarly, the information required to reconstruct the analytical precision for each element is seldom (if ever) reported. Ideally, authors would report the software-calculated sigma values for each analysis, which uses the number of counts on the peak and background of a specific EPMA spot to estimate the uncertainty related to counting statistics (Equation 4). Alternatively,

more approximate estimates of error can be calculated from Equations 2–3, but this requires knowledge of the counts on the primary calibration standards, as well as the beam current and count times used for each element. We were unable to find any relevant experimental papers reporting software-calculated errors or sufficient information to use Equations 2–4. However, we were able to obtain software-calculated precisions upon request from the authors for a subset of experimental Cpx analyses from Krawczynski et al. (2012) conducted on the old MIT JEOL 733 and the newer MIT JEOL8200 (installed ~2007), and from Neave et al. (2019) on the Hannover Cameca SX100 (installed ~2001, decommissioned ~2021). We supplement these estimates with precision from natural pyroxene analyses on the University of Cambridge Cameca SX100 (Gleeson et al., 2021) and secondary standard analyses for the Kakanui Augite from the Oregon State University Cameca SX100. We also obtained peak and background counts from primary standard analyses on the MIT JEOL 733 (installed in the 80s) and the Bristol JEOL JXA8530F (installed ~2012) to model precision as a function of count time and beam current.

For the following discussion, we focus on Na to highlight an element affected by analytical error that is pertinent to the majority of Cpx barometry parameterizations, because of its relationship to jadeite content. As expected, compiled analytical precisions from different EPMA systems increase in magnitude as Na_2O content decreases below 1 wt% (Fig. 6a, c), closely following the trajectory of modelled precision curves. The exact trajectory of these precision versus concentration curves depends on spectrometer efficiency (ratio of peak: background counts in a primary standard), as well as the energy of the beam (voltage, current) and the count time. As the majority of Cpx analyses are performed at 15 kV, variations in beam current and count time can be combined into a single variable, I*t (10s and 20 nA gives identical counting statistics to 20 s and 10 nA).

Using count data from the Bristol JEOL JXA8530F TAP crystal for Na on an Albite primary standard, we calculate that measurement of a Cpx with Na_2O=0.13 wt% if I*t=60 nA s has a precision of 25% (e.g., 10 s, 6 nA), while measurement if I*t=400 nA s has a precision of 9.7% (e.g, 20s, 20 nA, Fig. 6c). For the MIT JEOL 733 with a TAP crystal calibrated for Na on Albite, the precision for Na_2O=0.13 wt% is 60% for I*t=60 nA s, and 23% for I*t=400 nA s (Fig. 6a). The lower precision on the Bristol versus MIT JEOL for a given I*t value reflects the increase in detector efficiency on the newer Bristol instrument. This can also be seen by comparing the software-reported precision for the old MIT JEOL 733 (orange dots, Fig. 6a) to the newer MIT JEOL 8200 (red dots, Fig. 6a), where all other variables are kept constant (same calibration routine, same current and count times).

When information is available on both the software-reported analytical precision for each individual EPMA spot and the true phase variability observed in measured Cpx compositions within a single experimental charge, these can be compared. If variability for a specific element is dominated by analytical precision, the percentage variation calculated from multiple measurements of Cpx in that experimental charge (100*σ/Mean concentration) will be the same as the % precision value predicted from counting statistics. In contrast, if true phase variability is dominant (e.g. zoning, disequilibrium), the observed variability in measured Cpx compositions will greatly exceed the analytical precision. We were only able to obtain estimates of analytical precision for the experiments of Krawczynski et al. (2012) and Neave et al. (2019). In both sets of experiments, the analytical precision for Na_2O is very similar to the observed variability for measurements of Na_2O in Cpx (Fig. 6a, c). In contrast, the variability of Al_2O_3 in experimental Cpx greatly exceeds the analytical precision, indicating true phase variability (Fig. 6b, d). In general, variability in elements with >1 wt% concentration in the experiments of Neave et al. (2019) and Krawczynski et al. (2012) significantly exceed the analytical precision, while lower abundance elements (<1 wt%) show variability similar to

that expected from counting statistics (Fig. 6, Supporting Figs. 16–17). While the strong correlations between Al_2O_3 versus TiO_2 and Al_2O_3 versus SiO_2 in the experiments of Neave et al. (2019) are strongly indicative of sector zoning (compare Supporting Figs. 6, 11), the weaker correlations for the Krawczynski et al. (2012) data make it hard to know the exact origin of true phase heterogeneity without detailed elemental mapping of crystals (Supporting Fig. 8).

We wish to determine whether elemental variability for the other experiments in the LEPR database are similarly controlled by analytical precision for Na_2O, and true phase variability for higher concentration elements. While we cannot reconstruct the exact analytical precisions for these studies, we can use the curves calculated for the new Bristol JXA8530F and old MIT JEOL733 probes as end-member examples of detector efficiency to estimate precision for different I*t values. This approach is supported by the fact that the software-calculated Cameca SX100 errors from Hannover lie within the modelled lines for these two probes (Fig. 6c). To get an idea of common I*t values, we compile count times and beam currents from 39 randomly selected experiments in LEPR used to calibrate the Putirka (2008) and Petrelli et al. (2020) Cpx-only and Cpx-Liq expressions, as well as a number of Cpx containing experiments conducted since 2008 (see Supporting Table 1). This compilation is also hampered by insufficient reporting of analytical data. Of the 39 LEPR experimental studies, 31 stated the beam current while only 16 (~40%) gave the count time for Na_2O. The 22 experiments published since 2008 are somewhat better, with 21 providing beam current, and 14 (~60%) providing count times for Na_2O. Although incomplete, our compilation shows that I*t mostly varies between 60 and 400 nA s (Supporting Table 1). Interestingly, many papers include statements to the effect that well known or established analytical conditions were used for analysis without actually reporting what these were. The range of compiled I*t values shows that this is clearly insufficient, as there is no such thing as “normal” analytical conditions (Supporting Table 1).

When the worst-case scenario (60 nA s on the MIT JEOL733, orange line) and best-case scenario (400 nA s on the Bristol JX8530F, blue dashed line) are overlain on the reported 1 sigma values for element variability within a single experimental charge from LEPR (Fig. 6e-f), it is apparent that the majority of Cpx Na_2O variability reported within single experiments results from analytical precision. The various measures of software-reported precision we compiled for different EPMA facilities (e.g., Cambridge, OSU) lie in the middle of the cloud defined by LEPR experiments, further supporting this assertion. The small number of points that lie above the MIT JEOL733 line could be influenced by experimental scatter, or even lower spectrometer efficiency than the MIT JEOL733 (or I*t<60 nA s). In contrast to Na_2O, Al_2O_3 in LEPR experiments show significantly more variability than software-estimated precision, indicating that features such as sector zoning may be nearly ubiquitous in experimental Cpx (Fig. 6f).

Our modelling and compilations of analytical precision highlight a major issue with the way EPMA precision is being assessed and reported within the petrology community. If mentioned at all, precision is generally discussed with reference to repeated measurements of secondary standard materials (e.g., Neave et al., 2019; Waters et al., 2021). Although secondary standards are very helpful to assess accuracy and drift during an analytical session, they only provide useful insights into precision if secondary standards and samples have similar concentrations for a given element. This is a particular problem for Cpx, because the commonly used Kakanui augite secondary standard has 1.2–1.3 wt% Na_2O (Fig. 6b), whereas experimental Cpx produced at <10 kbar have median Na_2O contents of only 0.55 wt% (and most crustal Cpx have similarly low concentrations). The theoretical lines calculated for the MIT JEOL 733 show that analysis of Kakanui augite would indicate 5–10% error, but the lower Na_2O contents of crustal Cpx yield errors of up to ~40% (Fig. 6c). Thus, secondary standards must only be used to

estimate precision for elements where the standard and sample have very similar concentrations.

2.3.3. Effect of major element variability on calculated pressures

For experiments where individual Cpx measurements within a single experimental charge could be obtained, we calculate Cpx-only pressures for each reported measurement (Erdmann et al., 2016; Neave et al., 2019, Blatter et al., 2013; Krawczynski et al., 2012; Melekhova et al., 2015). Despite the fact that Cpx within a single experimental charge experienced a narrow range of pressures within their capsule, calculated pressures span up to ~ 4 kbar (Fig. 7a-e). The Cpx-only barometer of Putirka (2008) shows the widest range in most cases (red diamonds), with the barometers of Wang et al. (2021, black dots) and Petrelli et al. (2020, cyan squares) showing a slightly smaller range for a given experiment. The range of calculated pressures in a single experiment is in many cases comparable to the reported 1 sigma error on the barometer (coloured error bar). Visually, it is easy to see how this variation can lead to large reported errors on barometers if only a small number of Cpx are analysed. For example, if Neave et al. (2019) had measured just 1 Cpx, the pressure calculated using the Cpx-only barometer and thermometer of Putirka (2008, eq32a-32d) could range from ~4 to 10 kbar. In turn, when plotted against experimental pressure (3 kbar), this pressure calculation could lie 1 to 7 kbar off the 1:1 line. When all experiments in a test dataset are considered, these offsets cause very large RMSE/SEE estimates on the barometer.

However, it is still unclear from these discussions whether major elements (predominantly controlled by true phase variability) or minor elements (controlled by analytical precision) are producing this spread of calculated pressures in a single experimental charge. Qualitatively, when we plot the calculated pressures from five experiments against Na_2O for two barometers, the strong correlation between calculated pressures and Na indicates that analytical precision is a major contributor to the spread in calculated pressures (Fig. 7f).

To investigate the relative effect of analytical precision versus true phase variability more quantitatively, we use Monte Carlo simulations implemented in the Python3 thermobarometry tool Thermobar (Wieser et al., 2022b). For specific experimental charges from Krawczynski et al. (2012) and Neave et al. (2019), we create 5000 synthetic Cpx compositions with the concentration of each element distributed normally about the mean composition of the Cpx from each experiment, and the standard deviation equal to the average reported 1 sigma error from EPMA software for analyses from that experimental charge. Each major element in each of the 5000 Cpx is sampled randomly from a normal distribution. The uncoupled variations of these different oxides means that cation sums in these simulated Cpx do not lie substantially outside the distribution of cation sums in the measured Cpx (Supporting Fig. 18-19). We then calculate pressures and temperatures for these synthetic Cpx using a variety of Cpx-only barometers (Fig. 8–9). To aid visualization of the spread of simulated pressures and temperatures, we contour the results of the Monte Carlo simulations and overlay contours incorporating 67% and 95% of simulated pressures and temperatures using the Python3 tool Pyrolite (Williams et al., 2020). If analytical variability is the dominant cause of pressure-temperature variability, the Monte Carlo simulations will encompass the variability of calculated P and T for each measured Cpx composition. In contrast, if true phase variability dominates, calculated P and T for measured Cpx compositions (yellow and red dots) will plot well outside the PT region defined by the simulations (Fig. 8-9).

For experiment Y0272–1 from Neave et al. (2019), the 95% contour around the Monte Carlo simulation almost completely incorporates the spread of calculated pressures and temperatures in individual Cpx measured in that experiment for all three Cpx-only thermobarometers (yellow dots, Fig. 8a-c, see also Supporting Fig. 20). Thus, while experimental products show major element variability resulting from sector zoning (Neave et al., 2019), the dominant control on calculated pressures and temperatures results from analytical precision. For Cpx-

Liq calculations, no EPMA-estimates of glass analytical uncertainties could be obtained for Neave et al. (2019), so calculations were performed using the average glass composition paired with simulated Cpx compositions (so this calculation underestimated the true variability caused by analytical uncertainty). Despite neglecting analytical variability in the glass phase, the span of P-T in measured Cpx-Liq pairs is very similar to our Monte Carlo simulations for Putirka (2008) equation 33 for temperature, iterated with either equation 30 (Fig. 8e) or Neave and Putirka (2017) for pressure (Fig. 8e and Fig. 8d, respectively). It is noticeable on these figures that the machine-learning-based Cpx-only and Cpx-Liq thermobarometers from Petrelli et al. (2020) show significantly less spread in calculated pressures and temperatures both for measured experimental products, and our Monte Carlo simulations (Fig. 8c, 8f). However, using a different experiment, this barometer shows a much larger spread (Supporting Fig. 20), illustrating the unintuitive behaviour of regression tree machine-learning algorithms versus empirical expressions.

In the experiments of Krawczynski et al. (2012), Cpx in a single experiment have compositions such that sometimes jadeite is calculated using Na and sometimes using Al. This complicates the relationship between the spread of pressures and the analytical precision because Al is mostly affected by true phase variability (e.g., sector zoning) while Na is mostly affected by analytical precision. Our simulations do not show the same P-T extent as measured values. However, if one imagines shifting the simulation away from the mean, the spread shown by Cpx where jadeite is calculated from Na (yellow dots) is reasonably similar to the simulation, while Cpx with jadeite calculated from Al (red dots) lie well outside the Monte Carlo simulation (Fig. 9).

Overall, these comparisons indicate that apparent phase variability resulting from analytical precision alone can yield a wide range of pressures. Although analytical precision seems to dominate the spread of calculated pressures in experiments where jadeite is calculated using

Na, measuring sufficient Cpx to sufficiently average true phase variability is vital where jadeite is calculated from Al. When either source of elemental variability is insufficiently averaged by measuring a large number of Cpx, this can lead to large calculated errors for barometers. For x-y plots of calculated versus experimental pressure, the effect of measuring only a single Cpx on the y axis value is easy to visualize from Fig. 8–9.

We investigate whether insufficient averaging of analytical and/or true phase variation can explain the notable decline in the discrepancy between predicted and experimental pressure with increasing number of Cpx analyses per experiment (Fig. 4c-d). We use software-reported estimates of analytical precision from an experimental charge of Neave et al. (2019) to produce 5000 synthetic Cpx compositions. This simulates what would happen if 5000 discrete analyses were made of entirely homogenous experimental products, with variability in measured oxides resulting from counting statistics. We then calculate the composition obtained from sampling discrete numbers of Cpx (N=1 to N=100), and feed these averaged compositions into various Cpx-only barometers. We calculate the discrepancy between the calculated pressure for this averaged composition, and the pressure calculated from the mean composition of all 5000 Cpx. For each discrete number of averaged Cpx analyses, we overlay the mean discrepancy (black diamond), and the 95% quantile (yellow star) on the data (Fig. 10a-b). We repeat this process 700 times using a for loop in Python, meaning we have simulated randomly sampling one Cpx 700 different times, two Cpx 700 times, etc. A schematic showing the for loop and subsampling routine is provided in Supporting Fig. 21.

Fig. 10a-b demonstrates that when only one EPMA analysis is taken form a homogenous Cpx population, the calculated pressure can differ from the pressure calculated from the true composition by up to ±3–4 kbar for Putirka (2008, Fig. 10a) and ±2.5–3.5 kbar for Wang et al. (2021, Fig. 10b). The mean absolute discrepancy for N=1 Cpx is ±0.89 kbar for Putirka (2008) and ±0.55 kbar for Wang et al. (2021, blue stars), while the 95% quantile is ±2.09 kbar for

Putirka (2008) and ±1.39 kbar for Wang et al. (2021, yellow stars, Fig. 10a-b). The absolute discrepancy from each experiment, the mean, and 95% quantiles decline very rapidly between N=1 and N=7 Cpx. When >7 Cpx are averaged, there are very few experiments >1.5 kbar from the mean value calculated from all 5000 Cpx, and very few individual experiments >1 kbar (~5%). However, it must be remembered that we are only simulating analytical uncertainty; analyses will also be affected by true heterogeneity in experimental products.

To investigate the combined effect of analytical and experimental variability (i.e., the measured variability in a given experiment), we repeatedly resample the 18 reported Cpx from experiment B1038 of Krawczynski et al. (2012), averaging different numbers of measured Cpx compositions to create a theoretical "average" composition (see supporting Fig. 22 for a schematic of this loop). For N=1 Cpx, the mean offsets reach ~2 kbar, with 95% quantiles of ~4–5 kbar (Fig. 10c-d).

We also consider the effect of sampling on Cpx-Liq barometry, using individual measurements of experimental Cpx and glass from experiment B1038 from Krawczynski et al. (2012). First, we match up all possible pairs of measured experimental Cpx and Liq (N=360 pairs). Each pass through the loop, we randomly select 10 Liq which have been paired with a given Cpx, and calculate an average Liq composition. We then consider averaging different numbers of Cpx paired with these average Liq compositions (see Supporting Fig. 23 for schematic of this loop). This approach of using average liquid compositions means we are only investigating the effect of how many Cpx analyses are averaged, because there is no clear correlation in between number of Cpx and Liq analyses per experiment in our compiled dataset. Depending on the choice of barometer, mean offsets decline rapidly with increasing N from ~± 2 kbar for N=1 Cpx, with a 95% quantile of ~± 4–5 kbar (Fig. 10e-f).

Importantly, the large offsets for N=2–4 Cpx highlight a particular problem that can arise when measuring only a small number of Cpx. Specifically, when a Cpx has Na-Al contents such that the jadeite content is zero, averaging the composition of that Cpx with a second Cpx with Jd>0 can result in a very low (but non-zero) jadeite content. While Jd=0 will return a NaN for pressure (not a number), because most Cpx-Liq thermobarometers contain a log term involving the jadeite content (and log(0) = NaN), the log of a very low but non-zero jadeite content produces a very large negative number, yielding an anomalous pressure (see Supporting Information Fig. 24).

Our simulations (Fig. 10) demonstrate that insufficient EPMA analyses to characterize the true composition of experimental phases can account for the observation that experiments characterized by a small number of analyses can show large discrepancies between calculated and experimental pressures (Fig 4c-d). Most simply, imagine that barometers perfectly predict the relationship between composition and pressure. Even in this perfect scenario, measuring a small number of Cpx (± Liq) in each experiment can result in the measured composition not being representative of the true composition, resulting in offsets between calculated and experimental pressures. Of course, in some cases, a single measurement will obtain the correct value (i.e. sampling the mean of the normal distribution by fluke), accounting for the fact that some experiments analysing a small number of Cpx show small offsets on Fig 4 and 10. However, the smaller the number of Cpx analyses performed, the more likely it is that the composition of the Cpx obtained differs from the true composition. In reality, barometers are not perfectly accurate, which explains why there are still offsets between calculated and experimental pressure even when larger numbers of Cpx are analysed.

The y axis in these subsampling simulations represents the distance a single experiment may lie from the 1:1 line in a plot of experimental pressure versus calculated pressure, simply because of insufficient averaging of analytical and experimental variability. Given that ~43%

of experiments we have compiled performed ≤5 Cpx analyses per experiment, even if barometers perfectly recreate the relationship between pressure and temperature for the true composition of Cpx and Cpx-Liq pairs from that experiment, we would expect scatter about a 1:1 line of ~± 2–3 kbar based on insufficient averaging. In reality, the scatter off the 1:1 line will be larger than this, because insufficient averaging of experimental products affects the calibration of barometers, as well as the assessment of these barometers using test datasets. Thus, we suggest that insufficient averaging of analytical precision (with a contribution from true phase variability) is the ultimate reason barometers have SEE of ~2–4 kbar when applied to global test datasets, regardless of the exact calibration strategy.

2.4. Implications for thermobarometry on natural systems

The Monte Carlo simulations of calculated pressures and temperatures resulting from analytical uncertainty alone shown in Figures 7–8 for Cpx and Cpx-Liq are equally applicable to natural systems. Namely, even if erupted Cpx are entirely homogenous and come from a single magma storage region at a single pressure and temperature, calculated pressures may span ~4 kbar using Cpx-only thermobarometry, and ~6 kbar using Cpx-Liq thermobarometry simply resulting from analytical precision (assuming analytical conditions similar to those used by Neave et al., 2019 and Krawczynski et al., 2012, i.e., 100–150 nA s). When plotted in pressure-temperature space, completely random, normally distributed analytical error produces a strongly correlated pressure-temperature array (Fig. 8–9). It is crucial to recognise that a wide spread of pressures calculated for a natural system using popular Cpx-only and Cpx-Liq barometers should not automatically be interpreted as representing magma storage across a broad region of the crust (i.e., transcrustal magma storage). Rather it should be assumed that this an artifact of analytical uncertainty until proven otherwise. Specifically, Monte Carlo simulations with errors determined from software-calculated analytical uncertainty (rather than secondary standards) should be used to calculate the spread in pressures and temperatures that

result from analytical precision. If the spread of pressures and temperatures from natural samples exceeds the simulated spread (and even if it does not), the role of P-T spread resulting from sector zoning and other disequilibrium features should also be investigated (e.g., Hammer et al., 2016). True transcrustal storage should only be invoked after ruling out these null hypotheses.

Although the overall structure of pressure and temperature estimates should certainly be considered, averages of many individual measurements help to eliminate analytical and true phase variability. For example, Putirka et al. (1996) showed that the fit between calculated and experimental pressures are substantially improved when all experiments conducted at a given pressure are averaged, rather than considered individually (compare their Fig. 3a and Fig 4a). To avoid averaging out true variations in magma storage conditions, it may be best to perform and average multiple analyses within the core and rim of any given Cpx (e.g., Klügel et al., 2005).

3. SUMMARY AND FUTURE DIRECTIONS

There is broad consensus that improved methods for estimating the pressures of igneous processes and magma storage is vital to advance the field of igneous petrology (Hilley et al., 2022; McGuire et al., 2017). In the preceding sections we have highlighted a number of sources of uncertainty affecting Cpx-only and Cpx-Liq barometry, which are two of the most popular barometry tools. We show that insufficient averaging of measurements made with low analytical precision, combined with heterogeneity in experimental products, and interlaboratory offsets fundamentally limit the precision of Cpx-based barometric estimates to ±2–4 kbar for crustal Cpx. Below, we highlight a number of ways in which we can improve how experimental products are analysed and reported to improve the future calibration and application of Cpx-based barometers. These recommendations can be summarized as: 1)

collect more counts, 2) measure more phases in each experimental charge, 3) address interlaboratory biases and 4) better data reporting.

3.1. Can we simply collect more counts for Na in Cpx?

Our Monte Carlo simulations demonstrate that analytical precision associated with the measurement of Na_2O resulting from insufficient count times and/or beam currents is a major source of uncertainty affecting Cpx-only and Cpx-Liq barometry. Poor precision affects the experimental data used for barometer calibration and testing, as well as calculations of pressure in natural sample suites. Many papers suggest that they are using such short analysis times and low beam currents because of fears of Na migration (e.g., Neave et al., 2019). Although beam migration is a clear concern in hydrous glasses and Na-rich feldspars, to our knowledge there are no reports of Na migration within crustal pyroxenes.

To investigate the beam sensitivity of pyroxene, we perform tests of Na mobility during analysis at 15 kV, and 20, 40 and 100 nA using a 1 µm spot on the Oregon State Cameca SX100. We track changes in peak intensity, and calculated Na concentrations using typical analytical routines for a Na-rich end-member jadeite (~7.1 wt% Na_2O) and a Kakanui Augite with lower Na contents (~1.2 wt% Na_2O), as well as a hydrous rhyolite glass for comparison.

Peak intensities in the hydrous rhyolite glass show a rapid decrease with increasing exposure, even at 20 nA, as is widely documented (e.g., Morgan and London, 2005, Fig. 11a, black triangles). The jadeite is significantly less beam-sensitive, with peak counts only decreasing by 15-20% after ~ 5 minutes (and only at 40 and 100 nA, Fig. 11a-b). In contrast, we see no evidence for a decrease in Na peak intensities collected on the Kakanui augite even at 100 nA over ~6 minutes (Fig. 11b).

We also perform 6 repeated analyses at 100 nA at the same stage position on the jadeite and Kakanui augite, with a total beam-on time of ~60 s per analysis. Peak count times were Na (3.3 s), Ca (10 s), Al (10 s), Si (10 s) and Ti (10 s). We plot the concentration of each element quantified from the peak and background against the average beam-on time for each analysis. For the jadeite, the concentration of Na_2O declines reasonably coherently by ~10% after ~6 minutes of beam exposure (Fig. 11c). For the Kakanui Augite there is no coherent decrease in Na_2O, with concentrations varying well within the expected threshold given the low count time (Fig. 11d). Further details of additional tests are provided in the supporting information (Supporting Figs. S25-30). Overall, we conclude that in pyroxenes with relatively low Na_2O contents, there is no need to restrict count times or beam currents, as Na migration seems negligible.

Given the lack of measurable Na migration in natural Cpx, we suggest that the simplest way to increase precision on reported Na in future experiments and natural samples is a combination of longer count times and/or a higher beam current during Cpx analyses. Increasing the count time at a specific beam current is the best strategy if the interaction volume needs to be minimised (e.g., for analyses of small experimental products), while increasing the beam time and current together is most efficient if a tiny interaction volume is not critical.

In many analytical routines, increasing the count time on Na will not increase the total analytical time if other spectrometers are already counting minor elements for longer (e.g., Cr and Mn on the LIF). Additionally, in a number of studies, Na and Al are both being measured on the TAP or LTAP (e.g., Hammer et al., 2016; Krawczynski et al., 2012; McCane, 2022; Wieser et al., 2022a), with Al being counted significantly longer than Na, despite its higher

concentration in Cpx. If total analytical time is an issue, count times can be adjusted on the TAP/LTAP to count for longer on Na instead.

Although they have great utility for assessing accuracy and drift, secondary standards should only be used to assess precision if the standard has a very similar elemental concentration to the analyte. If elements are present in lower concentrations in natural samples, software-calculated precisions should be used to assess uncertainties resulting from counting statistics. Overall, we suggest that users optimize their EPMA acquisition parameters to achieve <5% precision for the range of Na_2O contents found in their samples.

3.2. Perform more measurements in each experimental charge.

Analytical noise is particularly problematic for calibration datasets if only a small number of Cpx in each experiment are measured. The large number of experiments performing <5 individual Cpx measurements, combined with low precision on Na_2O measurements, explains why no Cpx-based barometers can predict pressure in a global dataset of experiments with errors smaller than ±2–5 kbar (despite many different calibration strategies). Even if analytical precision is improved by increasing the number of counts, performing multiple Cpx analyses remains vital to minimize the effects of experimental heterogeneity (e.g., sector zoning, Neave et al. 2019). This is particularly true if jadeite is calculated from Al, or when using Cpx-Liq barometers relying on Al content (e.g., eq32c, Putirka, 2008) as Al and other major elements in Cpx and glass are influenced more by true experimental phase variability than analytical uncertainty.

3.3. Quantify and resolve interlaboratory offsets for glasses and silicate minerals

Even if analytical conditions are optimized to make measurements more precise, and a larger number of products are measured in each experiment, interlaboratory offsets may still introduce random, or even systematic offsets into barometry calibrations. To properly resolve the extent

of interlaboratory biases, we suggest that mineral round-robins are conducted on the current generation of EPMAs at institutions which are contributing a significant amount of experimental data (and ideally between all laboratories). Such round-robins will be vital to determine whether our assumption that mineral offsets may be as large as offsets measured for glasses is correct. It may be that by applying such corrections, more precise barometry calibrations can be obtained.

Longer-term, it is not practical to rely on large round-robins among all possible EPMA labs that may wish to perform mineral-melt barometry on natural samples, or conduct experiments used to calibrate these expressions. These interlaboratory biases highlight the need for the development of a new generation of homogenous reference materials to replace the heterogeneous NMNH standards. One recent suggestion, put forward in an open letter to the microanalysis community with over 90 co-signers (https://probesoftware.com/smf/index.php?topic=1415.0), is to create a global reference set of high purity, stoichiometric end-member synthetic compositional standards in approximately 500 to 1000 gram quantities. This would ensure that every e-beam microanalysis laboratory in the world could readily obtain sufficient material to last decades of polishing, use, re-polishing and re-use. Even better, such synthetic standard materials can always be reproduced in the future as necessary, since they would be selected such that their synthesis would be well-constrained by both purity and thermodynamics. These efforts are being formalized within the focused interest group microanalytical standards (FIGMAS) committee of the Microbeam Analysis Society (https://the-mas.org/about-us/focused-interest-group-figmas/).

3.4. Better reporting of compositional, analytical and metadata

It may be possible to improve barometry calibrations by excluding experiments with numbers of analyses below a certain threshold, or experiments where phases were only briefly characterized to identify phase occurrence, rather than to provide reliable phase compositions.

At a minimum, filtering based on numbers of analyses will require this information to be copied over from pdf tables in papers and entered into the LEPR dataset. However, to evaluate analytical noise within a single experiment rigorously, we also need an estimate of the analytical precision. For example, it may be more rigorous to include an experiment where only two Cpx were measured but at high precision (e.g., Na = 10%) versus an experiment with five Cpx with low analytical precision (e.g., Na = 50%, Fig. 6b). However, this information cannot be obtained for the majority of the LEPR database, particularly as many of the EPMA instruments used for these measurements have been decommissioned.

Thus, for future experimental work, we suggest that authors report the following information:

1. The beam current, voltage, crystal, primary calibration material, and peak and background count times for every element.
2. The software-calculated 1 sigma value for each analysis.
3. The elemental data for every spot analysis of every phase in each experimental charge and every natural mineral analysis, rather than providing a mean composition and standard deviation.
4. Detailed information on how thermal gradients were assessed, and any friction corrections.

Providing this information will allow future attempts at calibrating barometers to better filter the underlying data. We also encourage authors to think carefully about the influence of minor elements such as Cr on Cpx phase stability (Voigt et al., 2017) and to carefully report whether an attempt was made to measure an element but it was below the detection limit, or whether no measurement attempt was made. If an element was below detection limit, and an estimate of the detection limit is provided, the number can be more reliably imputed than when no information is given.

3.5. Remeasure existing experimental products

We recognise that experimental studies are seldom performed with the sole aim of calibrating thermobarometers. Instead, the authors may have simply wanted to constrain a phase diagram, so only a small number of Cpx were analysed in each experiment to confirm phase occurrence, and there was no reason for analytical conditions to be optimized for low concentration components like Na_2O, or to measure all elements (e.g., Cr_2O_3 in Cpx and glass). Although it will require a significant community effort to find and share the experimental charges, this is likely much less effort than redoing experiments from scratch, and it would be worthwhile to reanalyse a large proportion of the experimental charges compiled in LEPR. This would take advantage of the higher precision of modern EPMA instruments (compare the precision of the old and new MIT JEOL on Fig. 6c) and help to fill in the large amount of missing data in LEPR (Cr_2O_3, H_2O, P_2O_5 etc). Ideally, reanalysis would take place on a single EPMA instrument, or on a set of instruments where secondary standards are exchanged to correct for interlaboratory biases.

5. CONCLUSIONS

In their current state, Cpx-based barometers struggle to precisely and accurately constrain the location of magma storage in the crust (with errors of ±2–5 kbar, ~±8–11 km), In addition to fundamental thermodynamic limitations, we suggest that the poor performance of barometers results from the fact that the true composition of Cpx in experiments has not been precisely determined, because insufficient analyses were conducted to average out low analytical precision and true phase variability. Calibrating and testing Cpx-based barometers has been further hindered by interlaboratory offsets during EPMA analyses, and large amounts of missing elemental data reported by experimental studies. We suggest that pressures calculated from individual Cpx analyses in both experiments and natural samples must be evaluated in the context of the expected range of pressures obtained from the propagation of analytical

errors for that specific study. To invoke true transcrustal storage, it must be demonstrated that the range of calculated pressures greatly exceeds that expected from analytical precision alone.

We believe a new generation of more precise barometers could be calibrated through a community effort to obtain an experimental dataset which properly averages analytical imprecision (for low concentration elements such as Na_2O) and true phase variability (e.g., Al_2O_3 concentrations affected by sector zoning). There is growing recognition in the Machine Learning community that big data are not as important as good data. In a recent interview (2022), Machine Learning expert Andrew Ng states "In many industries where giant datasets simply do not exist, I think the focus has to shift from big data to good data." We suggest that the same reasoning should be applied to petrological thermobarometers. Ideally, an independent high quality test dataset would be isolated during model calibration and tuning to allow robust estimates of the precision that can be expected when these methods are applied to "unknown" samples. Improving Cpx-based barometers is vital for reliable interpretation of a volcanic plumbing system geometry (e.g., distinguishing between a single reservoir, discrete reservoirs, and true transcrustal magmatic systems).

6. DATA AND CODE AVAILABILITY

Jupyter Notebooks used to produce figures 2 to 11 in this paper are available on Penny Wieser's Github. https://github.com/PennyWieser/BarometersBehavingBadly_Wieser2022. Upon final acceptance version of this will be archived on Zenodo.

- Supporting_Data_1.xlsx –Contains Interlaboratory offsets from Gale et al. (2013), the Cpx calibration dataset used by Keith Putirka which we use to examine the prevalence of missing data, and the compilation of Cpx-Liq experiments used in this study (i.e. ArcPL).
- Supporting_Data_2.xlsx – Analysis of individual phases from the experiments of Krawczynski et al. (2012).

- Supporting_Data_3.xlsx – Estimates of analytical precision from a subset of experimental analyses by Krawczynski et al. (2012),
- Supporting_Data_4.xlsx –All Cpx-bearing experiments from the LEPR (downloaded in 2021).
- Supporting_Data_5.xlsx – Analysis of individual phases from the experiments of Neave et al. (2019).
- Supporting_Data_6.xlsx – Analysis of individual phases from the experiments of Erdmann et al. (2016), from their supporting information
- Supporting_Data_7.xlsx – Analysis of individual phases from the experiments of Melekhova et al. (2015).
- Supporting_Data_8.xlsx – Analysis of individual phases from the experiments of Waters et al. (2021).
- Supporting_Data_9.xlsx – Analysis of individual phases from the experiments of Blatter et al. (2013)
- Supporting_Data_9.xlsx – Analysis of individual phases from the experiments of Blatter et al. (2013)
- Supporting_Data_10.xlsx – Investigation of Na migration on the OSU SX100

ACKNOWLEDGEMENTS

PW thanks Keith Putirka for very helpful conversations regarding the calibration of his thermobarometers, Marie Takach and Frank Tepley for help investigating Na migration, Elena Melekhova for sharing her raw experimental data, Matthew Gleeson for sharing his software-calculated errors, and the NERC funded electron microprobe course held in Bristol in 2017 and the UK A Level physics curriculum for inspiring this manuscript (along with many hours spent on the Cambridge EPMA with Iris Buisman). We thank Ben Buse for sharing his spreadsheet for calculating analytical precision for different analytical conditions from the Bristol EPMA.

We thank Keith Putirka, Emily Johnson, two anonymous reviewers, and editorial handling from Madeleine Humphries for very helpful comments that greatly improved the manuscript. DAN acknowledges help from Renat Almeev and Andreas Klügel in digging out old datasets and support from a NERC Independent Research Fellowship (NE/T011106/1). PW, AK and CT acknowledge support from a National Science Foundation Grant 1948862, and start up funds from UC Berkeley to PW. Any use of trade, firm, or product names is for descriptive purposes only and does not imply endorsement by the U.S. Government.

REFERENCES

Akella, J., Kennedy, G.C., 1971. Melting of gold, silver, and copper-proposal for a new high-pressure calibration scale. J. Geophys. Res. 76, 4969–4977. https://doi.org/10.1029/JB076i020p04969

Almeev, R.R., Holtz, F., Ariskin, A.A., Kimura, J.-I., 2013. Storage conditions of Bezymianny Volcano parental magmas: results of phase equilibria experiments at 100 and 700 MPa. Contrib Mineral Petrol 166, 1389–1414. https://doi.org/10.1007/s00410-013-0934-x

Alonso-Perez, R., Müntener, O., Ulmer, P., 2009. Igneous garnet and amphibole fractionation in the roots of island arcs: experimental constraints on andesitic liquids. Contrib Mineral Petrol 157, 541–558. https://doi.org/10.1007/s00410-008-0351-8

Andújar, J., Scaillet, B., Pichavant, M., Druitt, T.H., 2015. Differentiation Conditions of a Basaltic Magma from Santorini, and its Bearing on the Production of Andesite in Arc Settings. Journal of Petrology 56, 765–794. https://doi.org/10.1093/petrology/egv016

Bacon, C.R., Carmichael, I.S.E., 1973. Stages in the P-T path of ascending basalt magma: An example from San Quintin, Baja California. Contr. Mineral. and Petrol. 41, 1–22. https://doi.org/10.1007/BF00377648

Baker, D.R., Eggler, D.H., 1987. Compositions of anhydrous and hydrous melts coexisting with plagioclase, augite, and olivine or low-Ca pyrxene from 1 atm to 8 kbar: Application to the Aleutian volcanic center of Atka. American Mineralogist 72.

Bartels, K.S., Kinzler, R.J., Grove, T.L., 1991. High pressure phase relations of primitive high-alumina basalts from Medicine Lake volcano, northern California. Contr. Mineral. and Petrol. 108, 253–270. https://doi.org/10.1007/BF00285935

Behrens, H., Meyer, M., Holtz, F., Benne, D., Nowak, M., 2001. The effect of alkali ionic radius, temperature, and pressure on the solubility of water in MAlSi3O8 melts (M=Li, Na, K, Rb). Chemical Geology 174, 275–289. https://doi.org/10.1016/S0009-2541(00)00320-X

Bell, S., 2001. Good Practice Guide No. 11, The Beginners guide to the uncertainty of measurement. National Physics Laboratory.

Berndt, J., 2004. An Experimental Investigation of the Influence of Water and Oxygen Fugacity on Differentiation of MORB at 200 MPa. Journal of Petrology 46, 135–167. https://doi.org/10.1093/petrology/egh066

Blatter, D.L., Sisson, T.W., Hankins, W.B., 2017. Voluminous arc dacites as amphibole reaction-boundary liquids. Contrib Mineral Petrol 172, 27. https://doi.org/10.1007/s00410-017-1340-6

Blatter, D.L., Sisson, T.W., Hankins, W.B., 2013. Crystallization of oxidized, moderately hydrous arc basalt at mid- to lower-crustal pressures: implications for andesite genesis. Contrib Mineral Petrol 166, 861–886. https://doi.org/10.1007/s00410-013-0920-3

Bogaerts, M., Scaillet, B., Auwera, J.V., 2006. Phase Equilibria of the Lyngdal Granodiorite (Norway): Implications for the Origin of Metaluminous Ferroan Granitoids. Journal of Petrology 47, 2405–2431. https://doi.org/10.1093/petrology/egl049

Bohlen, S.R., Boettcher, A.L., 1982. The quartz ⇆ coesite transformation: A precise determination and the effects of other components. J. Geophys. Res. 87, 7073–7078. https://doi.org/10.1029/JB087iB08p07073

Bohlen, S.R., Essene, E.J., Boettcher, A.L., 1980. Reinvestigation and application of olivine-quartz-orthopyroxene barometry. Earth and Planetary Science Letters 47, 1–10. https://doi.org/10.1016/0012-821X(80)90098-9

Botcharnikov, R.E., Koepke, J., Holtz, F., McCammon, C., Wilke, M., 2005. The effect of water activity on the oxidation and structural state of Fe in a ferro-basaltic melt. Geochimica et Cosmochimica Acta 69, 5071–5085. https://doi.org/10.1016/j.gca.2005.04.023

Brown, W.L., Parsons, I., 1981. Towards a more practical two-feldspar geothermometer. Contr. Mineral. and Petrol. 76, 369–377. https://doi.org/10.1007/BF00371478

Brugman, K., Phillips, M.G., Till, C.B., 2021. Experimental Determination of Mantle Solidi and Melt Compositions for Two Likely Rocky Exoplanet Compositions. JGR Planets 126. https://doi.org/10.1029/2020JE006731

Cadoux, A., Scaillet, B., Druitt, T.H., Deloule, E., 2014. Magma Storage Conditions of Large Plinian Eruptions of Santorini Volcano (Greece). Journal of Petrology 55, 1129–1171. https://doi.org/10.1093/petrology/egu021

Condamine, P., Tournier, S., Charlier, B., Médard, E., Triantafyllou, A., Dalou, C., Tissandier, L., Lequin, D., Cartier, C., Füri, E., Burnard, P.G., Demouchy, S., Marrocchi, Y., 2022. Influence of intensive parameters and assemblies on friction evolution during piston-cylinder experiments. American Mineralogist 107, 1575–1581. https://doi.org/10.2138/am-2022-7958

Costa, F., 2004. Petrological and Experimental Constraints on the Pre-eruption Conditions of Holocene Dacite from Volcan San Pedro (36 S, Chilean Andes) and the Importance of Sulphur in Silicic Subduction-related Magmas. Journal of Petrology 45, 855–881. https://doi.org/10.1093/petrology/egg114

Di Carlo, I., 2006. Experimental Crystallization of a High-K Arc Basalt: the Golden Pumice, Stromboli Volcano (Italy). Journal of Petrology 47, 1317–1343. https://doi.org/10.1093/petrology/egl011

Draper, D.S., Johnston, A.D., 1992. Anhydrous PT phase relations of an Aleutian high-MgO basalt: an investigation of the role of olivine-liquid reaction in the generation of arc high-alumina basalts. Contr. Mineral. and Petrol. 112, 501–519. https://doi.org/10.1007/BF00310781

Emmanuel, T., Maupong, T., Mpoeleng, D., Semong, T., Mphago, B., Tabona, O., 2021. A survey on missing data in machine learning. J Big Data 8, 140. https://doi.org/10.1186/s40537-021-00516-9

Erdmann, M., Koepke, J., 2016. Silica-rich lavas in the oceanic crust: experimental evidence for fractional crystallization under low water activity. Contrib Mineral Petrol 171, 83. https://doi.org/10.1007/s00410-016-1294-0

Erdmann, S., Martel, C., Pichavant, M., Bourdier, J.-L., Champallier, R., Komorowski, J.-C., Cholik, N., 2016. Constraints from Phase Equilibrium Experiments on Pre-eruptive Storage Conditions in Mixed Magma Systems: a Case Study on Crystal-rich Basaltic Andesites from Mount Merapi, Indonesia. J. Petrology 57, 535–560. https://doi.org/10.1093/petrology/egw019

Feig, S.T., Koepke, J., Snow, J.E., 2010. Effect of oxygen fugacity and water on phase equilibria of a hydrous tholeiitic basalt. Contrib Mineral Petrol 160, 551–568. https://doi.org/10.1007/s00410-010-0493-3

Firth, C., Adam, J., Turner, S., Rushmer, T., Brens, R., Green, T.H., Erdmann, S., O'Neill, H., 2019. Experimental constraints on the differentiation of low-alkali magmas beneath the Tonga arc:

Implications for the origin of arc tholeiites. Lithos 344–345, 440–451. https://doi.org/10.1016/j.lithos.2019.07.008

Fournelle, J., 2012. Complications with Using Natural Minerals as Microbeam Standards: Pyroxenes. Presented at the American Geophysical Union, Fall Meeting 2012, abstract id. V23C-2827.

Gaetani, G.A., Grove, T.L., 1998. The influence of water on melting of mantle peridotite. Contributions to Mineralogy and Petrology 131, 323–346. https://doi.org/10.1007/s004100050396

Gale, A., Dalton, C.A., Langmuir, C.H., Su, Y., Schilling, J.-G., 2013. The mean composition of ocean ridge basalts: MEAN MORB. Geochem. Geophys. Geosyst. 14, 489–518. https://doi.org/10.1029/2012GC004334

Gleeson, M.L.M., Gibson, S.A., Stock, M.J., 2021. Upper Mantle Mush Zones beneath Low Melt Flux Ocean Island Volcanoes: Insights from Isla Floreana, Galápagos. Journal of Petrology 61, egaa094. https://doi.org/10.1093/petrology/egaa094

Grove, T.L., Elkins-Tanton, L.T., Parman, S.W., Chatterjee, N., M﹟ntener, O., Gaetani, G.A., 2003. Fractional crystallization and mantle-melting controls on calc-alkaline differentiation trends. Contributions to Mineralogy and Petrology 145, 515–533. https://doi.org/10.1007/s00410-003-0448-z

Hamada, M., Fujii, T., 2008. Experimental constraints on the effects of pressure and H2O on the fractional crystallization of high-Mg island arc basalt. Contrib Mineral Petrol 155, 767–790. https://doi.org/10.1007/s00410-007-0269-6

Hammer, J., Jacob, S., Welsch, B., Hellebrand, E., Sinton, J., 2016. Clinopyroxene in postshield Haleakala ankaramite: 1. Efficacy of thermobarometry. Contrib Mineral Petrol 171, 7. https://doi.org/10.1007/s00410-015-1212-x

Harlow, G.E., 1997. K in clinopyroxene at high pressure and temperature; an experimental study. American Mineralogist 82, 259–269. https://doi.org/10.2138/am-1997-3-403

Hart, S.R., Dunn, T., 1993. Experimental cpx/melt partitioning of 24 trace elements. Contr. Mineral. and Petrol. 113, 1–8. https://doi.org/10.1007/BF00320827

Hays, J., 1966. Lime-alumina-silica. Carnegie Inst Washington Yearbook 65.

Higgins, O., Sheldrake, T., Caricchi, L., 2022. Machine learning thermobarometry and chemometry using amphibole and clinopyroxene: a window into the roots of an arc volcano (Mount Liamuiga, Saint Kitts). Contrib Mineral Petrol 177, 10. https://doi.org/10.1007/s00410-021-01874-6

Hilley, G., 2022. SZ4D Implementation Plan. Stanford Digital Repository. https://doi.org/10.25740/HY589FC7561

Hughes, E.C., Buse, B., Kearns, S.L., Blundy, J.D., Kilgour, G., Mader, H.M., 2019. Low analytical totals in EPMA of hydrous silicate glass due to sub-surface charging: Obtaining accurate volatiles by difference. Chemical Geology 505, 48–56. https://doi.org/10.1016/j.chemgeo.2018.11.015

Hunt, J., Clift, P., Lacasse, C., Vallier, T., Werner, R., 1998. INTERLABORATORY COMPARISON OF ELECTRON PROBE MICROANALYSIS OF GLASS GEOCHEMISTRY. Proceedings of the Ocean Drilling Program, Scientific Results, Vol. 152.

Husen, A., Almeev, R.R., Holtz, F., 2016. The Effect of H2O and Pressure on Multiple Saturation and Liquid Lines of Descent in Basalt from the Shatsky Rise. Journal of Petrology 57, 309–344. https://doi.org/10.1093/petrology/egw008

Jarosewich, E., 2002. Smithsonian Microbeam Standards. J. Res. Natl. Inst. Stand. Technol. 107, 681. https://doi.org/10.6028/jres.107.054

Jarosewich, E., Nelen, J.A., Norberg, J.A., 1980. Reference Samples for Electron Microprobe Analysis*. Geostandards and Geoanalytical Research 4, 43–47. https://doi.org/10.1111/j.1751-908X.1980.tb00273.x

Johannes, W., Bell, P.M., Mao, H.K., Boettcher, A.L., Chipman, D.W., Hays, J.F., Newton, R.C., Seifert, F., 1971. An interlaboratory comparison of piston-cylinder pressure calibration using the

albite-breakdown reaction. Contr. Mineral. and Petrol. 32, 24–38. https://doi.org/10.1007/BF00372231

Jorgenson, C., Higgins, O., Petrelli, M., Bégué, F., Caricchi, L., 2022. A Machine Learning-Based Approach to Clinopyroxene Thermobarometry: Model Optimization and Distribution for Use in Earth Sciences. JGR Solid Earth 127. https://doi.org/10.1029/2021JB022904

Klügel, A., Hansteen, T.H., Galipp, K., 2005. Magma storage and underplating beneath Cumbre Vieja volcano, La Palma (Canary Islands). Earth and Planetary Science Letters 236, 211–226. https://doi.org/10.1016/j.epsl.2005.04.006

Koepke, J., Botcharnikov, R.E., Natland, J.H., 2018. Crystallization of late-stage MORB under varying water activities and redox conditions: Implications for the formation of highly evolved lavas and oxide gabbro in the ocean crust. Lithos 323, 58–77. https://doi.org/10.1016/j.lithos.2018.10.001

Krawczynski, M.J., Grove, T.L., Behrens, H., 2012. Amphibole stability in primitive arc magmas: effects of temperature, H2O content, and oxygen fugacity. Contrib Mineral Petrol 164, 317–339. https://doi.org/10.1007/s00410-012-0740-x

Kuehn, S.C., Froese, D.G., Shane, P.A.R., 2011. The INTAV intercomparison of electron-beam microanalysis of glass by tephrochronology laboratories: Results and recommendations. Quaternary International 246, 19–47. https://doi.org/10.1016/j.quaint.2011.08.022

Leahy, G.M., Collins, J.A., Wolfe, C.J., Laske, G., Solomon, S.C., 2010. Underplating of the Hawaiian Swell: evidence from teleseismic receiver functions: Underplating of the Hawaiian Swell. Geophysical Journal International 183, 313–329. https://doi.org/10.1111/j.1365-246X.2010.04720.x

Lerner, A.H., Wallace, P., Shea, T., 2021. The petrologic and degassing behavior of sulfur and other magmatic volatiles from the 2018 eruption of Kīlauea, Hawai'i: melt concentrations, magma storage depths, and magma recycling. Bulletin Volcanology 83:43, 1–32.

Lindsley, D.H., Andersen, D.J., 1983. A two-pyroxene thermometer. J. Geophys. Res. 88, A887. https://doi.org/10.1029/JB088iS02p0A887

Llovet, X., Galan, G., 2003. Correction of secondary X-ray fluorescence near grain boundaries in electron microprobe analysis: Application to thermobarometry of spinel lherzolites. American Mineralogist 88, 121–130. https://doi.org/10.2138/am-2003-0115

Mandler, B.E., Donnelly-Nolan, J.M., Grove, T.L., 2014. Straddling the tholeiitic/calc-alkaline transition: the effects of modest amounts of water on magmatic differentiation at Newberry Volcano, Oregon. Contrib Mineral Petrol 168, 1066. https://doi.org/10.1007/s00410-014-1066-7

McCane, J., 2022. VARIATION IN CLINOPYROXENE TEXTURE, COMPOSITION, AND CRYSTALLIZATION DEPTH OF LATE CRETACEOUS TO EARLY EOCENE LAMPROPHYRIC ROCKS FROM ALKALINE CALC-ALKALINE MAGMATIC COMPLEXES OF MONTANA, USA. Masters of Science, Department of Geosciences, Colorado State University.

McGuire, J., Plank, T., Barrientos, S., et al, 2017. The SZ4D initiative: Understanding the processes that underlie Subduction zone hazards in 4D. A vision documnt submited to the National Science Foundation.

Melekhova, E., Blundy, J., Robertson, R., Humphreys, M.C.S., 2015. Experimental Evidence for Polybaric Differentiation of Primitive Arc Basalt beneath St. Vincent, Lesser Antilles. Journal of Petrology 56, 161–192. https://doi.org/10.1093/petrology/egu074

Mercer, C.N., Johnston, A.D., 2008. Experimental studies of the P–T–H2O near-liquidus phase relations of basaltic andesite from North Sister Volcano, High Oregon Cascades: constraints on lower-crustal mineral assemblages. Contrib Mineral Petrol 155, 571–592. https://doi.org/10.1007/s00410-007-0259-8

Morgan, G.B., London, D., 2005. Effect of current density on the electron microprobe analysis of alkali aluminosilicate glasses. American Mineralogist 90, 1131–1138. https://doi.org/10.2138/am.2005.1769

Mutch, E.J.F., Blundy, J.D., Tattitch, B.C., Cooper, F.J., Brooker, R.A., 2016. An experimental study of amphibole stability in low-pressure granitic magmas and a revised Al-in-hornblende geobarometer. Contrib Mineral Petrol 171, 85. https://doi.org/10.1007/s00410-016-1298-9

Nandedkar, R.H., Ulmer, P., Müntener, O., 2014. Fractional crystallization of primitive, hydrous arc magmas: an experimental study at 0.7 GPa. Contrib Mineral Petrol 167, 1015. https://doi.org/10.1007/s00410-014-1015-5

Neave, D.A., Bali, E., Guðfinnsson, G.H., Halldórsson, S.A., Kahl, M., Schmidt, A.-S., Holtz, F., 2019. Clinopyroxene–Liquid Equilibria and Geothermobarometry in Natural and Experimental Tholeiites: the 2014–2015 Holuhraun Eruption, Iceland. Journal of Petrology 60, 1653–1680. https://doi.org/10.1093/petrology/egz042

Neave, D.A., Putirka, K.D., 2017. A new clinopyroxene-liquid barometer, and implications for magma storage pressures under Icelandic rift zones. American Mineralogist 102, 777–794. https://doi.org/10.2138/am-2017-5968

Parat, F., Streck, M., Holtz, F., Almeev, R.R., 2014. Experimental study into the petrogenesis of crystal-rich basaltic to andesitic magmas at Arenal volcano. Contributions to Mineralogy and Petrology.

Parman, S.W., Grove, T.L., Kelley, K.A., Plank, T., 2011. Along-Arc Variations in the Pre-Eruptive H2O Contents of Mariana Arc Magmas Inferred from Fractionation Paths. Journal of Petrology 52, 257–278. https://doi.org/10.1093/petrology/egq079

Petrelli, M., Caricchi, L., Perugini, D., 2020. Machine Learning Thermo-Barometry: Application to Clinopyroxene-Bearing Magmas. J. Geophys. Res. Solid Earth 125. https://doi.org/10.1029/2020JB020130

Pichavant, M., 2002. Physical conditions, structure, and dynamics of a zoned magma chamber: Mount Pelée (Martinique, Lesser Antilles Arc). J. Geophys. Res. 107, 2093. https://doi.org/10.1029/2001JB000315

Pichavant, M., Macdonald, R., 2007. Crystallization of primitive basaltic magmas at crustal pressures and genesis of the calc-alkaline igneous suite: experimental evidence from St Vincent, Lesser Antilles arc. Contrib Mineral Petrol 154, 535–558. https://doi.org/10.1007/s00410-007-0208-6

Powell, R., Holland, T.J.B., 2008. On thermobarometry. J Metamorph Geol 26, 155–179. https://doi.org/10.1111/j.1525-1314.2007.00756.x

Profeta, L., Ducea, M.N., Chapman, J.B., Paterson, S.R., Gonzales, S.M.H., Kirsch, M., Petrescu, L., DeCelles, P.G., 2016. Quantifying crustal thickness over time in magmatic arcs. Sci Rep 5, 17786. https://doi.org/10.1038/srep17786

Putirka, K., 1999. Clinopyroxene + liquid equilibria to 100 kbar and 2450 K. Contributions to Mineralogy and Petrology 135, 151–163. https://doi.org/10.1007/s004100050503

Putirka, K., 1997. Magma transport at Hawaii: Inferences based on igneous thermobarometry. Geology 25, 69. https://doi.org/10.1130/0091-7613(1997)025<0069:MTAHIB>2.3.CO;2

Putirka, K., Johnson, M., Kinzler, R., Longhi, J., Walker, D., 1996. Thermobarometry of mafic igneous rocks based on clinopyroxene-liquid equilibria, 0-30 kbar. Contributions to Mineralogy and Petrology 123, 92–108. https://doi.org/10.1007/s004100050145

Putirka, K.D., 2008. Thermometers and Barometers for Volcanic Systems. Reviews in Mineralogy and Geochemistry 69, 61–120. https://doi.org/10.2138/rmg.2008.69.3

Pyle, D., 1999. Data Preparation for Data Mining. Morgan Kauffman, San Francisco.

Rader, E.L., Larsen, J.F., 2013. Experimental phase relations of a low MgO Aleutian basaltic andesite at XH2O = 0.7–1. Contrib Mineral Petrol 166, 1593–1611. https://doi.org/10.1007/s00410-013-0944-8

Riker, J.M., Blundy, J.D., Rust, A.C., Botcharnikov, R.E., Humphreys, M.C.S., 2015. Experimental phase equilibria of a Mount St. Helens rhyodacite: a framework for interpreting crystallization paths in degassing silicic magmas. Contrib Mineral Petrol 170, 6. https://doi.org/10.1007/s00410-015-1160-5

Rose, T.R., Sorenson, S., Post, J., 2008. The impurities in the Rockport fayalite microbeam standard: How bad are they? Presented at the American Geophysical Union, Fall Meeting 2009, abstract id. V31E-2008.

Rubin, D.B., 1976. Inference and missing data. Biometrika 63, 581–592. https://doi.org/10.1093/biomet/63.3.581

Rutherford, M.J., Sigurdsson, H., Carey, S., Davis, A., 1985. The May 18, 1980, eruption of Mount St. Helens: 1. Melt composition and experimental phase equilibria. J. Geophys. Res. 90, 2929. https://doi.org/10.1029/JB090iB04p02929

Sisson, T.W., Grove, T.L., 1993. Temperatures and H2O contents of low-MgO high-alumina basalts. Contr. Mineral. and Petrol. 113, 167–184. https://doi.org/10.1007/BF00283226

Sisson, T.W., Ratajeski, K., Hankins, W.B., Glazner, A.F., 2005. Voluminous granitic magmas from common basaltic sources. Contrib Mineral Petrol 148, 635–661. https://doi.org/10.1007/s00410-004-0632-9

Tamayama, M., Eyring, H., 1967. Study of Pressure Calibration and Pressure Distribution in a Piston-Cylinder High Pressure Press. Review of Scientific Instruments 38, 1009–1018. https://doi.org/10.1063/1.1720958

Twala, B., 2009. AN EMPIRICAL COMPARISON OF TECHNIQUES FOR HANDLING INCOMPLETE DATA USING DECISION TREES. Applied Artificial Intelligence 23, 373–405. https://doi.org/10.1080/08839510902872223

Ubide, T., Mollo, S., Zhao, J., Nazzari, M., Scarlato, P., 2019. Sector-zoned clinopyroxene as a recorder of magma history, eruption triggers, and ascent rates. Geochimica et Cosmochimica Acta 251, 265–283. https://doi.org/10.1016/j.gca.2019.02.021

Ulmer, P., Kaegi, R., Müntener, O., 2018. Experimentally Derived Intermediate to Silica-rich Arc Magmas by Fractional and Equilibrium Crystallization at 1·0 GPa: an Evaluation of Phase Relationships, Compositions, Liquid Lines of Descent and Oxygen Fugacity. Journal of Petrology 59, 11–58. https://doi.org/10.1093/petrology/egy017

Villiger, S., 2004. The Liquid Line of Descent of Anhydrous, Mantle-Derived, Tholeiitic Liquids by Fractional and Equilibrium Crystallization--an Experimental Study at 1{middle dot}0 GPa. Journal of Petrology 45, 2369–2388. https://doi.org/10.1093/petrology/egh042

Voigt, M., Coogan, L.A., von der Handt, A., 2017. Experimental investigation of the stability of clinopyroxene in mid-ocean ridge basalts: The role of Cr and Ca/Al. Lithos 274–275, 240–253. https://doi.org/10.1016/j.lithos.2017.01.003

Wang, X., Hou, T., Wang, M., Zhang, C., Zhang, Z., Pan, R., Marxer, F., Zhang, H., 2021. A new clinopyroxene thermobarometer for mafic to intermediate magmatic systems. Eur. J. Mineral. 33, 621–637. https://doi.org/10.5194/ejm-33-621-2021

Waters, L.E., Cottrell, E., Coombs, M.L., Kelley, K.A., 2021. Generation of Calc-Alkaline Magmas during Crystallization at High Oxygen Fugacity: An Experimental and Petrologic Study of Tephras from Buldir Volcano, Western Aleutian Arc, Alaska, USA. Journal of Petrology 62, egaa104. https://doi.org/10.1093/petrology/egaa104

Weill, D., Rice, J., Shaffer, M., Donovan, J.J., 2013. Electron Beam MicroAnalysis Theory and Application.

White, R.S., McKenzie, D., O'Nions, R.K., 1992. Oceanic crustal thickness from seismic measurements and rare earth element inversions. J. Geophys. Res. 97, 19683. https://doi.org/10.1029/92JB01749

Wieser, P., Petrelli, M., Lubbers, J., Wieser, E., Ozaydin, S., Kent, A., Till, C., 2022. Thermobar: An open-source Python3 tool for thermobarometry and hygrometry. Volcanica 5, 349–384. https://doi.org/10.30909/vol.05.02.349384

Wieser, Penny E., Edmonds, M., Gansecki, C., Maclennan, J., Jenner, F.E., Kunz, B., Antoshechkina, P., Trusdell, F., Lee, R.L., Eimf, 2022. Explosive Activity on Kīlauea's Lower East Rift Zone Fueled by a Volatile-Rich, Dacitic Melt. Geochem Geophys Geosyst 23. https://doi.org/10.1029/2021GC010046

Wieser, P. E., Iacovino, K., Matthews, S., Moore, G., Allison, C.M., 2022. VESIcal: 2. A Critical Approach to Volatile Solubility Modeling Using an Open-Source Python3 Engine. Earth and Space Science 9. https://doi.org/10.1029/2021EA001932

Wieser, P.E., Lamadrid, H., Maclennan, J., Edmonds, M., Matthews, S., Iacovino, K., Jenner, F.E., Gansecki, C., Trusdell, F., Lee, R.L., Ilyinskaya, E., 2021. Reconstructing Magma Storage Depths for the 2018 Kīlauean Eruption From Melt Inclusion CO_2 Contents: The Importance of Vapor Bubbles. Geochem Geophys Geosyst 22. https://doi.org/10.1029/2020GC009364

Williams, M., Schoneveld, L., Mao, Y., Klump, J., Gosses, J., Dalton, H., Bath, A., Barnes, S., 2020. pyrolite: Python for geochemistry. JOSS 5, 2314. https://doi.org/10.21105/joss.02314

Yang, H.-J., Kinzler, R.J., Grove, T.L., 1996. Experiments and models of anhydrous, basaltic olivine-plagioclase-augite saturated melts from 0.001 to 10 kbar. Contributions to Mineralogy and Petrology 124, 1–18. https://doi.org/10.1007/s004100050169

Figure Captions

Figure 1 – Schematic diagram showing the three main categories of uncertainty associated with thermobarometry.

Figure 2 – Assessing the influence of interlaboratory biases on Cpx-only and Cpx-Liq thermobarometry. a-b) Interlaboratory correction factors from Gale et al. (2013) relative to Lamont (plotting at 1, 1). c-d) Calculated Cpx-only and Cpx-Liq pressures and temperatures for the average reported composition from Experiment 41c-106 of Krawczynski et al. (2012, 4.9 kbar, 1248.15 K), corrected as if Cpx and Liq compositions were measured in different laboratories. e-f) as for c-d, using Experiment B1038 (8 kbar, 1323.15 K). Additional experiments are shown in Supplementary Figs. 2–4. Commonly stated 1σ errors for each thermobarometer are shown for comparison. The SEE for eq32b is the fit to N=1173 data, eq32d is the fit to N=910 anhydrous experiments, and eq33 is the fit to N=1174 data (all from figures in Putirka, 2008). The SEE for Neave and Putirka (2017) is that given in their abstract.

Fig. 3 – For each of the N=852 experiments in ArcPL, we calculate pressure (a-b) and temperature (c-d) using the measured Cr content (shown on the x axis), and using Cr=0 wt%. The difference between the calculation using measured Cr and Cr=0 wt% is the y coordinate. Different colors and symbols represent different thermobarometry combinations used to

calculated these pressures and temperatures. Commonly stated 1σ errors for these thermobarometer are shown for comparison. In addition to those described in the caption of Fig. 2 from Putirka (2008), eq32c is the fit to a global dataset, the SEE from Petrelli et al. (2020) are the fit to a test dataset, and the error from Putirka (1996) eqT1 is that stated in the conclusion of that paper.

Fig. 4. Number of discrete Cpx analyses performed in each experimental charges plotted against experimental pressure (a), and as a histogram with a bin width of 1 (b). (c-d) For each experimental run, we calculate the absolute difference between the pressure calculated using the Cpx-only barometers of Wang et al. (2021) and Putirka (2008) eq32d-32b and the experimental pressure. In general, experimental runs with a smaller number of Cpx analyses show the largest absolute discrepancies. Symbols are semi-transparent, so darker colors represent a tighter clustering of data. The blue stars show the mean value for each discrete number of Cpx in c and d, and for each pressure bin (0±0.5 kbar, 1±0.5 kbar etc.). The yellow stars show the 95% quantile.

Figure 5 – a) Correlation matrix showing the correlation coefficient (R^2) between different oxides in the 42 clinopyroxenes measured by Neave et al. (2019) in experiment Y0201–2, with cells colored based on this v R^2 value. b-c) 500 synthetic Cpx analyses with major elements distributed normally using the reported mean and standard deviation of the 42 clinopyroxenes measured in the experiment (yellow dots) versus measured compositions in red dots.

Figure 6 – Analytical precision as a function of Na_2O content and analytical conditions. a) Theoretical precision versus concentration curves calculated for 4 different beam conditions on the MIT JEOL733 are shown in orange. EPMA software-calculated precisions for individual

Cpx analyses are shown in red circles from Krawczynski et al. (2012) on the MIT JEOL8200 and orange circles from the older JEOL733. Phase variation/precision calculated from each experiment of Krawczynski et al. (2012, combining analyses from both probes) are shown as yellow squares. Analyses were performed with I*t =150 nA s. b) same for Al_2O_3. c) Software-calculated precision for Cpx measurements from Neave et al. (2019) on the University of Hannover SX100 (cyan dots) with phase variation overlain (blue squares). The necessary count rates to use equation 2 could not be obtained from this instrument, so we overlay curves calculated using various analytical conditions for the old MIT JEOL733 and newer Bristol JEOL JXA8530F. c) Same for Al_2O_3. Theoretical lines are not shown, as there is substantially more variation in instrument efficiency and analytical conditions between different labs for Al compared to Na (See Supporting Table 1). d-e) Experimental precision for Cpx in different experimental charges reported in the LEPR dataset are shown as grey dots. We also overlay software-calculated precisions from MIT and Hannover, as well as measurements on the University of Cambridge Cameca SX100 from Gleeson et al. (2021), and measurements of Kakanui augite on the Oregon State Cameca SX100. We overlay theoretical precision lines representing best-case (newer Bristol JEOL JXA8530F, I*t =400 nA s) and worst-case scenarios (older MIT JEOL733, I*t =60 nA s).

Fig. 7. a-e) Pressures and temperatures calculated from individual Cpx compositions from specific experiments using Cpx-only thermobarometers from Petrelli et al. (2020), Putirka (2008), and Wang et al. (2021). Error bars showing published/commonly quoted 1 sigma error each thermobarometer (see caption for Fig. 2-3). a) shows the pressures and temperatures calculated from the 42 Cpx from experiment Y0200–3 of Neave et al. (2019). The yellow star shows the P-T conditions at which the experiment was conducted. b) shows experiment BM49 from Melekhova et al. (2015), c) shows Exp CE10 from Erdmann et al. (2016), d) shows Exp

41c-110 from Krawczynski et al. (2012), and e) shows Exp2374 from Blatter et al. 2013. In f), for 3 different experiments, we show the strong correlation between Na_2O in the Cpx and calculated pressure using the Putirka (2008) barometer (diamonds) and the Wang et al. (2021) barometer (circles). Experiments showing a larger spread of Na_2O values (Neave et al. 2019, Melekhova et al. 2015) show a much wider spread of pressures than the Blatter et al. (2013) experiment.

Figure 8– Monte Carlo simulations showing the spread of Cpx-only and Cpx-Liq pressures resulting from electron microprobe-calculated analytical precision of experimental Cpx from Exp Y0272–1 of Neave et al. (2019). Measured Cpx compositions are overlain in a-c, and all possible combinations of measured Cpx and Liquids in d-e). The error bar on each plot shows the reported error on each thermobarometer, and the yellow star shows the analytical conditions. In a-b, and d-e) including experimental conditions compresses the plot, so the direction is marked with a yellow arrow. In d-f), Monte Carlo simulations show errors for Cpx and the average glass composition. Monte Carlo simulations and thermobarometry calculations performed in Thermobar, contours showing 67% and 95% of simulations calculated using Pyrolite. Supporting Fig. 20 shows the same plots for experiment B1084–10.

Figure 9 -As in Fig. 8 but for Exp B1038 from Krawczynski et al. (2012). In d-f), Monte Carlo simulations show errors for both Cpx and Glass. The 95% contour using only analytical noise for Cpx (and not glass) is shown in grey for comparison with Fig. 8 (where the analytical error on glass analyses from Neave et al. 2019 was not available).

Fig. 10 – Demonstration of the absolute pressure offset that can be introduced by measuring insufficient Cpx from any given experimental study. a-b) Groups of 1 to 100 Cpx were

randomly sampled from an underlying distribution of 5000 Cpx simulated using reported EPMA errors for the experiment of Neave et al. (2019) Y0272–1. The difference in pressure calculated for this group is compared to the average pressure calculated for all 5000 Cpx, and plotted as a single dot (see Supporting Fig. 21). c-d) To simulate the combined influence of true phase variability and analytical errors, we repeatedly resample and average the 18 measured Cpx from Krawczynski et al. (2012, see Supporting Fig. 22). e-f) Random sampling of measured Cpx-Liq pairs from Krawczynski et al. (2012, see Supporting Fig. 23). On all plots, the y axis shows the absolute discrepancy between the pressure calculated during each run through the for loop and the average pressure. In a-d), this is the average PT for the entire simulated cloud of Cpx, in e-f) it's the average for the reported mean Cpx and glass composition from the experiment). For each discrete number of Cpx, we calculate the mean (blue star) and 95% quantile (yellow star).

Fig. 11 – Investigation of Na migration. a-b) tracking the number of counts on the Na peak with increasing beam exposure on a hydrous rhyolite, a jadeite and a Kakanui augite. Polynomial fits are included through the data to help with visualization. Note the compressed y axis scale on b. c-d) Change in elemental concentration for six repeated quantitative analyses on the same location in jadeite versus Kakanui augite. The approximate beam exposure time is shown as a secondary axis (although different elements were acquired at slightly different points during each acquisition).

(a) Model Errors

Calibration range

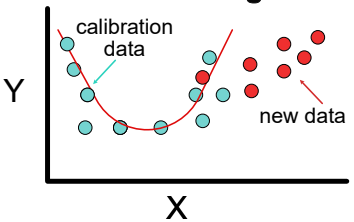

Model overfitting

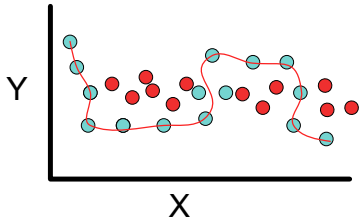

Weak relationship

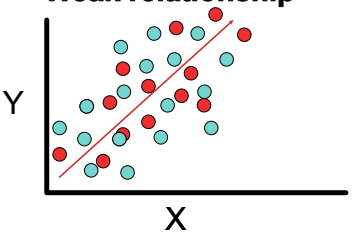

Incomplete data

SiO_2	TiO_2	H_2O		Cr_2O_3
51	2	1	...	0.4
53	1.9	6		×
47	1.8	2.6		0.03
51	2.1	×		×
56	2.3	×		0.01

(b) Analytical Errors

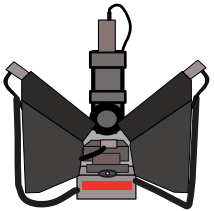

Counting Statistics

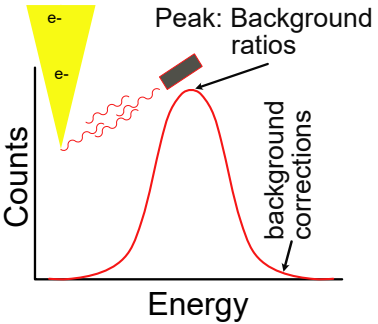

Beam Damage

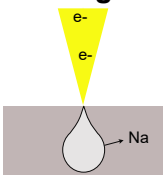

Instrument drift

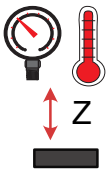

Primary standards

Variability between & within chips

Coat thickness

Different primary standards

Oxide build up

(c) Experimental Errors

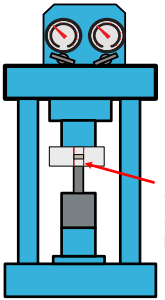

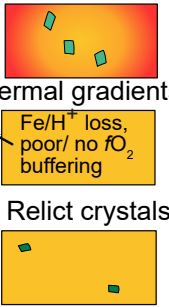

Phase Inhomogeneity

Zoning

Quench/kinetic effects

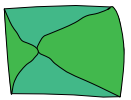

Sector zoning

Insufficient time to reach equilibrium

Missing elements vs. real systems

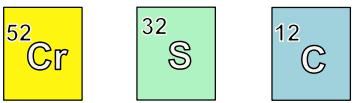

d) Combined analytical +exp issues

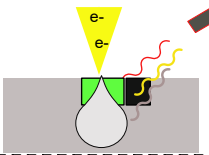

Interaction volume > phase
Secondary fluorescence

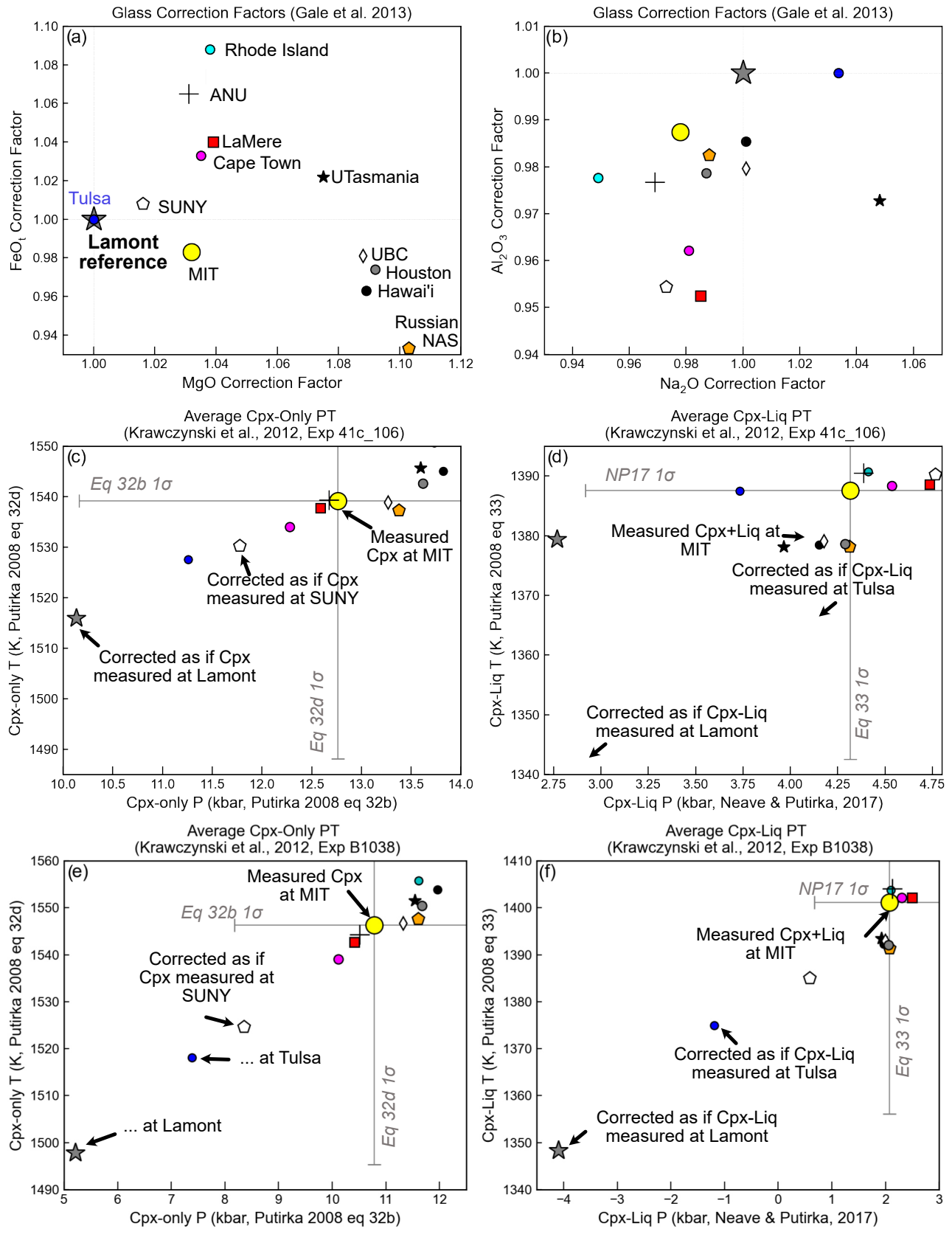
Glass Correction Factors (Gale et al. 2013)
(a)
Rhode Island
ANU
LaMere
Cape Town
UTasmania
Tulsa
SUNY
Lamont reference
MIT
UBC
Houston
Hawai'i
Russian NAS
FeO$_t$ Correction Factor
MgO Correction Factor
Glass Correction Factors (Gale et al. 2013)
(b)
Al_2O_3 Correction Factor
Na_2O Correction Factor
Average Cpx-Only PT
(Krawczynski et al., 2012, Exp 41c_106)
(c)
Eq 32b 1σ
Eq 32d 1σ
Measured Cpx at MIT
Corrected as if Cpx measured at SUNY
Corrected as if Cpx measured at Lamont
Cpx-only T (K, Putirka 2008 eq 32d)
Cpx-only P (kbar, Putirka 2008 eq 32b)
Average Cpx-Liq PT
(Krawczynski et al., 2012, Exp 41c_106)
(d)
NP17 1σ
Eq 33 1σ
Measured Cpx+Liq at MIT
Corrected as if Cpx-Liq measured at Tulsa
Corrected as if Cpx-Liq measured at Lamont
Cpx-Liq T (K, Putirka 2008 eq 33)
Cpx-Liq P (kbar, Neave & Putirka, 2017)
Average Cpx-Only PT
(Krawczynski et al., 2012, Exp B1038)
(e)
Measured Cpx at MIT
Eq 32b 1σ
Eq 32d 1σ
Corrected as if Cpx measured at SUNY
... at Tulsa
... at Lamont
Cpx-only T (K, Putirka 2008 eq 32d)
Cpx-only P (kbar, Putirka 2008 eq 32b)
Average Cpx-Liq PT
(Krawczynski et al., 2012, Exp B1038)
(f)
NP17 1σ
Eq 33 1σ
Measured Cpx+Liq at MIT
Corrected as if Cpx-Liq measured at Tulsa
Corrected as if Cpx-Liq measured at Lamont
Cpx-Liq T (K, Putirka 2008 eq 33)
Cpx-Liq P (kbar, Neave & Putirka, 2017)

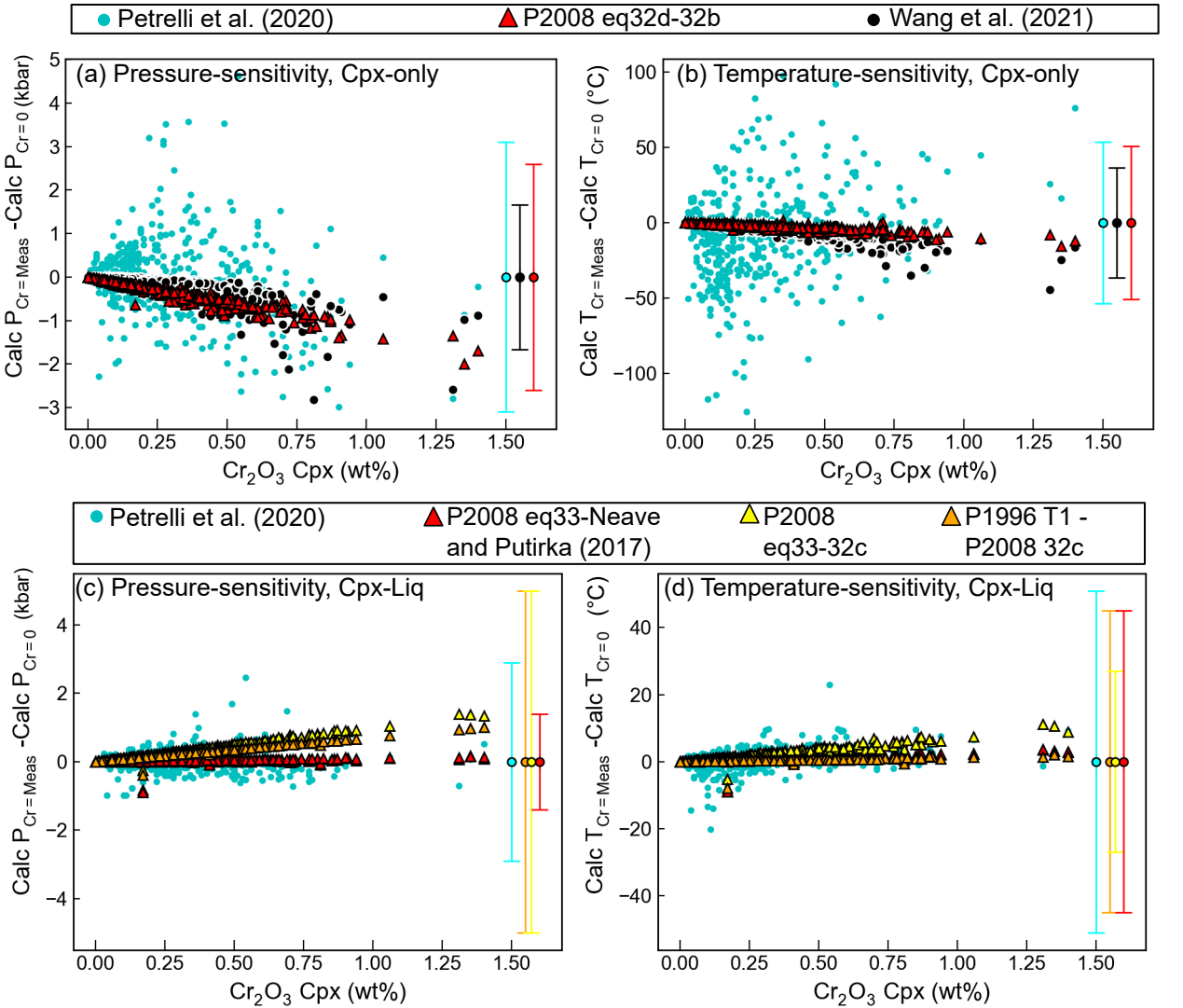
Petrelli et al. (2020)
P2008 eq32d-32b
Wang et al. (2021)
(a) Pressure-sensitivity, Cpx-only
Calc P Cr=Meas -Calc P Cr=0 (kbar)
Cr2O3 Cpx (wt%)
(b) Temperature-sensitivity, Cpx-only
Calc T Cr=Meas -Calc T Cr=0 (°C)
Cr2O3 Cpx (wt%)
Petrelli et al. (2020)
P2008 eq33-Neave and Putirka (2017)
P2008 eq33-32c
P1996 T1 - P2008 32c
(c) Pressure-sensitivity, Cpx-Liq
Calc P Cr=Meas -Calc P Cr=0 (kbar)
Cr2O3 Cpx (wt%)
(d) Temperature-sensitivity, Cpx-Liq
Calc T Cr=Meas -Calc T Cr=0 (°C)
Cr2O3 Cpx (wt%)

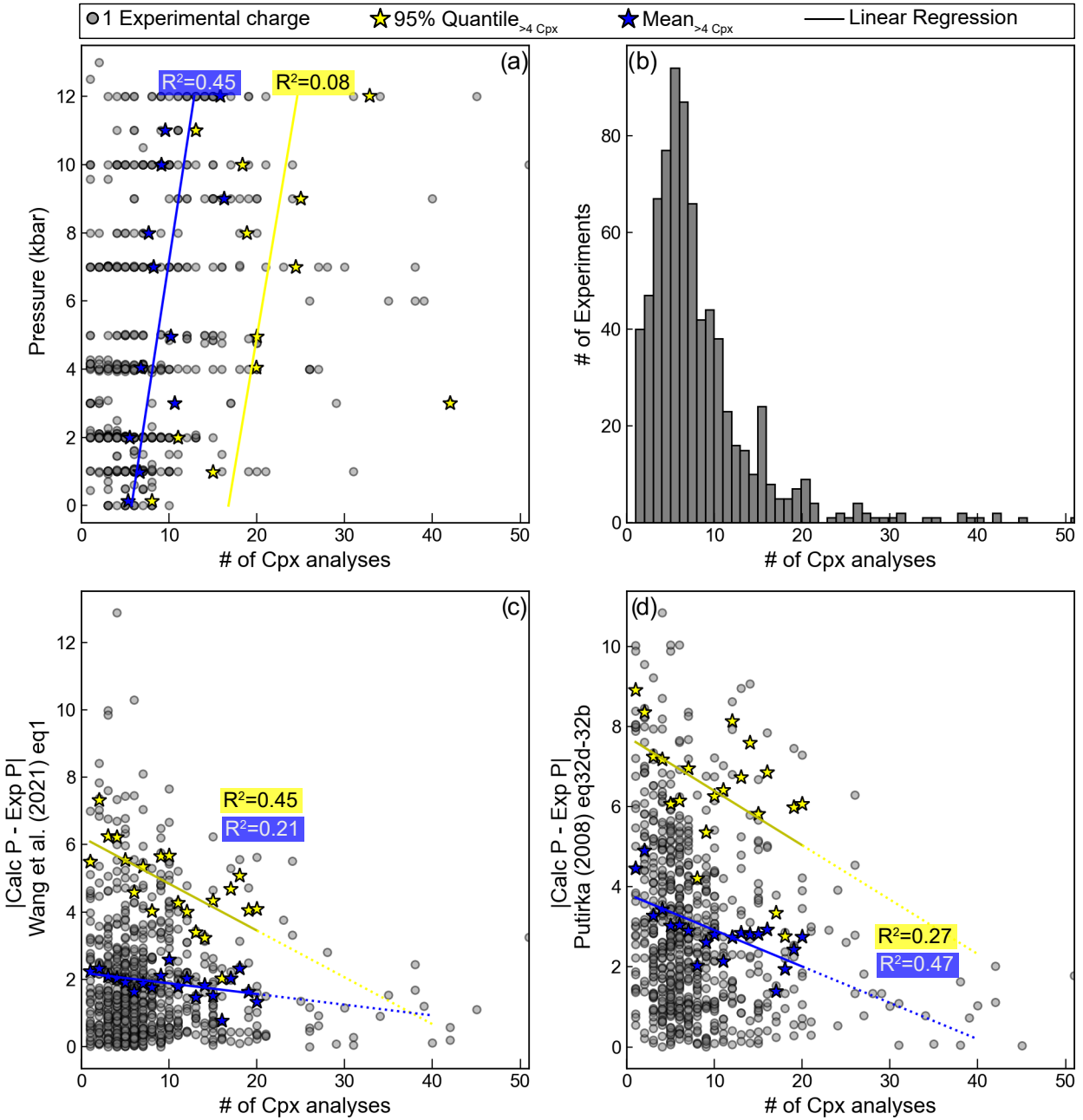
1 Experimental charge
95% Quantile>4 Cpx
Mean>4 Cpx
Linear Regression
(a)
R²=0.45
R²=0.08
Pressure (kbar)
# of Cpx analyses
(b)
# of Experiments
# of Cpx analyses
(c)
R²=0.45
R²=0.21
|Calc P - Exp P|
Wang et al. (2021) eq1
# of Cpx analyses
(d)
R²=0.27
R²=0.47
|Calc P - Exp P|
Putirka (2008) eq32d-32b
# of Cpx analyses

Experiment Y0201-2, Neave et al. (2019), N=42

(a) Correlation matrix Cpx

	SiO_2	TiO_2	Al_2O_3	FeO_t	MnO	MgO	CaO	Na_2O	Cr_2O_3
SiO_2	1.00	0.63	0.58	0.11	0.06	0.31	0.05	0.06	0.00
TiO_2	0.63	1.00	0.80	0.12	0.00	0.56	0.06	0.10	0.03
Al_2O_3	0.58	0.80	1.00	0.05	0.00	0.66	0.11	0.17	0.01
FeO_t	0.11	0.12	0.05	1.00	0.01	0.01	0.38	0.02	0.00
MnO	0.06	0.00	0.00	0.01	1.00	0.01	0.00	0.00	0.00
MgO	0.31	0.56	0.66	0.01	0.01	1.00	0.26	0.18	0.02
CaO	0.05	0.06	0.11	0.38	0.00	0.26	1.00	0.14	0.01
Na_2O	0.06	0.10	0.17	0.02	0.00	0.18	0.14	1.00	0.00
Cr_2O_3	0.00	0.03	0.01	0.00	0.00	0.02	0.01	0.00	1.00

R^2: 1.0, 0.8, 0.6, 0.4, 0.2, 0.0

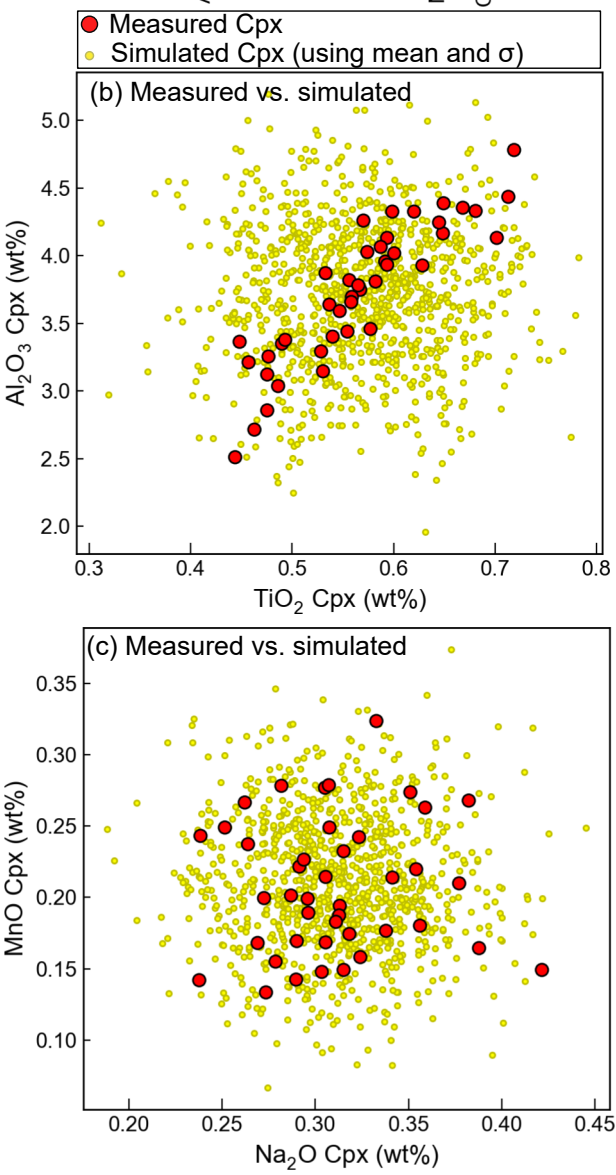

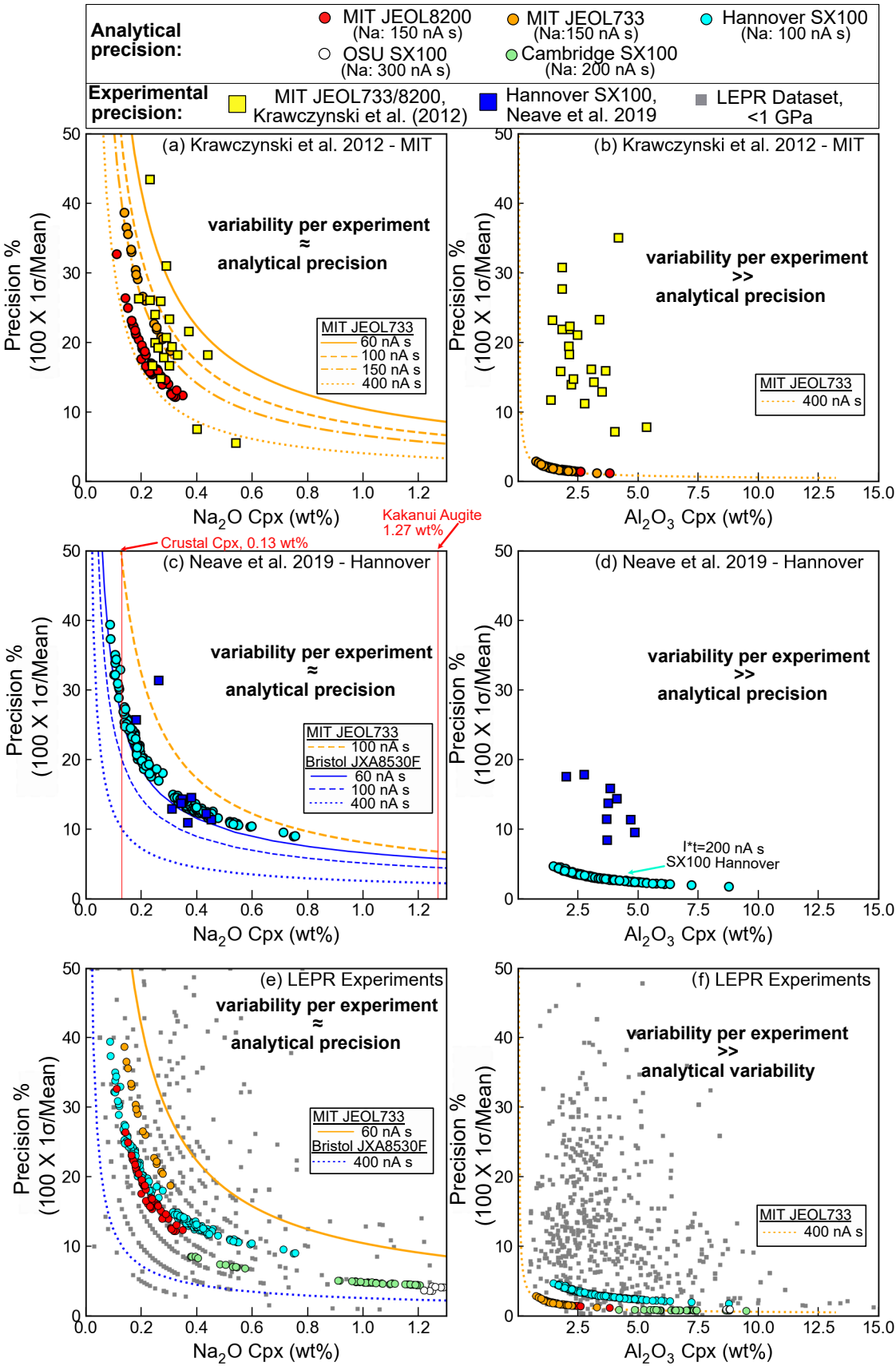
Analytical precision:
MIT JEOL8200 (Na: 150 nA s)
MIT JEOL733 (Na:150 nA s)
Hannover SX100 (Na: 100 nA s)
OSU SX100 (Na: 300 nA s)
Cambridge SX100 (Na: 200 nA s)
Experimental precision:
MIT JEOL733/8200, Krawczynski et al. (2012)
Hannover SX100, Neave et al. 2019
LEPR Dataset, <1 GPa
(a) Krawczynski et al. 2012 - MIT
variability per experiment ≈ analytical precision
MIT JEOL733
60 nA s
100 nA s
150 nA s
400 nA s
(b) Krawczynski et al. 2012 - MIT
variability per experiment >> analytical precision
MIT JEOL733
400 nA s
(c) Neave et al. 2019 - Hannover
Crustal Cpx, 0.13 wt%
Kakanui Augite 1.27 wt%
variability per experiment ≈ analytical precision
MIT JEOL733
100 nA s
Bristol JXA8530F
60 nA s
100 nA s
400 nA s
(d) Neave et al. 2019 - Hannover
variability per experiment >> analytical precision
I*t=200 nA s
SX100 Hannover
(e) LEPR Experiments
variability per experiment ≈ analytical precision
MIT JEOL733
60 nA s
Bristol JXA8530F
400 nA s
(f) LEPR Experiments
variability per experiment >> analytical variability
MIT JEOL733
400 nA s
Precision % (100 X 1σ/Mean)
Na2O Cpx (wt%)
Al2O3 Cpx (wt%)

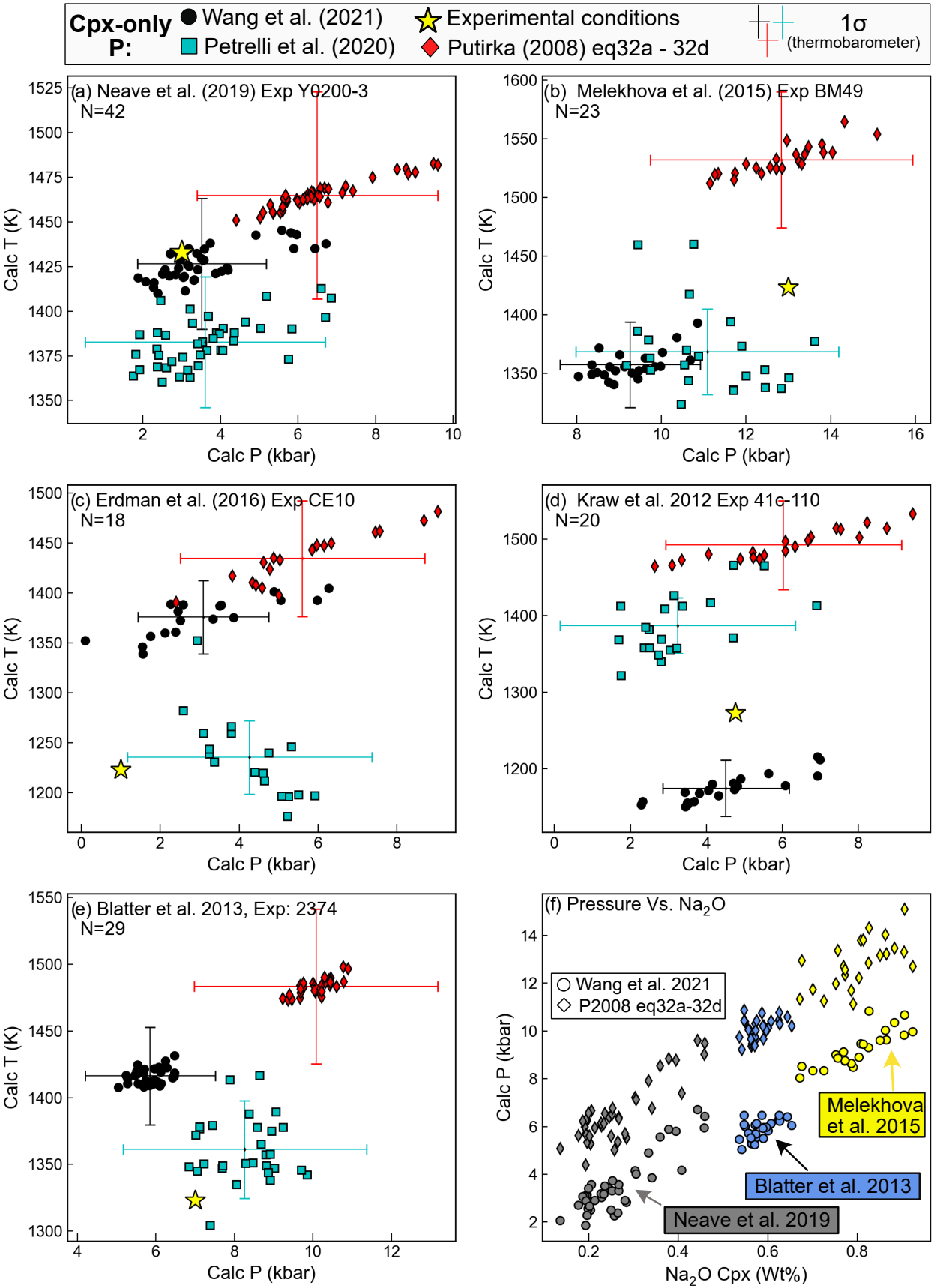
Cpx-only P:
Wang et al. (2021)
Petrelli et al. (2020)
Experimental conditions
Putirka (2008) eq32a - 32d
1σ (thermobarometer)
(a) Neave et al. (2019) Exp Y0200-3
N=42
(b) Melekhova et al. (2015) Exp BM49
N=23
(c) Erdman et al. (2016) Exp CE10
N=18
(d) Kraw et al. 2012 Exp 41c-110
N=20
(e) Blatter et al. 2013, Exp: 2374
N=29
(f) Pressure Vs. Na2O
Wang et al. 2021
P2008 eq32a-32d
Melekhova et al. 2015
Blatter et al. 2013
Neave et al. 2019
Calc T (K)
Calc P (kbar)
Na2O Cpx (Wt%)

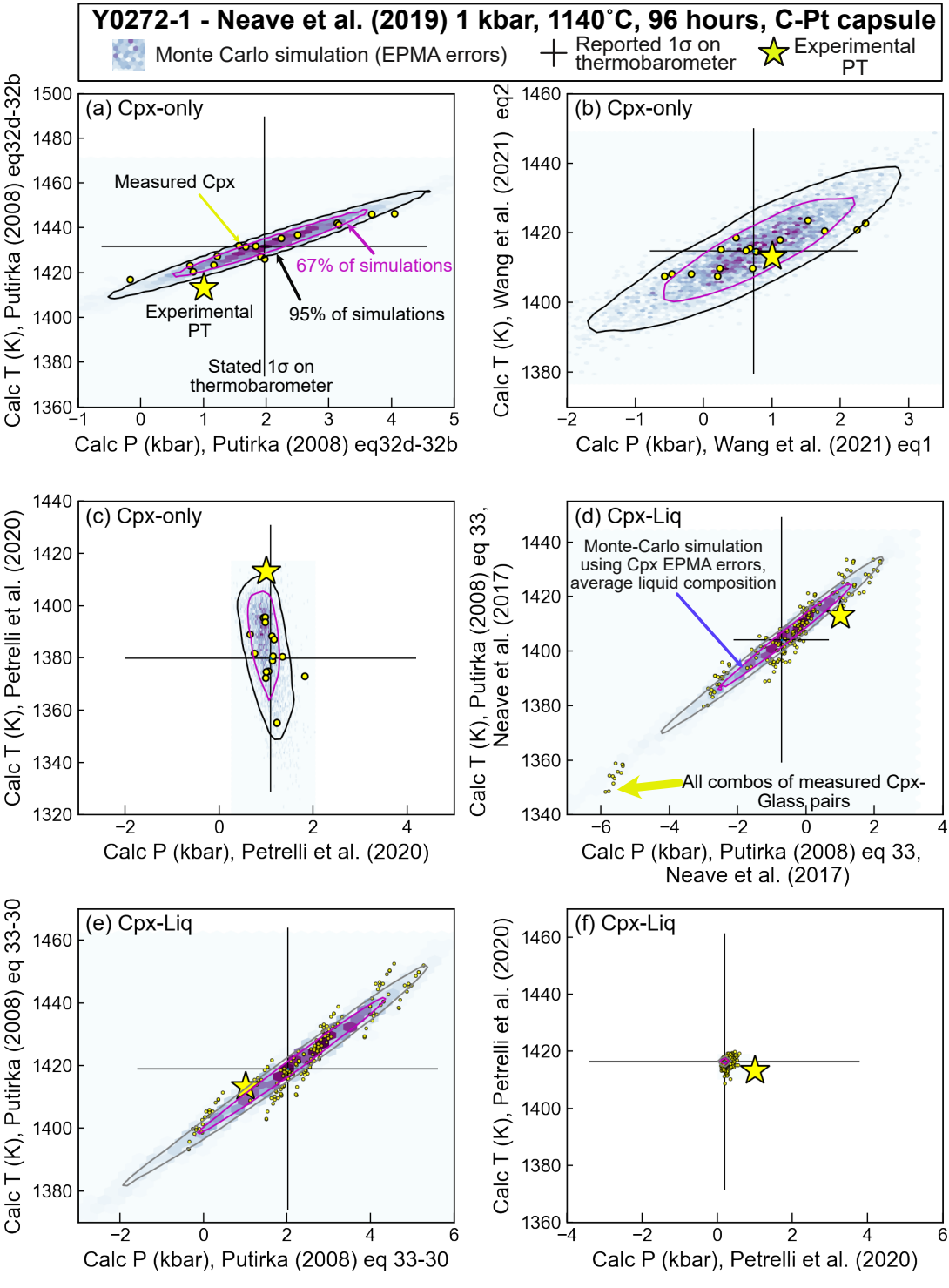
Y0272-1 - Neave et al. (2019) 1 kbar, 1140˚C, 96 hours, C-Pt capsule
Monte Carlo simulation (EPMA errors)
Reported 1σ on thermobarometer
Experimental PT
(a) Cpx-only
Measured Cpx
67% of simulations
95% of simulations
Experimental PT
Stated 1σ on thermobarometer
Calc T (K), Putirka (2008) eq32d-32b
Calc P (kbar), Putirka (2008) eq32d-32b
(b) Cpx-only
Calc T (K), Wang et al. (2021) eq2
Calc P (kbar), Wang et al. (2021) eq1
(c) Cpx-only
Calc T (K), Petrelli et al. (2020)
Calc P (kbar), Petrelli et al. (2020)
(d) Cpx-Liq
Monte-Carlo simulation using Cpx EPMA errors, average liquid composition
All combos of measured Cpx-Glass pairs
Calc T (K), Putirka (2008) eq 33, Neave et al. (2017)
Calc P (kbar), Putirka (2008) eq 33, Neave et al. (2017)
(e) Cpx-Liq
Calc T (K), Putirka (2008) eq 33-30
Calc P (kbar), Putirka (2008) eq 33-30
(f) Cpx-Liq
Calc T (K), Petrelli et al. (2020)
Calc P (kbar), Petrelli et al. (2020)

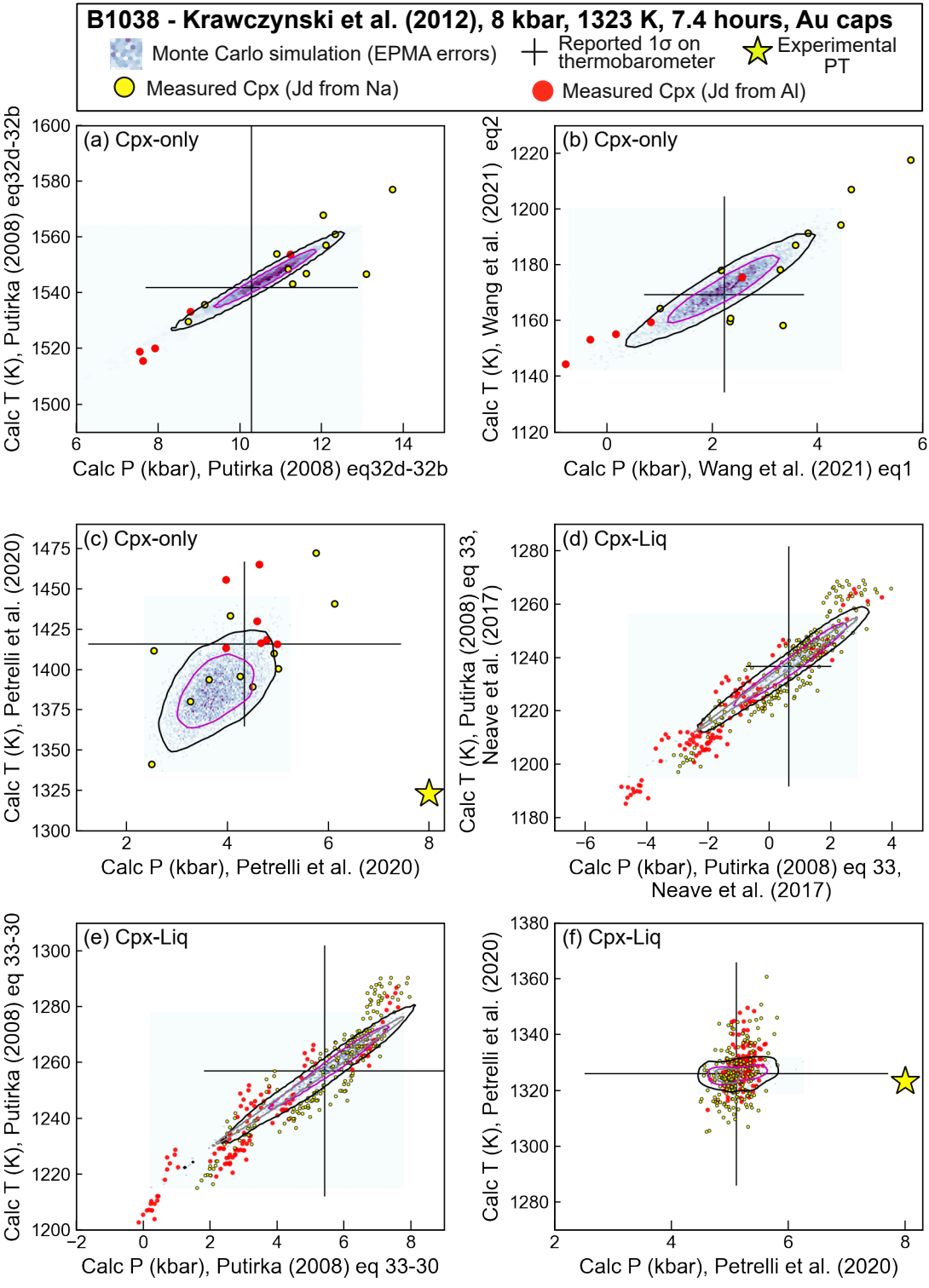
B1038 - Krawczynski et al. (2012), 8 kbar, 1323 K, 7.4 hours, Au caps
Monte Carlo simulation (EPMA errors)
Reported 1σ on thermobarometer
Experimental PT
Measured Cpx (Jd from Na)
Measured Cpx (Jd from Al)
(a) Cpx-only
Calc T (K), Putirka (2008) eq32d-32b
Calc P (kbar), Putirka (2008) eq32d-32b
(b) Cpx-only
Calc T (K), Wang et al. (2021) eq2
Calc P (kbar), Wang et al. (2021) eq1
(c) Cpx-only
Calc T (K), Petrelli et al. (2020)
Calc P (kbar), Petrelli et al. (2020)
(d) Cpx-Liq
Calc T (K), Putirka (2008) eq 33, Neave et al. (2017)
Calc P (kbar), Putirka (2008) eq 33, Neave et al. (2017)
(e) Cpx-Liq
Calc T (K), Putirka (2008) eq 33-30
Calc P (kbar), Putirka (2008) eq 33-30
(f) Cpx-Liq
Calc T (K), Petrelli et al. (2020)
Calc P (kbar), Petrelli et al. (2020)

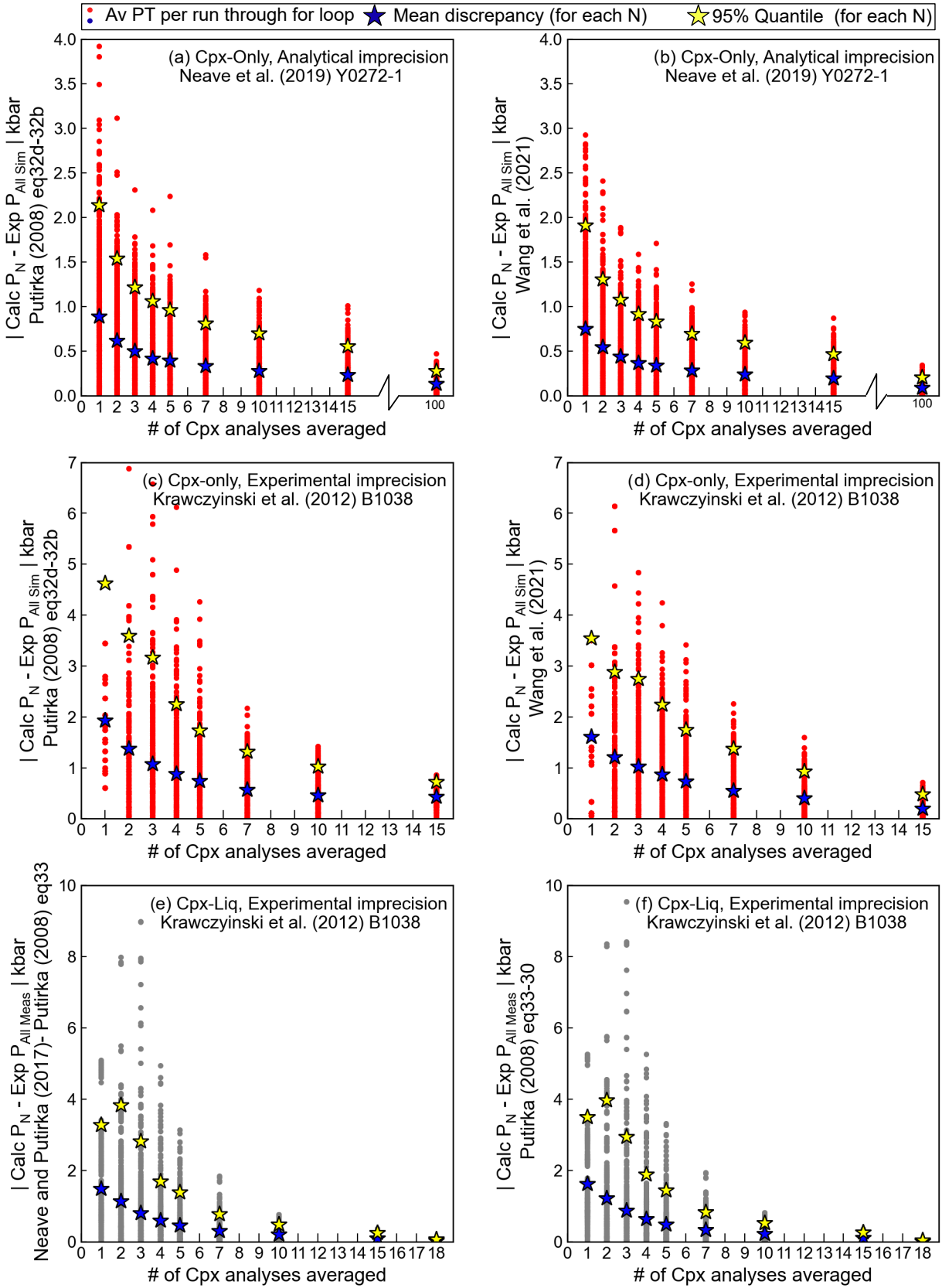
Av PT per run through for loop
Mean discrepancy (for each N)
95% Quantile (for each N)
(a) Cpx-Only, Analytical imprecision
Neave et al. (2019) Y0272-1
| Calc P_N - Exp P_All Sim | kbar
Putirka (2008) eq32d-32b
# of Cpx analyses averaged
(b) Cpx-Only, Analytical imprecision
Neave et al. (2019) Y0272-1
| Calc P_N - Exp P_All Sim | kbar
Wang et al. (2021)
# of Cpx analyses averaged
(c) Cpx-only, Experimental imprecision
Krawczyinski et al. (2012) B1038
| Calc P_N - Exp P_All Sim | kbar
Putirka (2008) eq32d-32b
# of Cpx analyses averaged
(d) Cpx-only, Experimental imprecision
Krawczyinski et al. (2012) B1038
| Calc P_N - Exp P_All Sim | kbar
Wang et al. (2021)
# of Cpx analyses averaged
(e) Cpx-Liq, Experimental imprecision
Krawczyinski et al. (2012) B1038
| Calc P_N - Exp P_All Meas | kbar
Neave and Putirka (2017)- Putirka (2008) eq33
# of Cpx analyses averaged
(f) Cpx-Liq, Experimental imprecision
Krawczyinski et al. (2012) B1038
| Calc P_N - Exp P_All Meas | kbar
Putirka (2008) eq33-30
# of Cpx analyses averaged

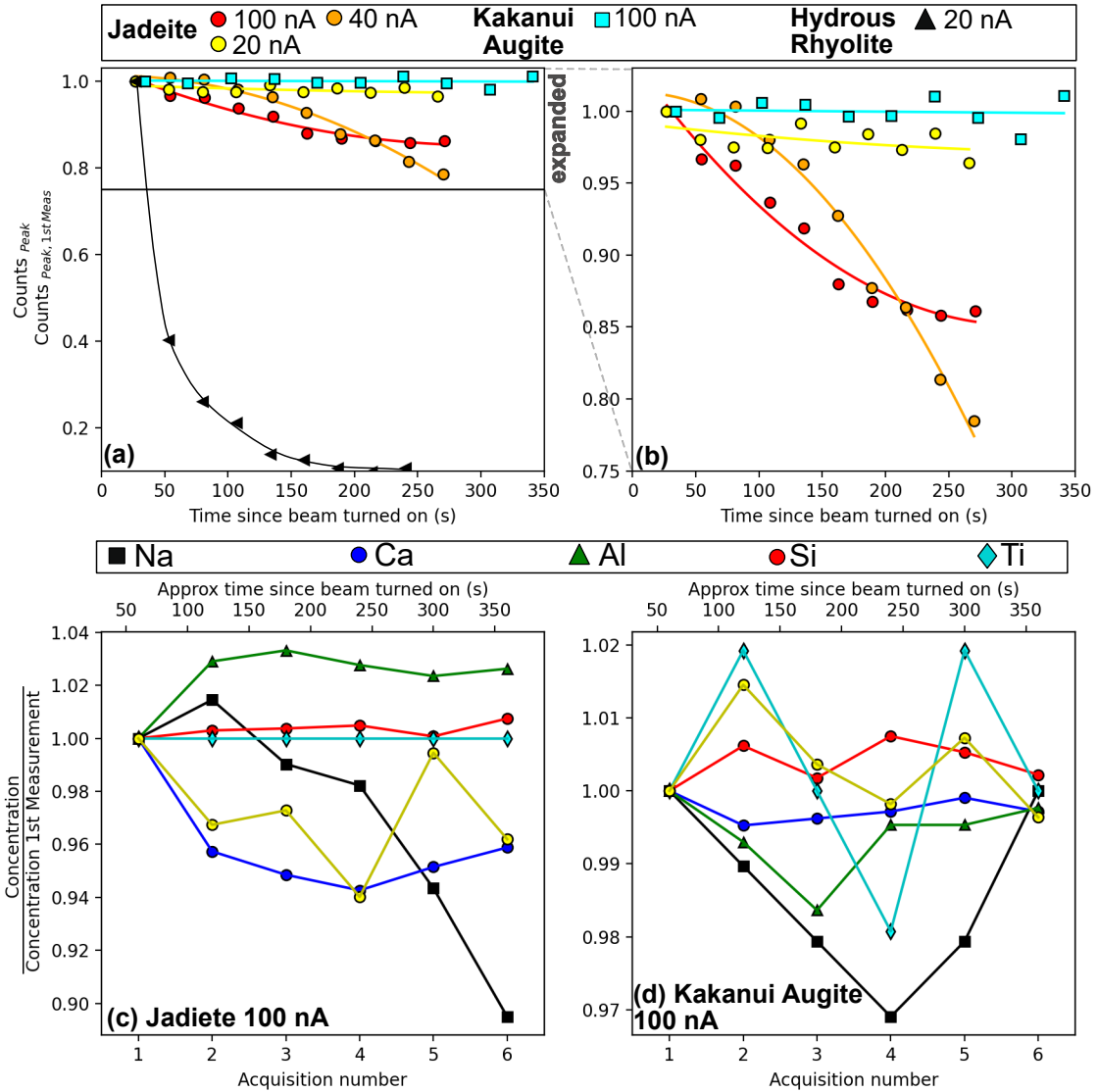
Jadeite
100 nA
40 nA
20 nA
Kakanui Augite
100 nA
Hydrous Rhyolite
20 nA
Counts Peak / Counts Peak, 1st Meas
expanded
(a)
(b)
Time since beam turned on (s)
Na
Ca
Al
Si
Ti
Approx time since beam turned on (s)
Concentration / Concentration 1st Measurement
(c) Jadiete 100 nA
(d) Kakanui Augite 100 nA
Acquisition number

Supplementary Information for Barometers Behaving Badly

Penny E. Wieser[1*, 2], Adam Kent[2], Christy B. Till[3], John Donovan[4], David A. Neave[5], Dawnika Blatter[6], Michael J. Krawczynski[7]

1. **Corresponding author**: Penny_wieser@berkeley.edu, 541–908–4572. Department of Earth and Planetary Sciences, McCone Hall, UC Berkeley, 94720, USA

2. College of Earth, Ocean and Atmospheric Sciences, Oregon State University, 97331, USA

3. School of Earth and Space Exploration, Arizona State University, Tempe, AZ 85281, USA

4. Department of Earth Sciences, University of Oregon, 97403, USA.

5. Department of Earth and Environmental Sciences, The University of Manchester, Oxford Road, Manchester M13 9PL, UK

6. U.S. Geological Survey, Volcano Science Center, 345 Middlefeld Road, Menlo Park, CA 94025, USA

7. Department of Earth and Planetary Sciences, Washington University in St. Louis, 1 Brookings Drive, St. Louis, MO 63130, USA

1. Compilation of beam currents and count times used for Na

Supporting Table 1- *Compilation of beam current and count times for Na analyses in a subset of the LEPR dataset conducted at <1 GPa used to calibrate most existing thermobarometers. Missing or incomplete/ambigous data are colored orange.*

Reference	Beam Current (I)	Count time (t)	I*t	Instrument
Akella (1976)				
Baker and Eggler (1987)	12 nA			Penn State + Smithsonian
Gee and Sack (1988)	30 nA	2-10 s	60-300	JEOL Superprobe Northwestern, ARL UC Berkeley
Carroll and Wyllie (1989)	5 nA			JEOL at Caltech, Cameca at Brown
Kennedy et al. (1990)	10 nA			MIT MAC-5 and JEOL 733

Nielsen et al. (1992)	20 nA	10 s	200	SX50, OSU
Fram and Longhi (1992)	5 nA			
Rushmer (1993)				SX50 (no loc, authors at ETH)
Baker et al. (1994)	10 nA			JEOL 733, Caltech
Baker et al. (1994)				MIT MAC-5 and JEOL 733
Draper and Johnston (1992)	20 nA	10 s	200	Cameca SX50, UOregon
Kawamoto (1996)				JEOL JSM-840 e, University of Tokyo
Springer and Seck (1997)	10 nA	5 s	50	camebax
Tsuruta and Takahashi (1998)	12 nA	10-40 s (don't specify for each element)	120-480	JEOL-JXA8800, Tokyo institute of technology
Métrich and Rutherford (1998)	15 nA			Camebax, Brown
Blundy et al. (1998)	15 nA			JEOL 833, University of Bristol
Draper and Green (1999)	20 nA	15 s	300 s	SX50, Macquarie
McCoy and Lofgren (1999)				JEOL JXA-8900R, Smithsonian
Wang and Takahashi (1999)	No information whatsoever on how phase compositions were measured (not even analytical technique)			
Minitti and Rutherford (2000)	15 nA			
Tielpo et al. (2000)				JEOL JXA-840A, Pavia
Blatter and Carmichael (2001)	20 nA			SX50, UC Berkeley
Wood and Trigila (2001)	15 nA	10-60 (don't say which element is which)	150 - 900	JEOL 8600, Bristol
Berndt et al. (2001)	18 nA	5 s	90	Camebax,
Toplis and Corgne (2002)	10 nA	Says 10s major 30s minor elements (no list)	300	Cameca SX50, Nancy
Scaillet (2003)	6 nA	10 s	60	(authors at Orleans)
Pertermann (2003)	7.5-15 nA	30 s	225-450	JXA8900R, Minnesota
Prouteau (2003)	6 nA	10 s	60	SX50, Orleans
Wasylenki (2003)	30 nA			Caltech JEOL733
Laporte et al. (2004)	15 nA	10s	150	SX-100, authors at Clermont-Ferrand
Maaløe (2004)	Uses EDS – no further information about analytical conditions. E.g. unclear if any standards used.			JEOL-2400 SEM
Barclay (2004)	20 nA	10 s	200	SX50, UC Berkeley
Feig et al. (2006)	15 nA	5 s	75	SX100,
Di Carlo (2006)	6 nA	10 s	60	SX-50, Orleans

Scoates et al. (2006)	10 nA	10 s	100	Cameca SX-50, Universite´ de Pierre
Alonso-Perez et al. (2009)	20 nA			SX50/JEOL 8600
Pertermann and Lundstrom (2006)	Use EDS on JEOL JSM 840 SEM with natural and synthetic standards. Some repeat analyses on JXA 8900, no mention of analytical conditions.			
new compilation				
Costa (2004)	12 nA	10 s	120	SX50 Orleans
Berndt (2004)	15 nA	5 s	75	SX100 Hannover
Pichavant and Macdonald (2007)	6 nA	6- 10 s	36-60	2 different Cameca, Orleans
Hamada and Fujii (2008)	12 nA			JEOL JXA8800R,
Feig et al. (2010)	15 nA	5 s	75	SX100, nd
Krawczynski et al. (2012)	10 nA	15 s	150	JEOL
Mandler et al. (2014)				JEOL JXA8200 Superprobe
Rader and Larsen (2013)	10 nA			Cameca SX-50, University of Alaska
Blatter et al. (2013)	15 nA	20 s	300	JEOL JXA-8900 Menlo Park
Almeev et al. (2013)	15 nA	8 s	120	SX100 Hannover
Cadoux et al. (2014)	6 nA	10 s	60	SX50 Orleans
Parat et al. (2014)	10 nA	10 s	100	SX100 montpellier
Melekhova et al. (2015)	No info for mineral analyses			SX100 Bristol
Andújar et al. (2015)	6 nA	10 s	60	SX50 Orleans
Nandedkar et al. (2014)	20 nA	20 s	400	JEOL JXA8200, nd, ETH?
Erdmann et al. (2016)	10 nA	10-20 s	100-200	
Husen et al. (2016)	10 nA	10 s	100	SX100 Hannover
Koepke et al. (2018)	15 nA	5 s	75	SX100,
Ulmer et al. (2018)	20 nA	20-30 s	400-600	ARL SEMQ/ SX50/JEOL JXA8200.
Neave et al. (2019)	10 nA	10 s	100	SX100 Hannover
Firth et al. (2019)	10 nA			SX100 Anu, Canberra, Macquarie
Waters et al. (2021)	10 nA	20 s	200	JEOL 8900 Superprobe, NHM

2. Further investigation of interlaboratory offsets

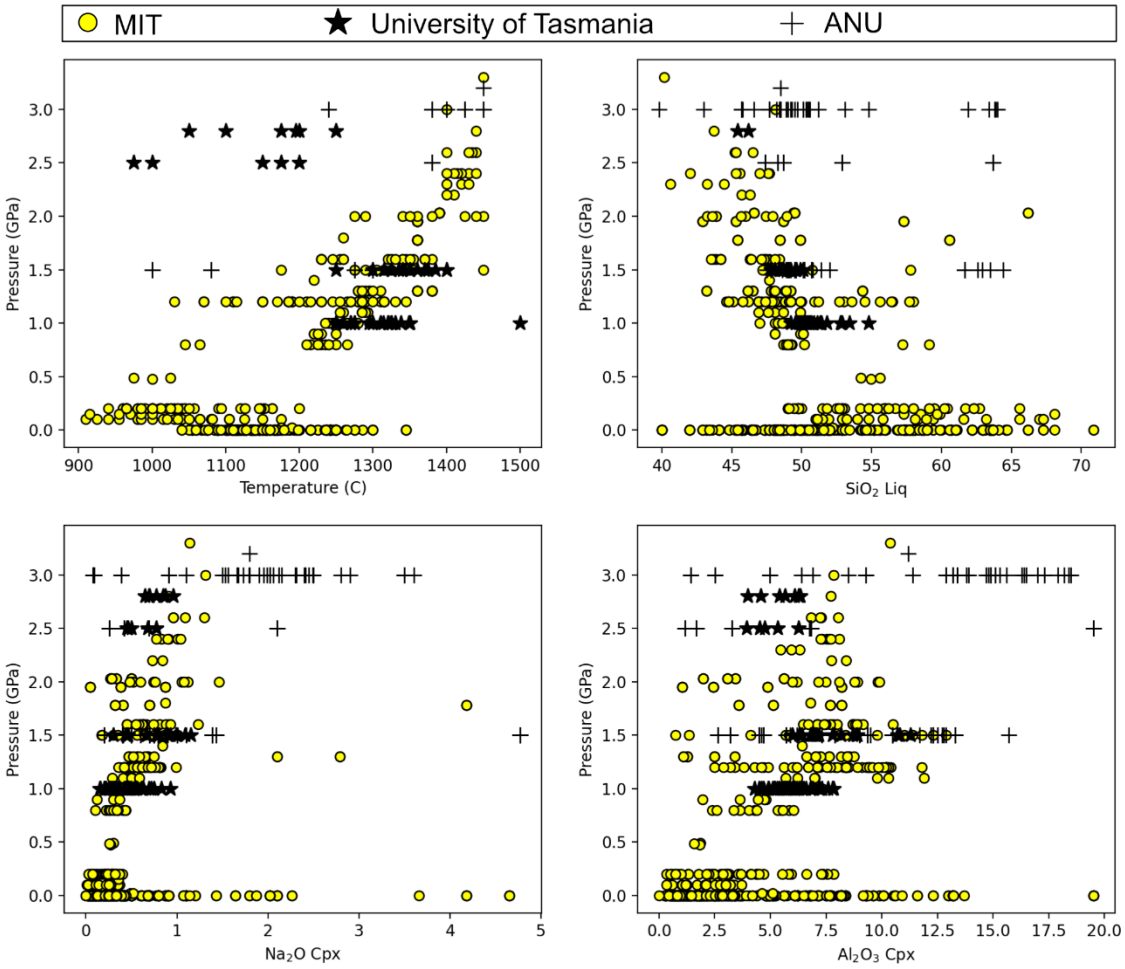

Supplementary Fig. 1 – Non-uniform distribution of P-T-X space covered by different laboratories.

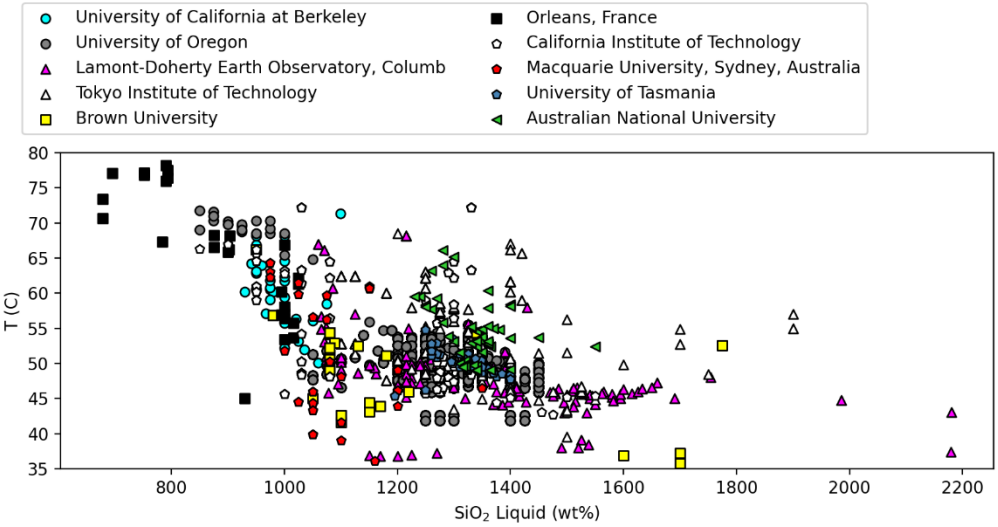
University of California at Berkeley
University of Oregon
Lamont-Doherty Earth Observatory, Columb
Tokyo Institute of Technology
Brown University
Orleans, France
California Institute of Technology
Macquarie University, Sydney, Australia
University of Tasmania
Australian National University
T (C)
SiO2 Liquid (wt%)

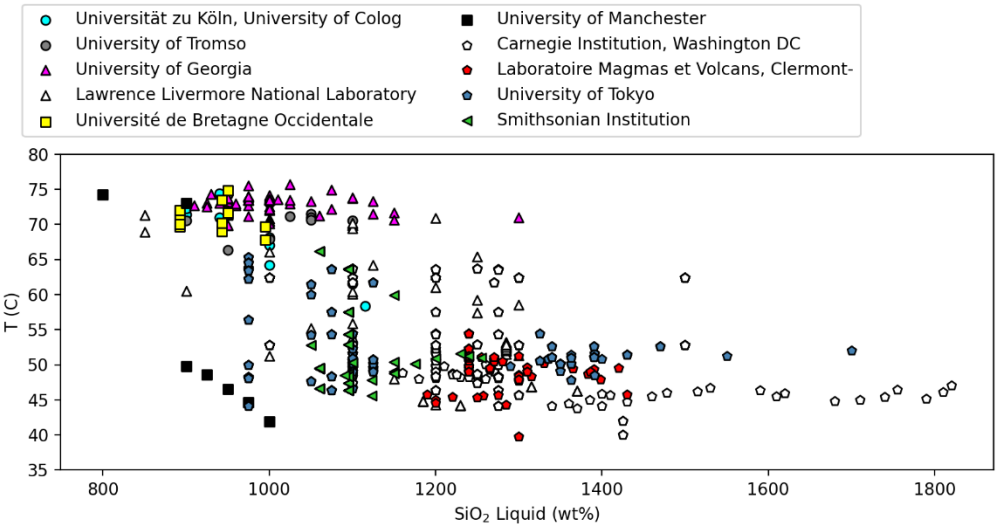
Universität zu Köln, University of Colog
University of Tromso
University of Georgia
Lawrence Livermore National Laboratory
Université de Bretagne Occidentale
University of Manchester
Carnegie Institution, Washington DC
Laboratoire Magmas et Volcans, Clermont-
University of Tokyo
Smithsonian Institution
T (C)
SiO2 Liquid (wt%)

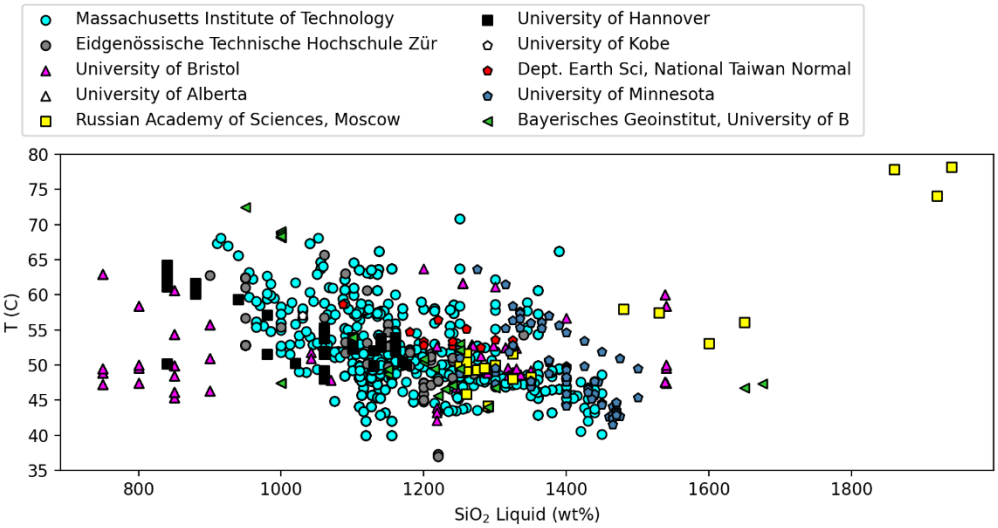
Massachusetts Institute of Technology
Eidgenössische Technische Hochschule Zür
University of Bristol
University of Alberta
Russian Academy of Sciences, Moscow
University of Hannover
University of Kobe
Dept. Earth Sci, National Taiwan Normal
University of Minnesota
Bayerisches Geoinstitut, University of B
T (C)
SiO2 Liquid (wt%)

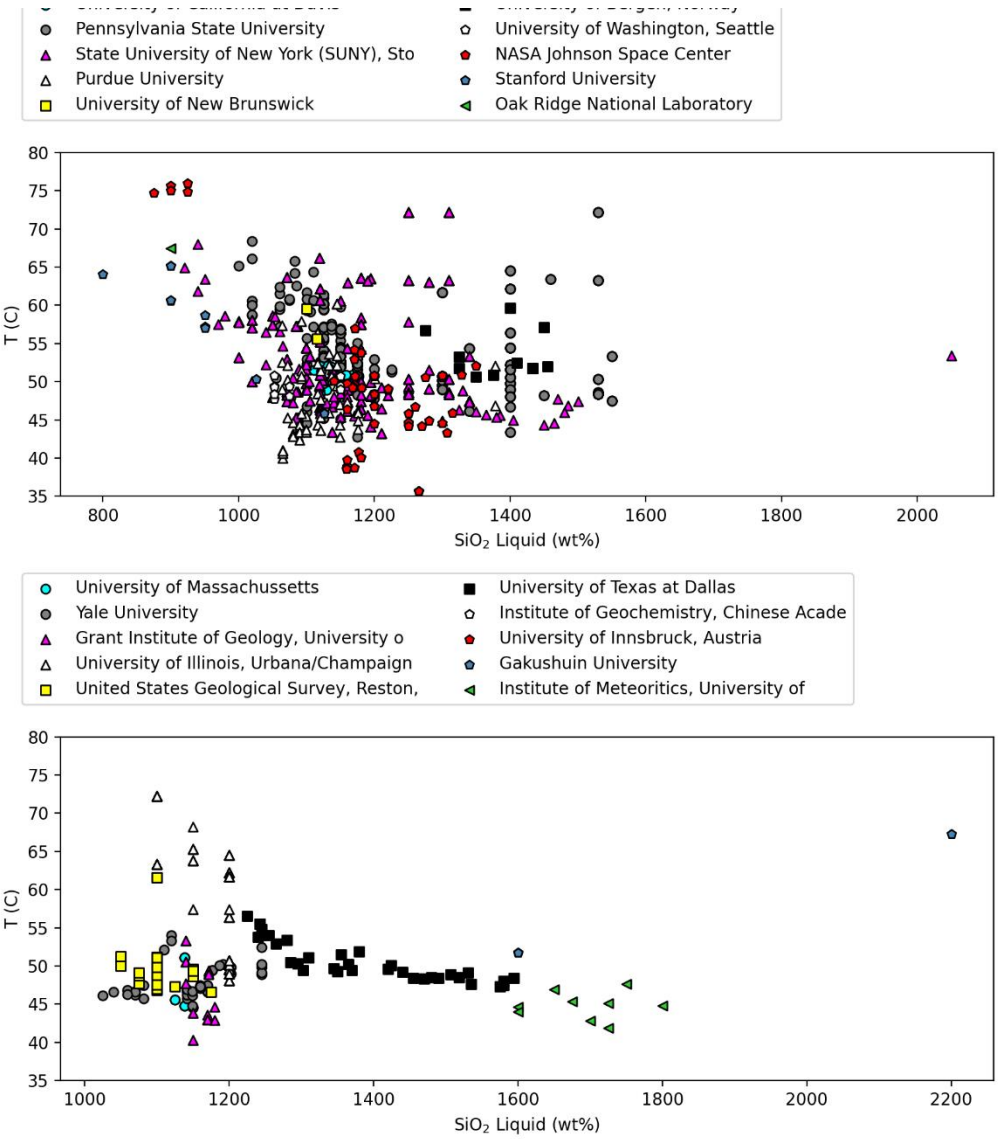

Supplementary Fig. 2 – Range of SiO_2-T space covered by 47 different laboratories in the LEPR dataset.

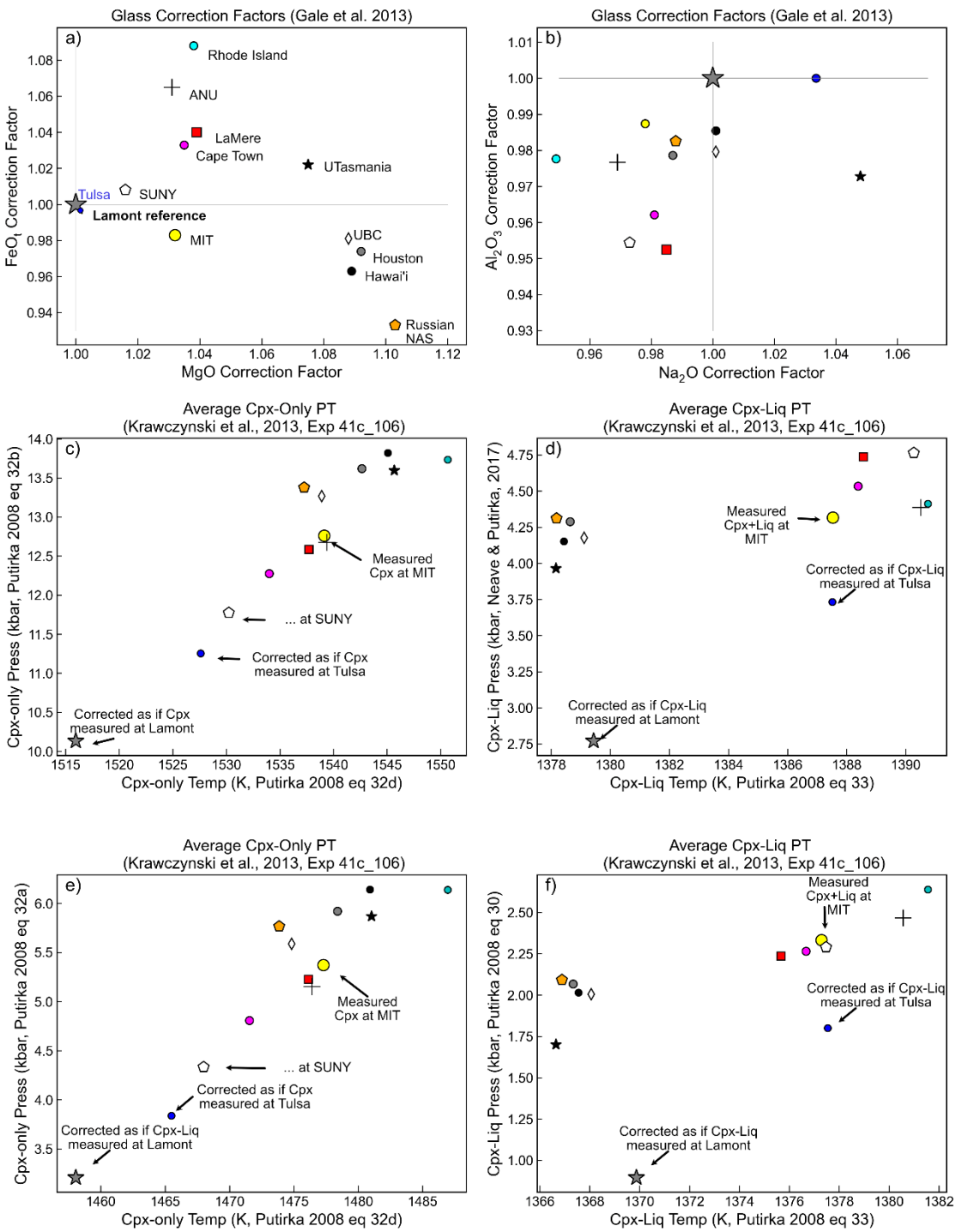

Supporting Fig. 3 – First 4 panels as in main text, panel e-d showing the differences using eq32a for Cpx-only pressures (e) and equation 30 for Cpx-Liq pressures (d).

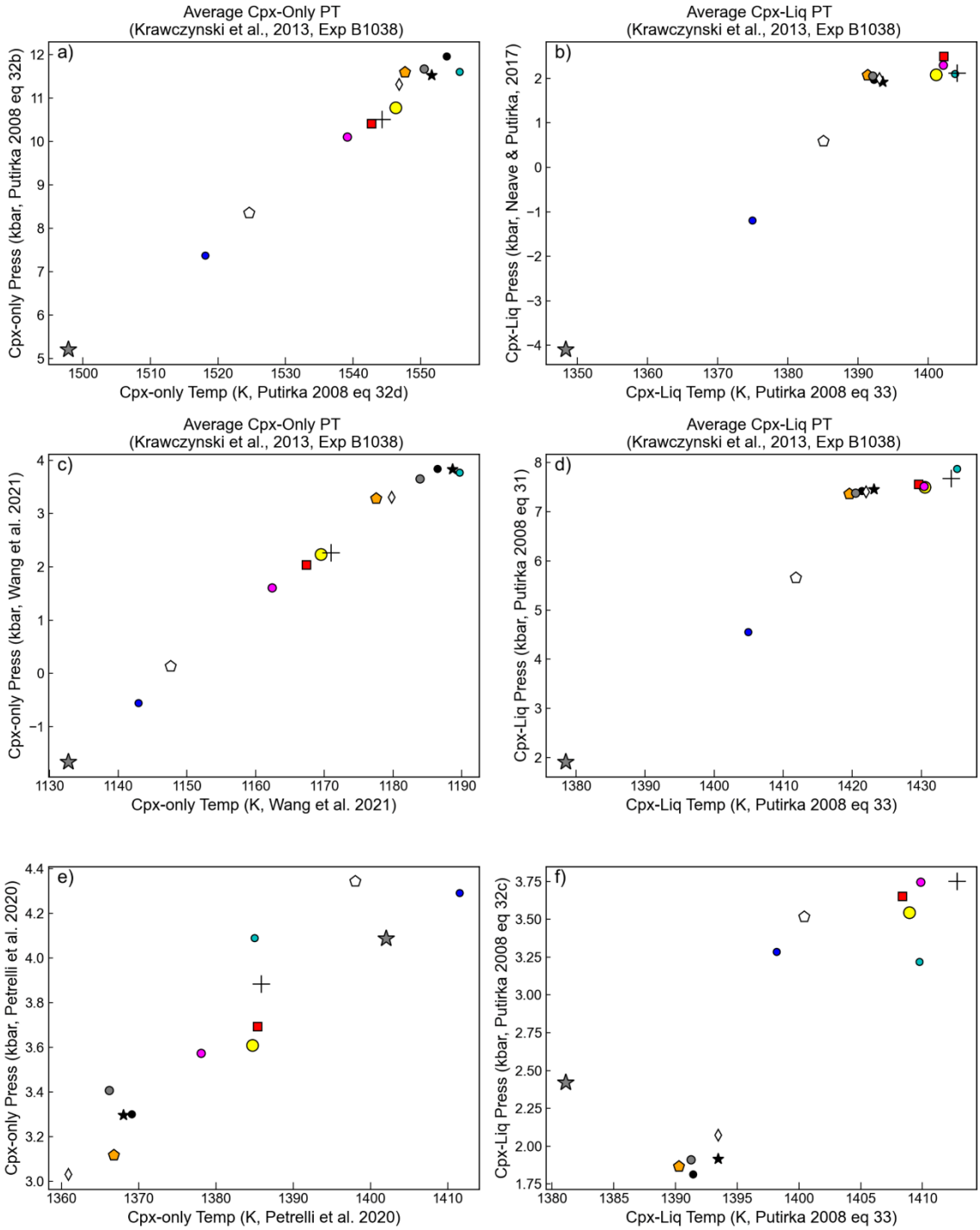

Supporting Fig. 4 – Using the same experiment as the bottom two panels in Fig. 2 of the main text for B1038 but showing discrepancies using different sets of barometers.

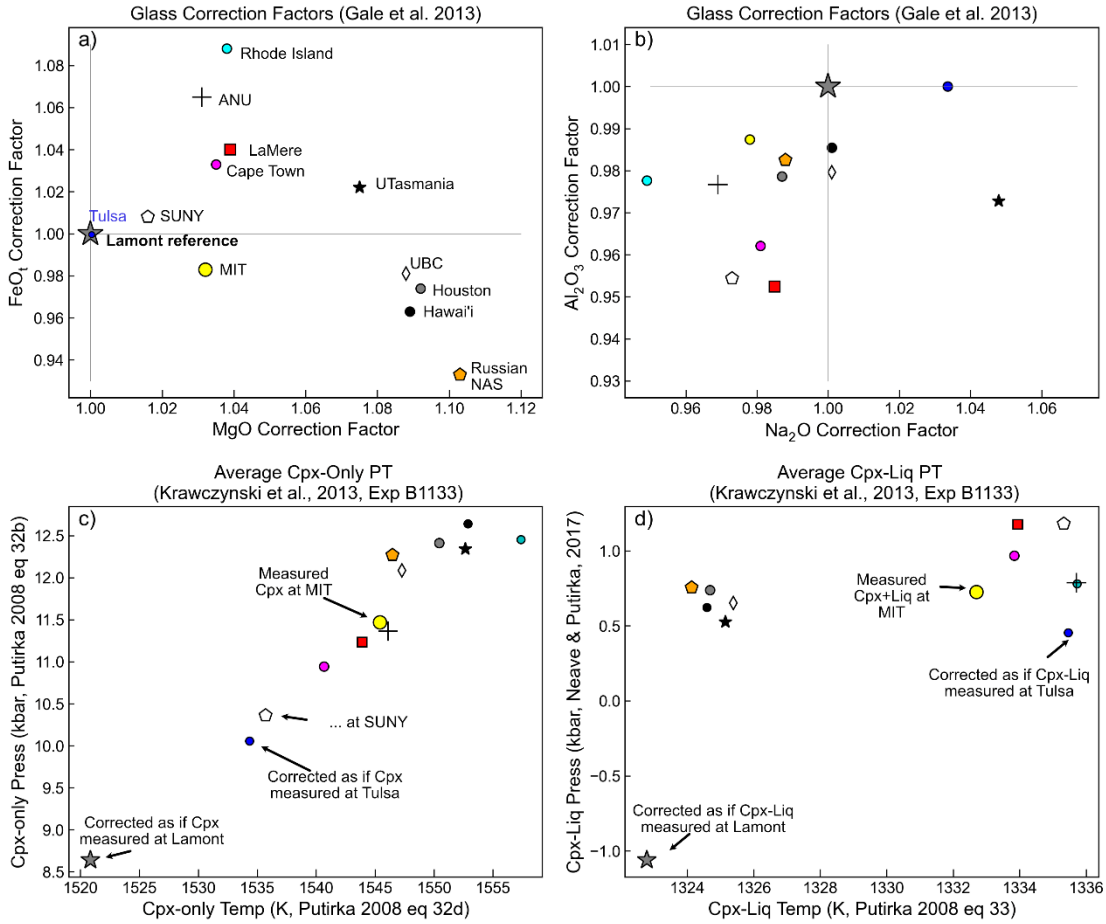

Supporting Fig. 5 – As for Fig. 2 of the main text but showing offsets for Experiment B1133.

3. Covariance in Experimental Cpx Compositions

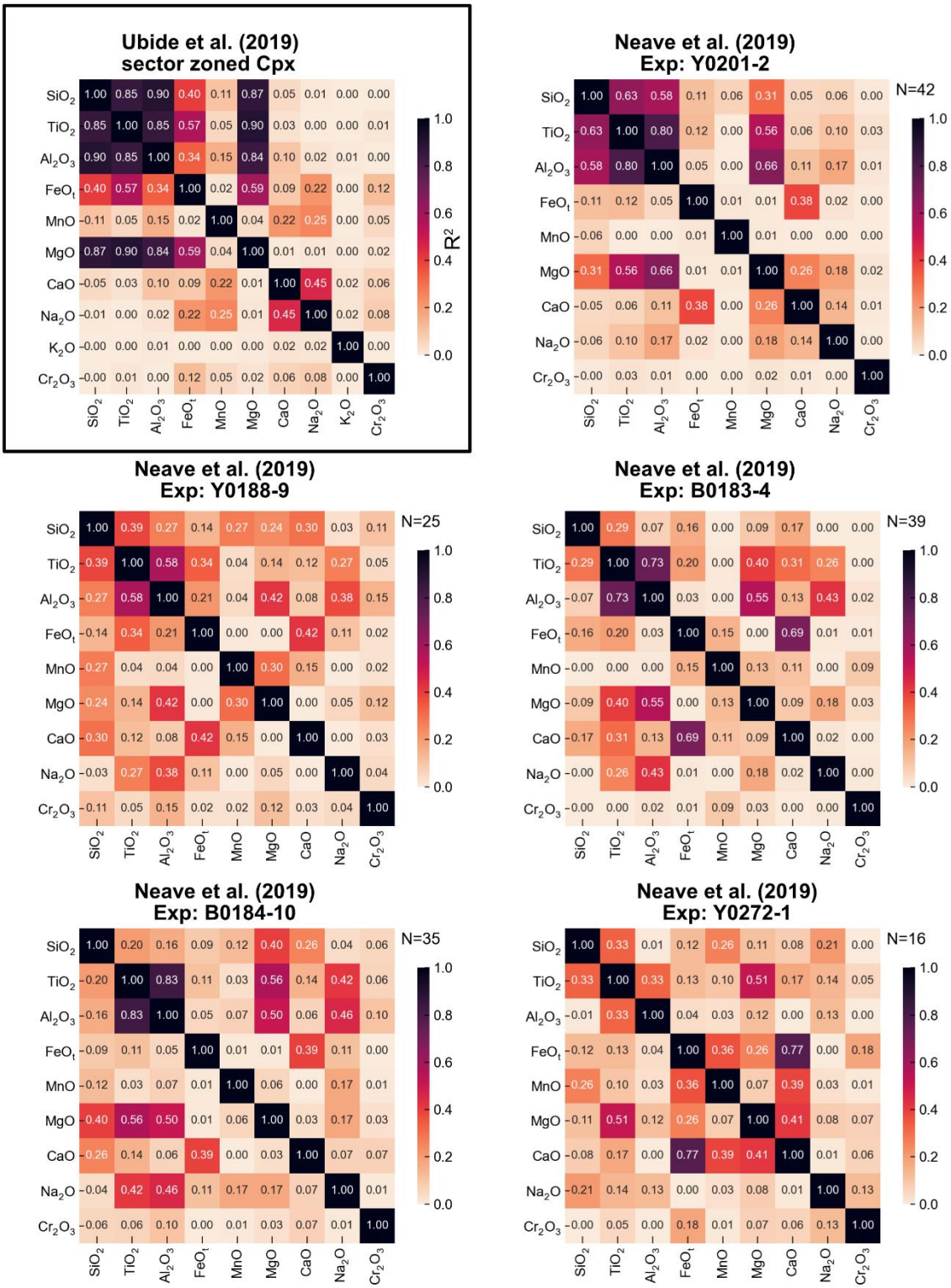

Supporting Fig. 6. Correlation matrix of pyroxenes from different experiments of Neave et al. (2019) with the color bar showing the R^2 value. The correlation matrix for the sector-zoned Cpx of Ubide et al. (2019) are shown for reference.

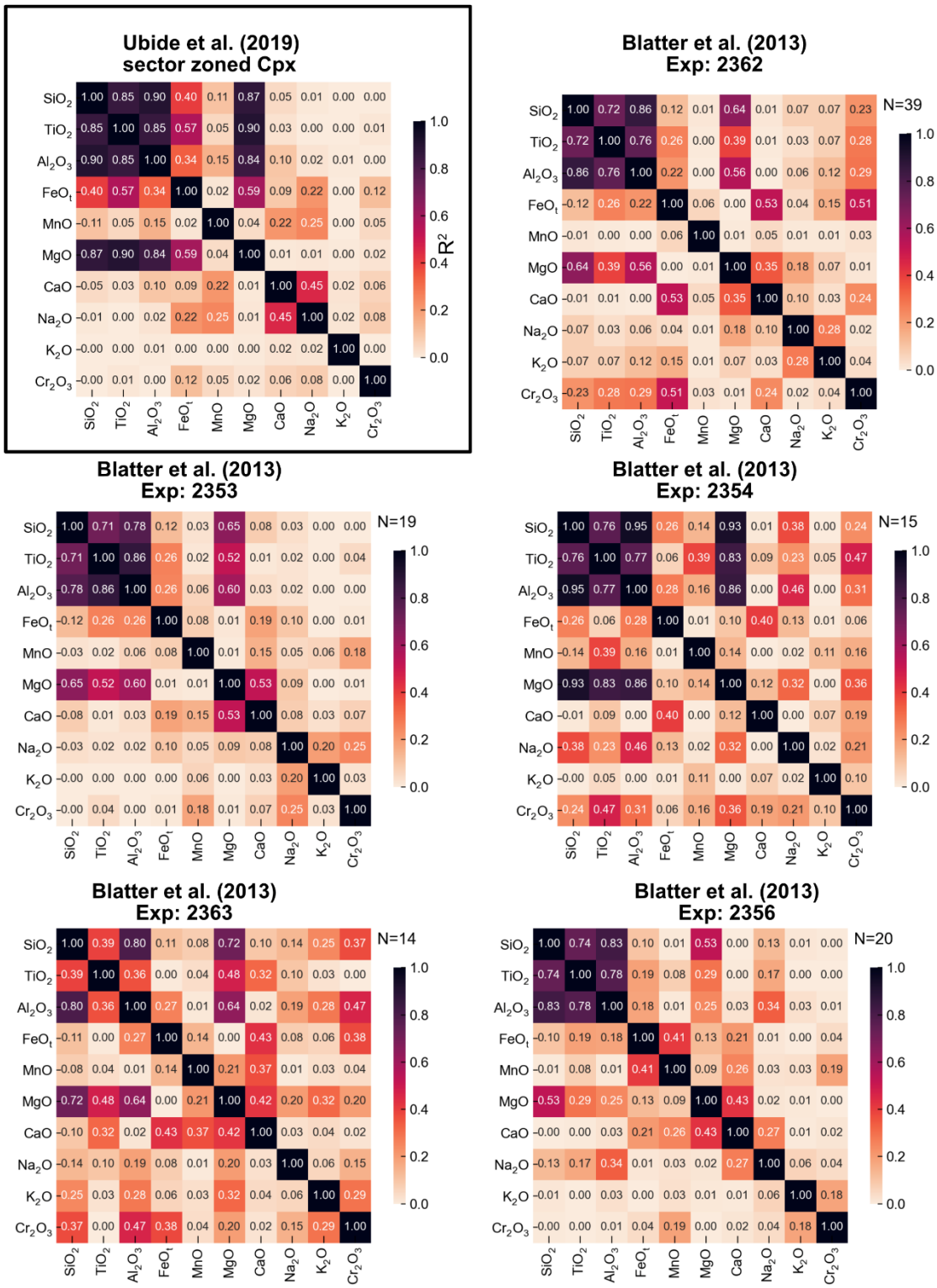

Supporting Fig 7 - Correlation matrix of pyroxenes from different experiments of Blatter et al. (2013) with the color bar showing the R^2 value. The correlation matrix for the sector-zoned Cpx of Ubide et al. (2019) are shown for reference.

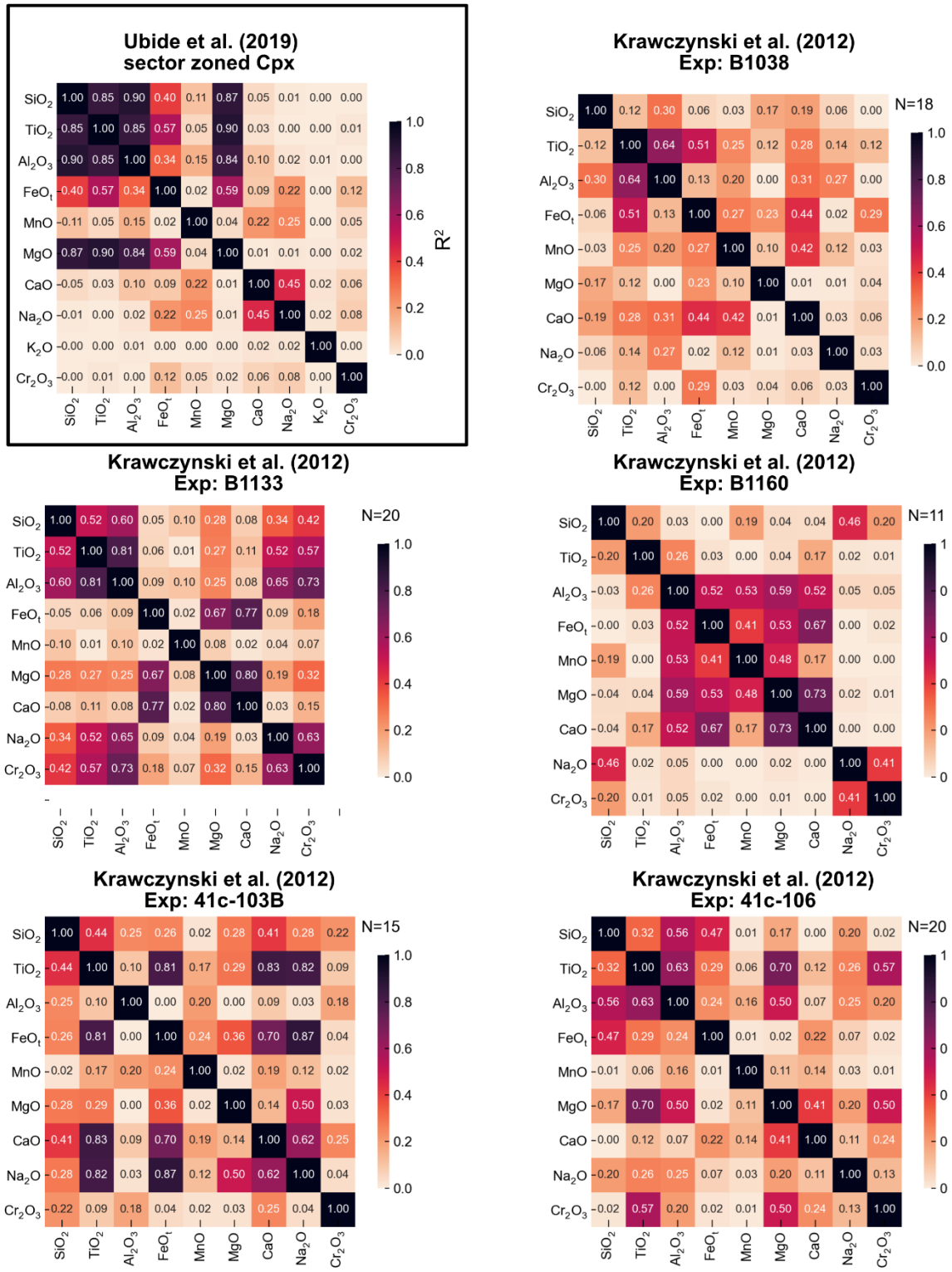

Supporting Fig 8 - Correlation matrix of pyroxenes from different experiments of Krawczynski et al. (2012) with the color bar showing the R^2 value. The correlation matrix for the sector-zoned Cpx of Ubide et al. (2019) are shown for reference.

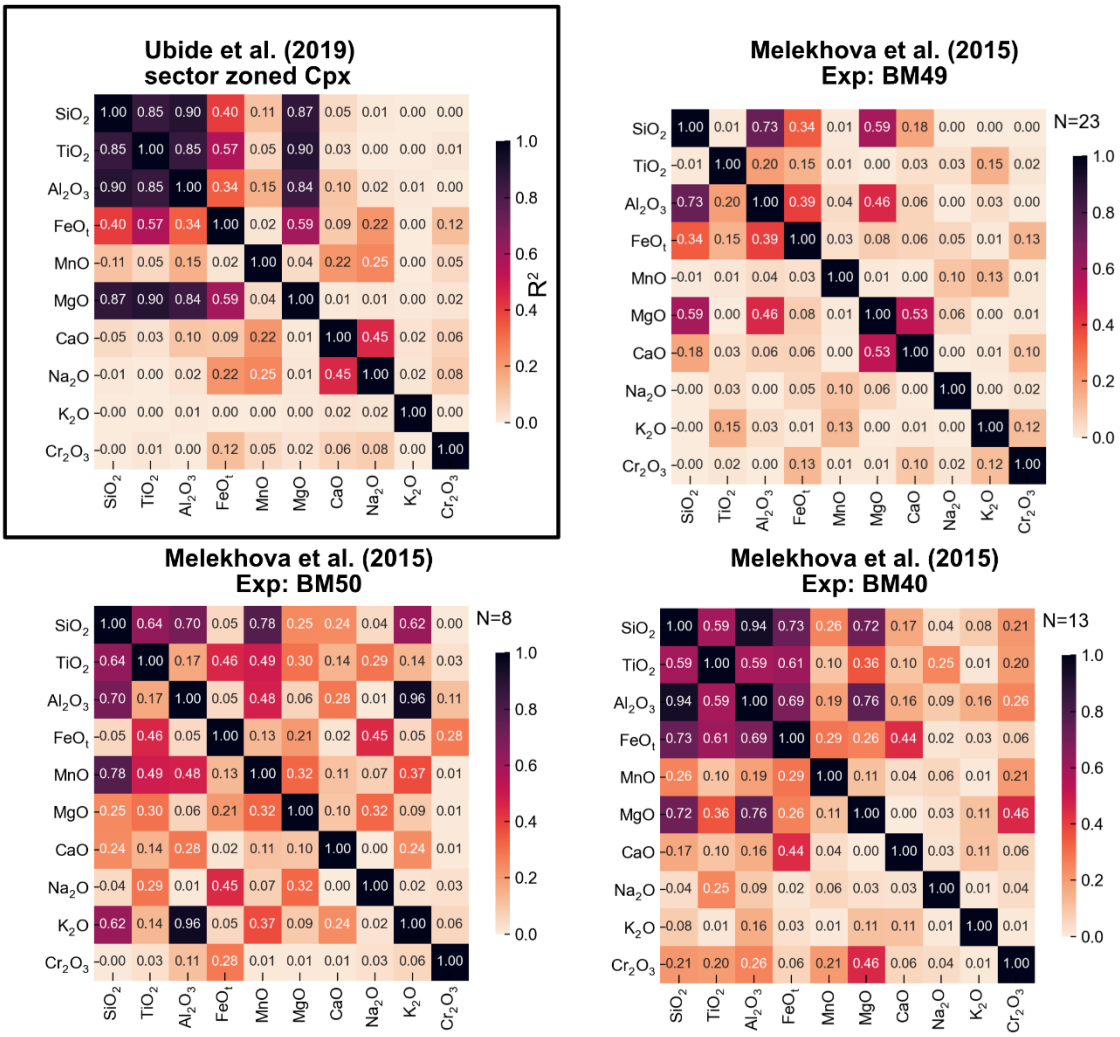

Supporting Fig 9 - Correlation matrix of pyroxenes from different experiments of Melekhova et al. (2015) with the color bar showing the R^2 value. The correlation matrix for the sector-zoned Cpx of Ubide et al. (2019) are shown for reference.

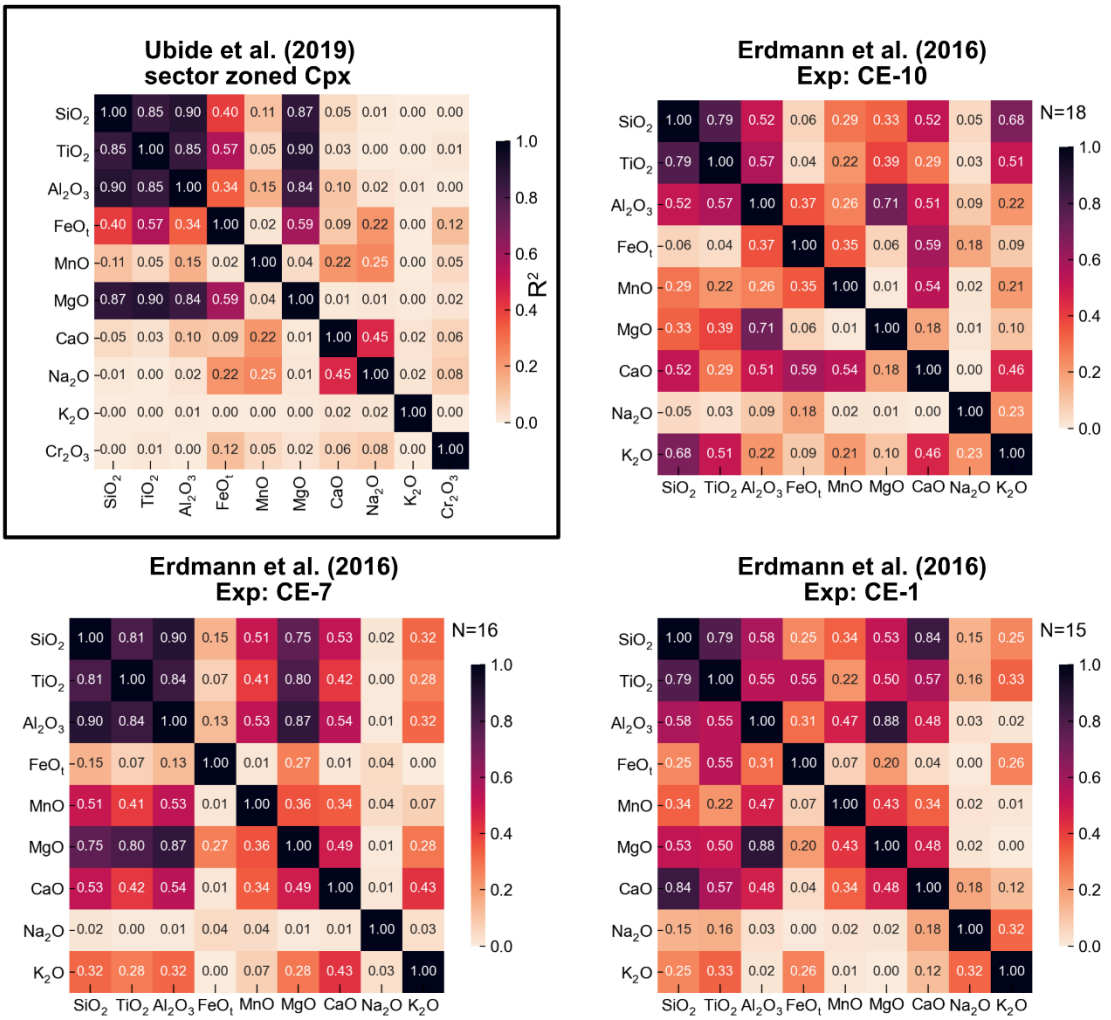

Supporting Fig 10 - Correlation matrix of pyroxenes from different experiments of Erdmann et al. (2016) with the color bar showing the R^2 value. The correlation matrix for the sector-zoned Cpx of Ubide et al. (2019) are shown for reference.

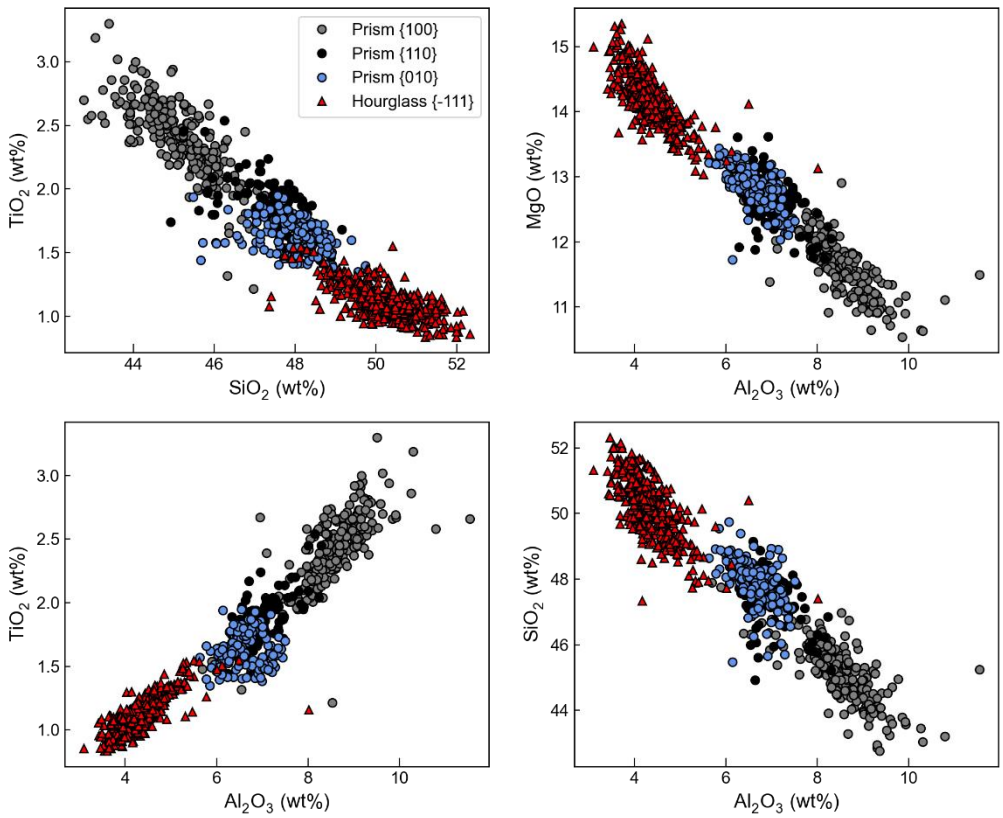

Supporting Fig. 11 : Major element correlations in sector zoned pyroxenes from Ubide et al. (2019), colored by sector.

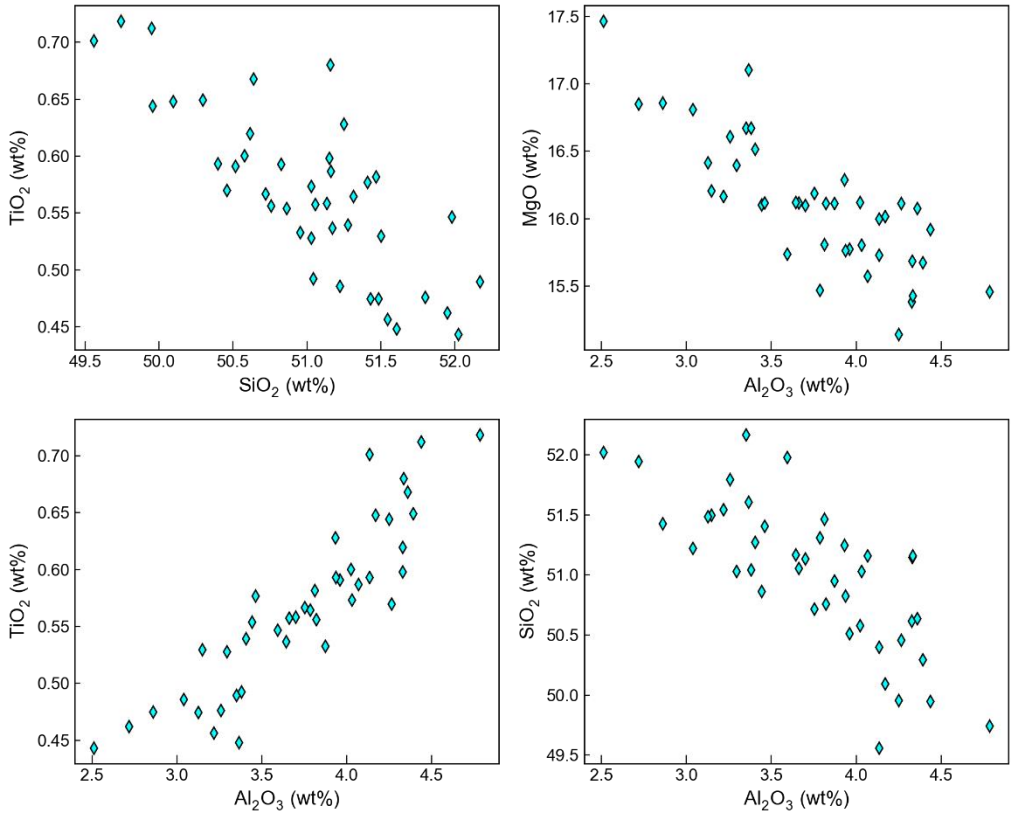

Supporting Figure 12 – Correlations between elements in Exp. Y0201-2 from Neave et al. (2017).

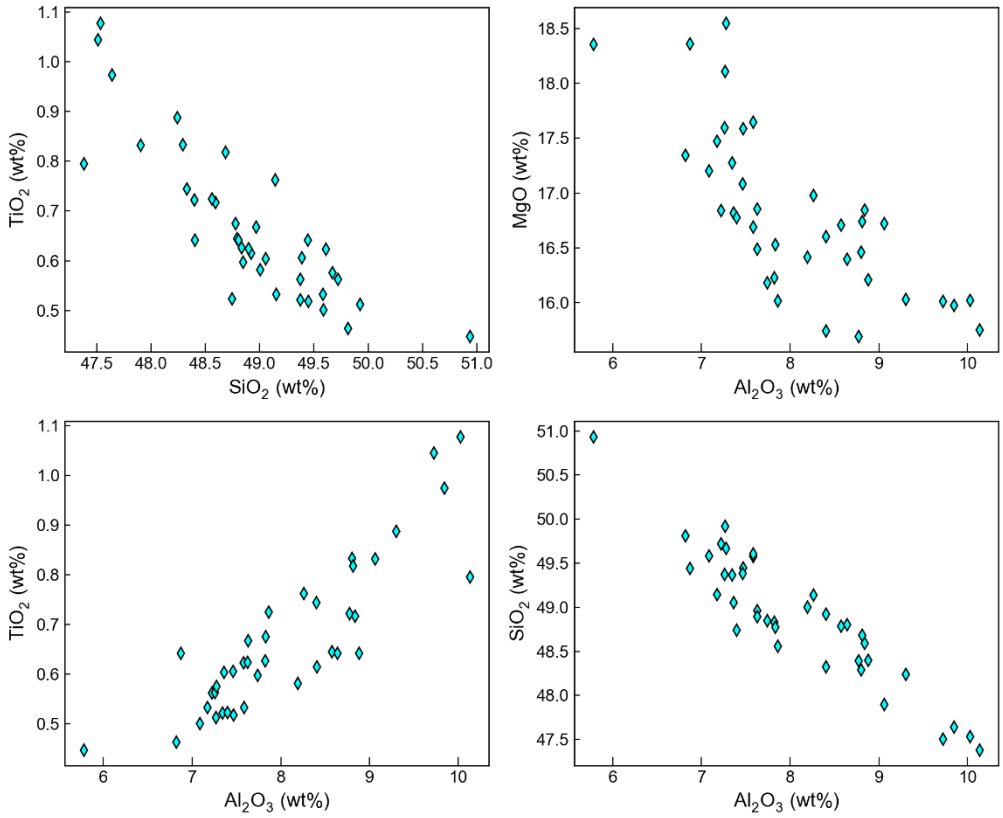

Supporting Figure 13 – Correlations between elements in Exp. 2362 from Blatter et al. (2013)

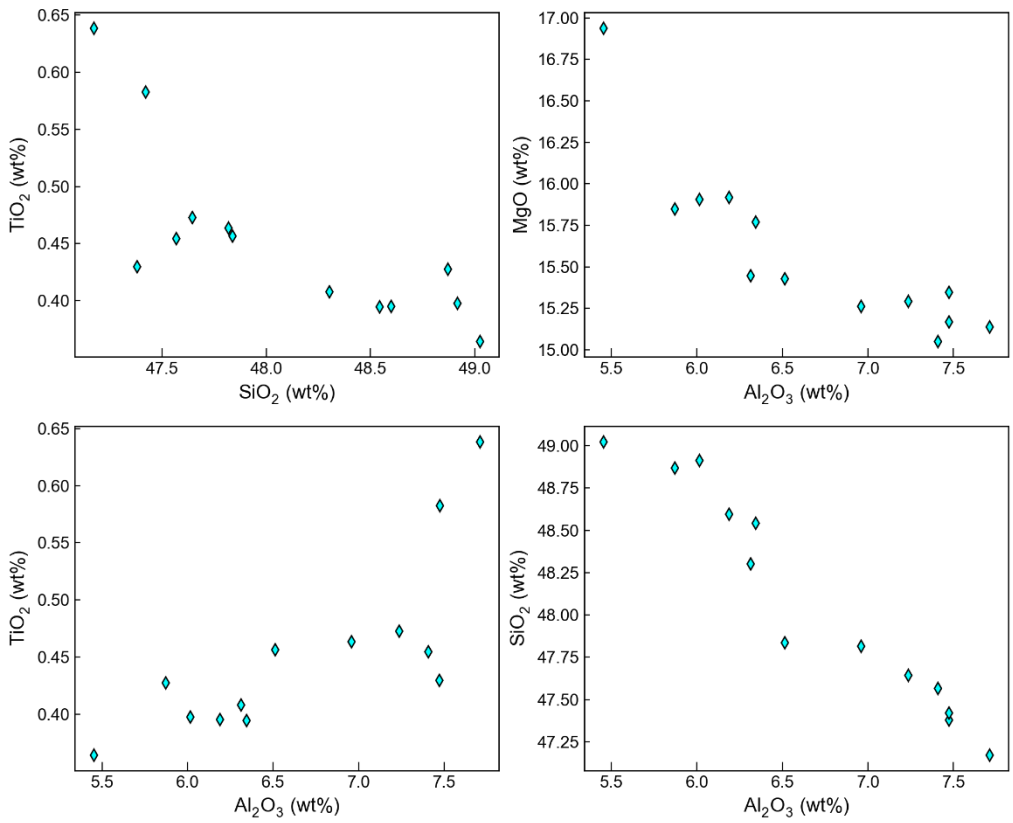

Supporting Figure 14 – Correlations between elements in Exp. BM40 from Melekhova et al. (2015)

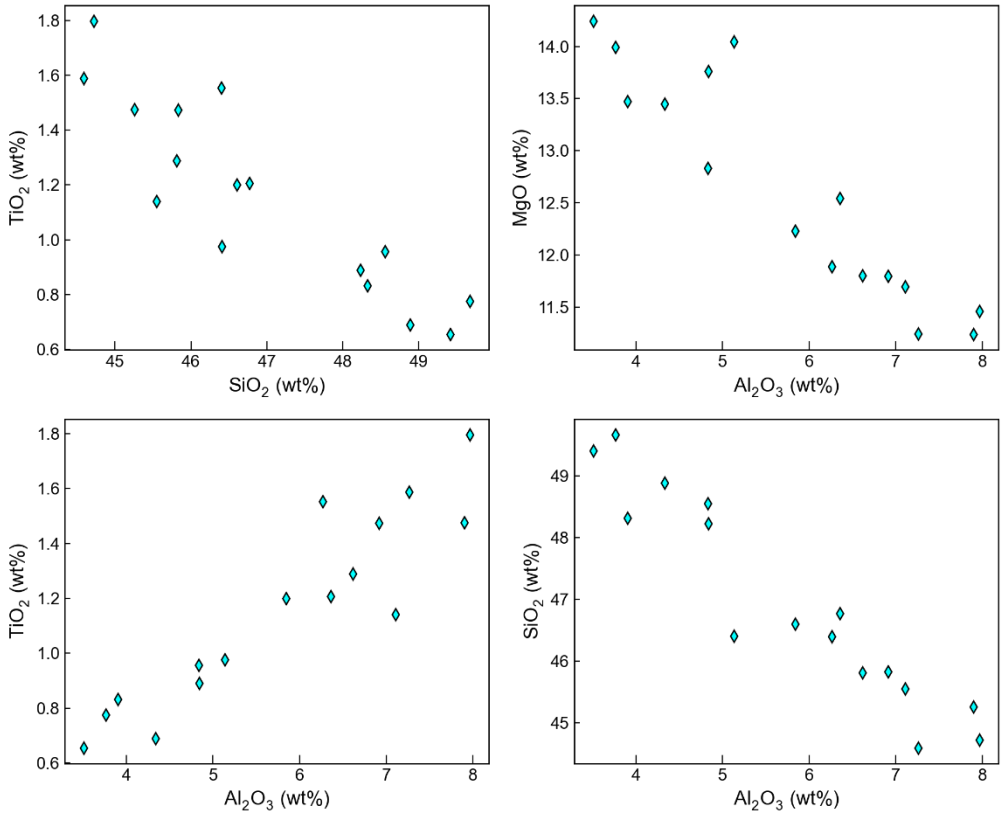

Supporting Figure 15 – Correlations between elements in Exp. CE-7 from Erdmann et al. (2016).

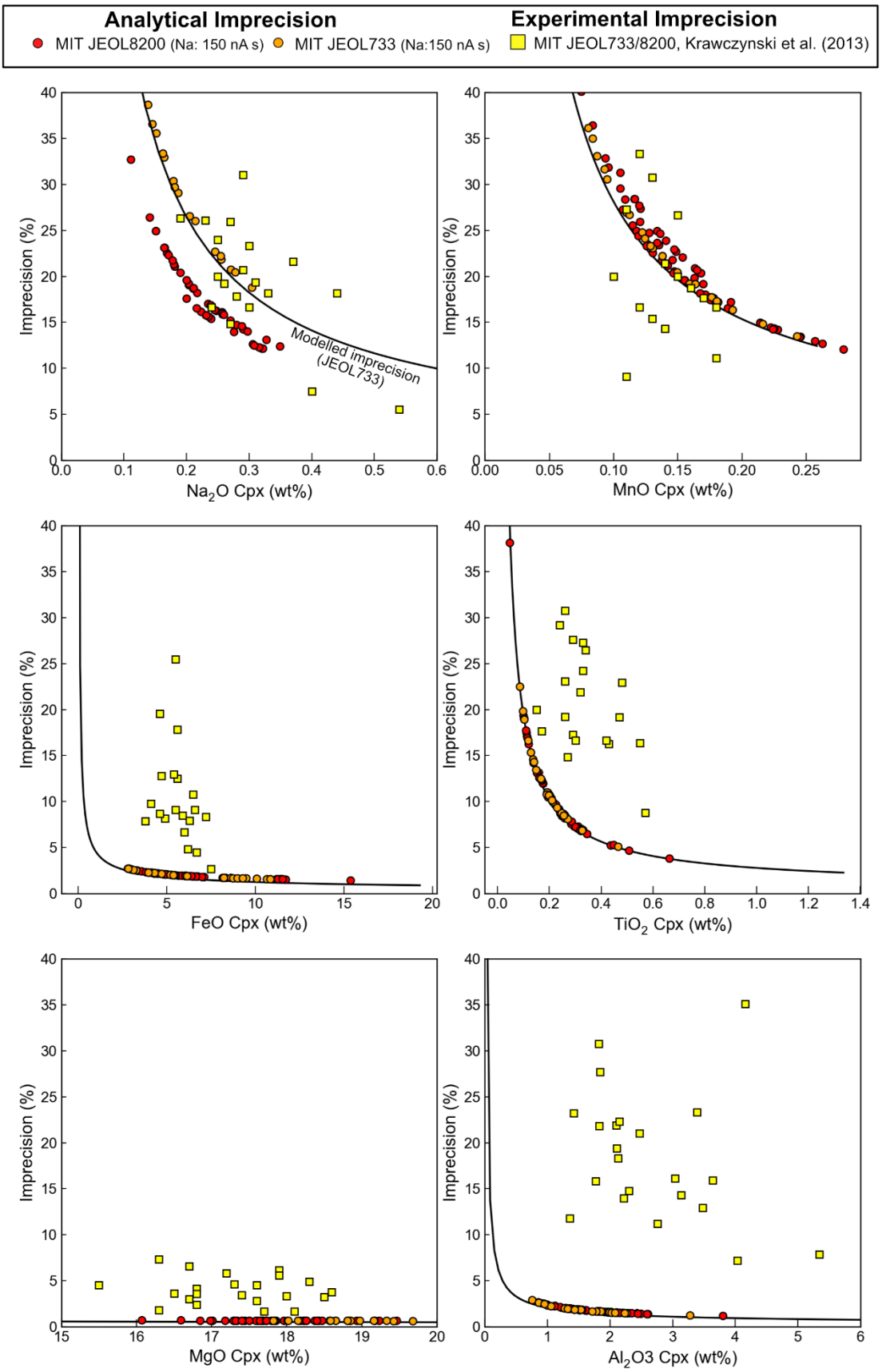

Supporting Fig. 16 – Figures comparing analytical imprecision (orange and red dots) to the variability observed in each experiment of Krawczynski et al. (2012- yellow squares).

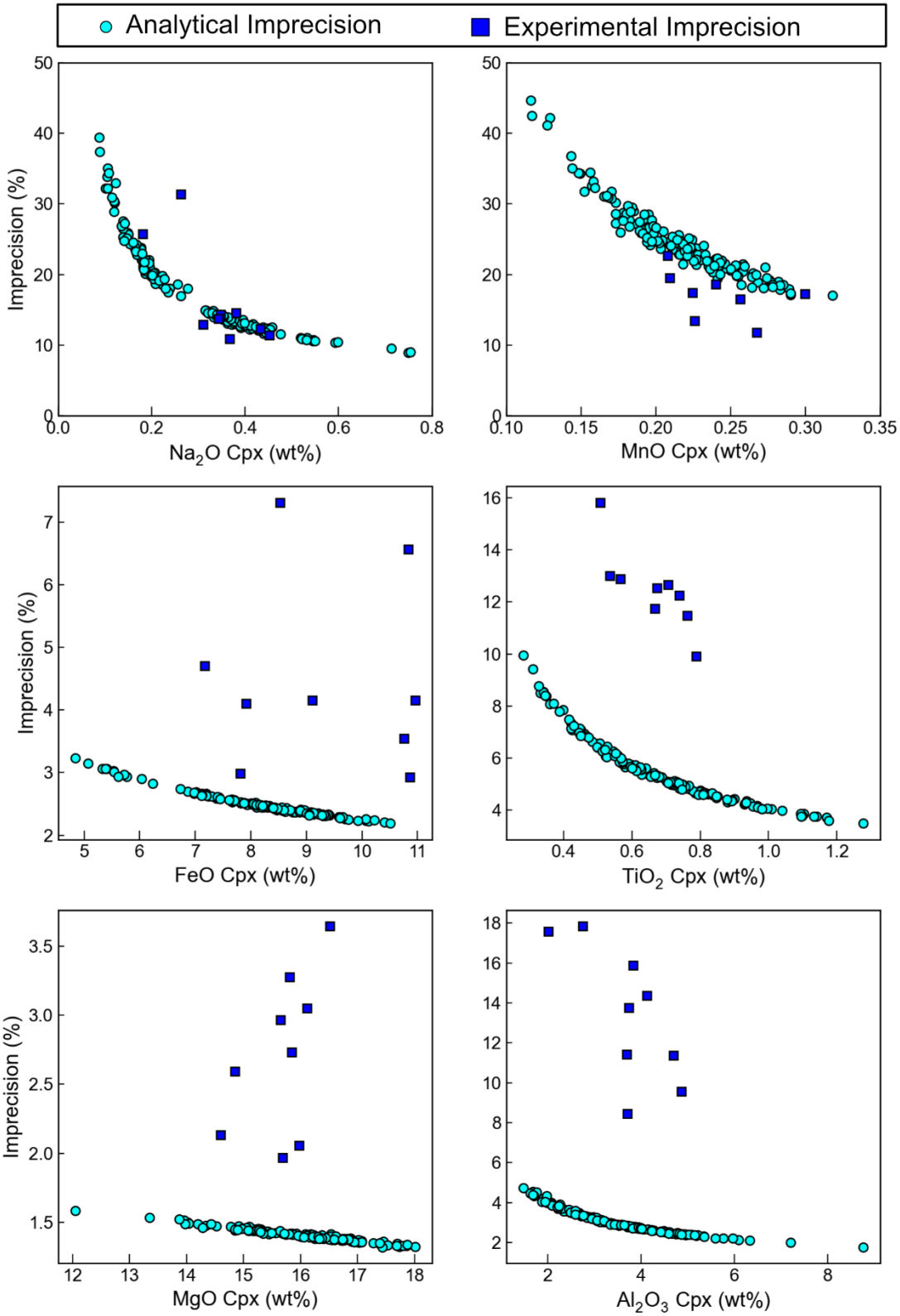

Supporting Fig. 17 - Figures comparing analytical imprecision (cyan dots) to the variability observed in each experiment of Neave et al. (2019; blue squares).

4. Additional Information regarding Monte Carlo Simulations

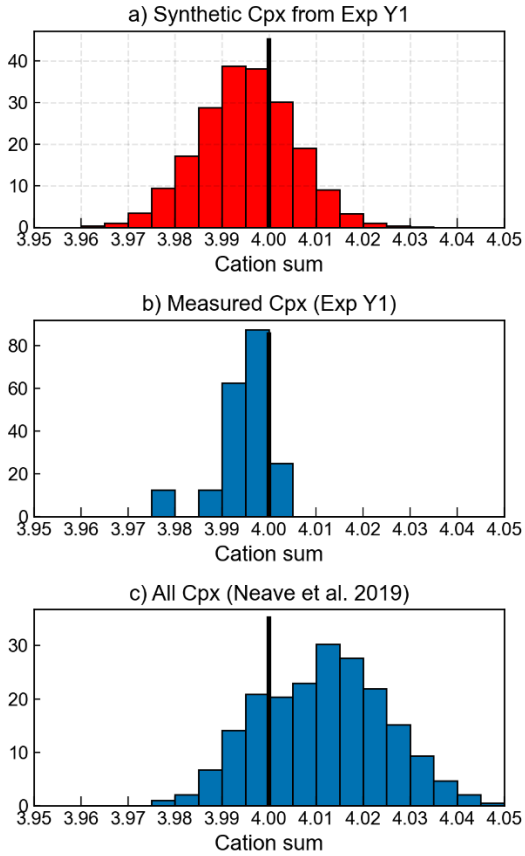

Supporting Fig. 18 – Distribution of cation sums in synthetic Cpx (part a) vs measured Cpx in that experiment, and measured Cpx in all experiments of Neave et al. (2019). Y axis shows probability density.

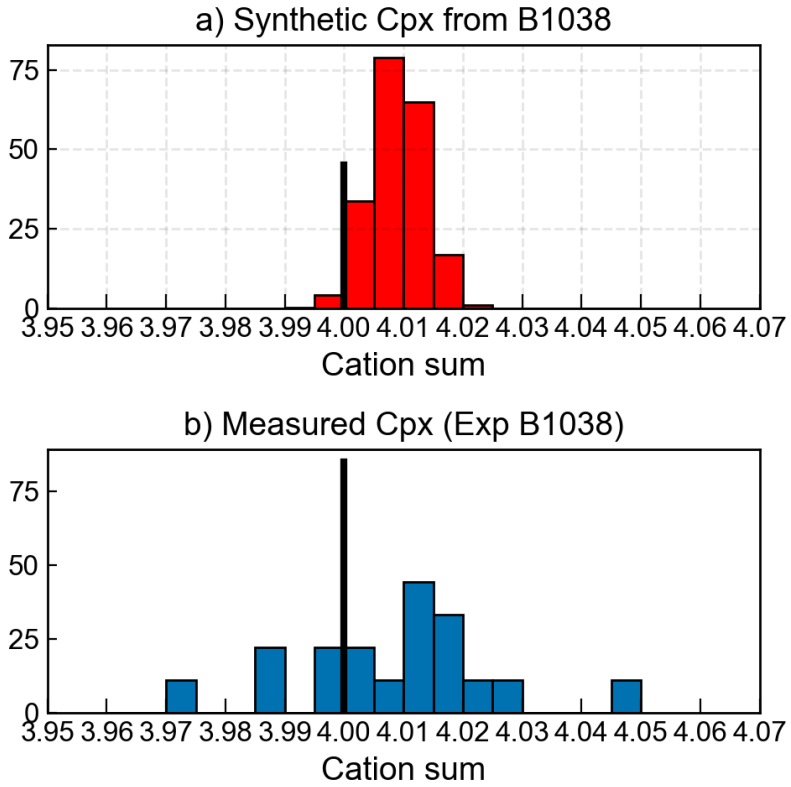

Supporting Fig. 19 – Cation sums for simulated Cpx from Krawczynski et al. (2012) compared to those in the experiment we are trying to simulate.

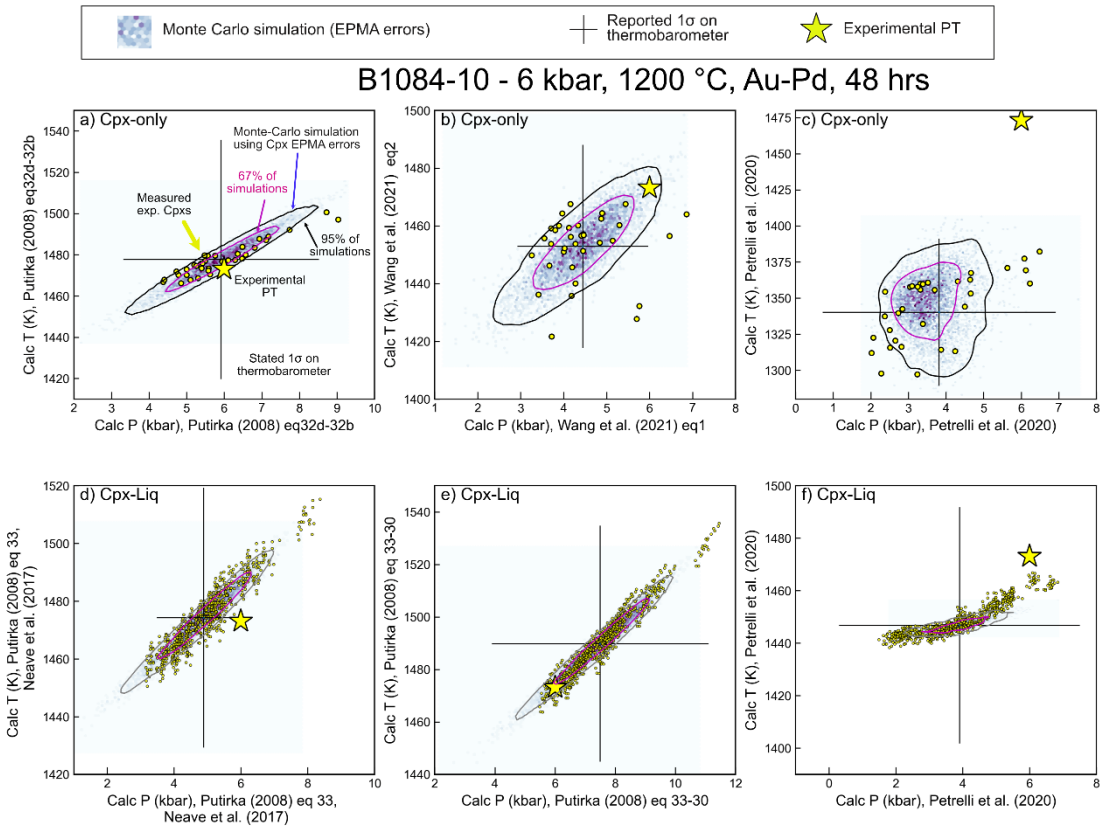

Supporting Figure 20 – As for Fig. 8 in the main text, but showing experiment B1084-10 from Neave et al. (2019).

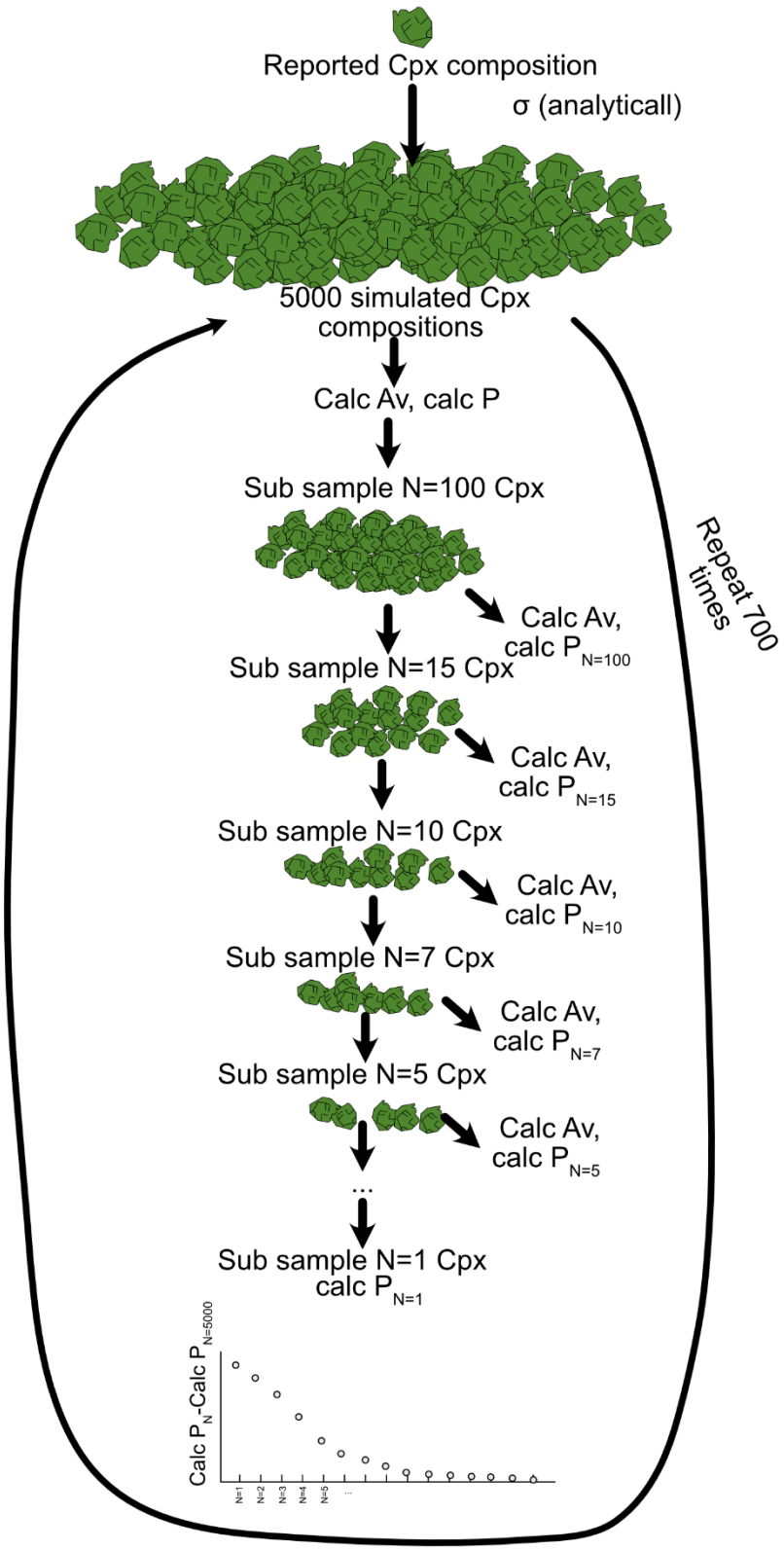

Supporting Fig. 21 – Schematic of the for-loop used to calculate the discrepancy in pressure as a function of the number of Cpx averaged for the Neave et al. (2017) experiment shown in Fig. 10a-b.

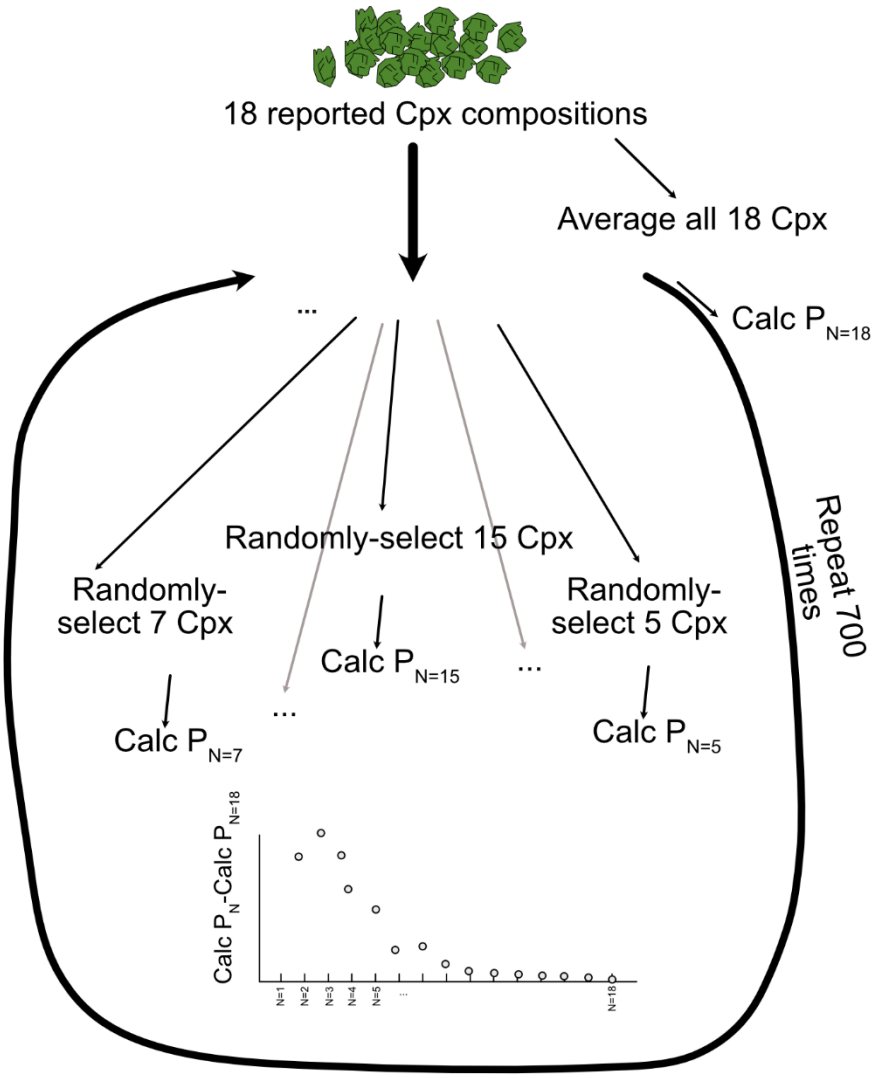

Supporting Fig 22– Schematic of the for loop used for subsampling the Cpx of Krawczynski et al. (2012) in Fig 10 c-d of the main text.

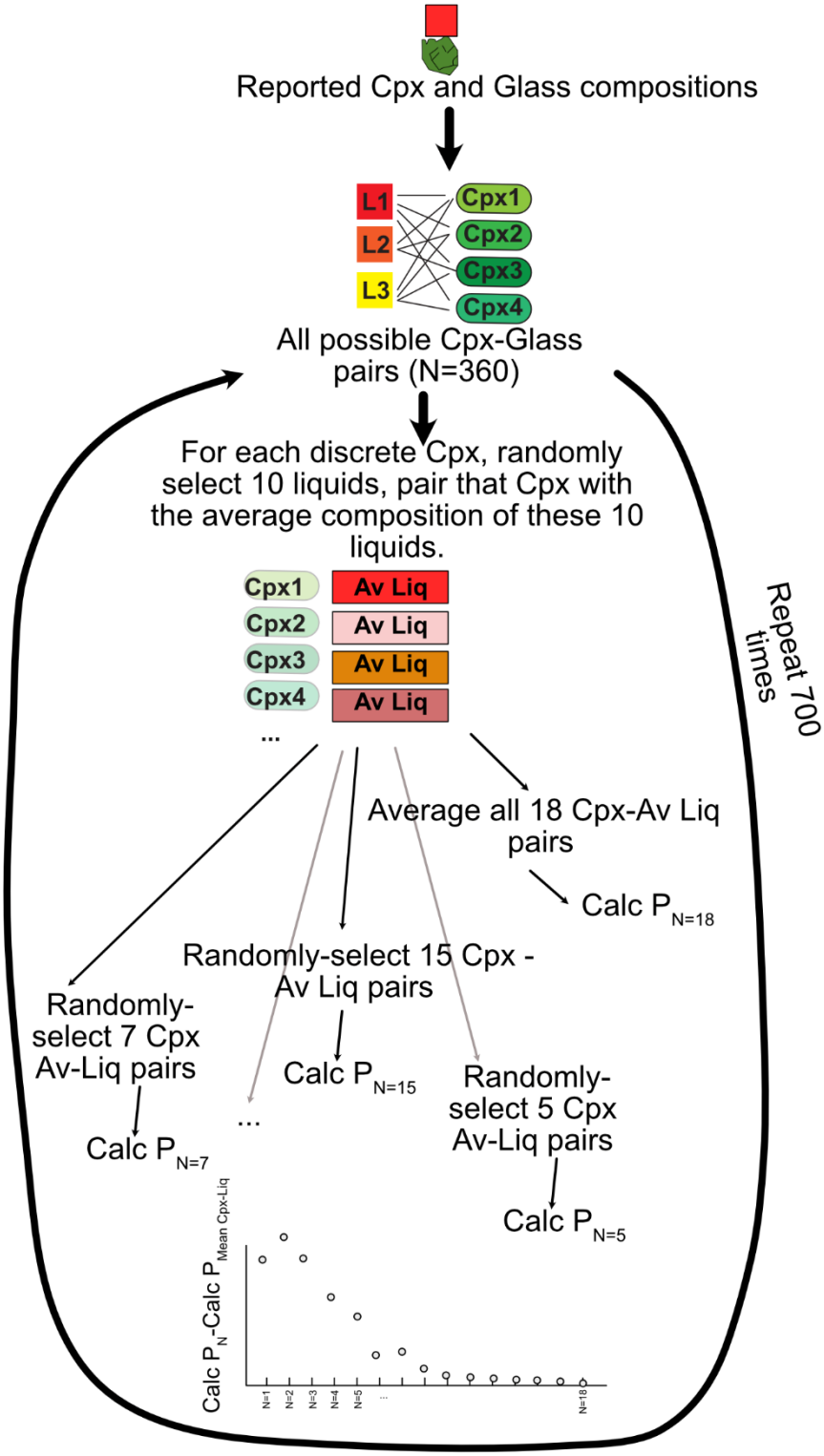

Supporting Fig 23– Schematic of the for loop used for subsampling the Cpx-Liq experiments of Krawczynski et al. (2012) in Fig 10 e-f of the main text.

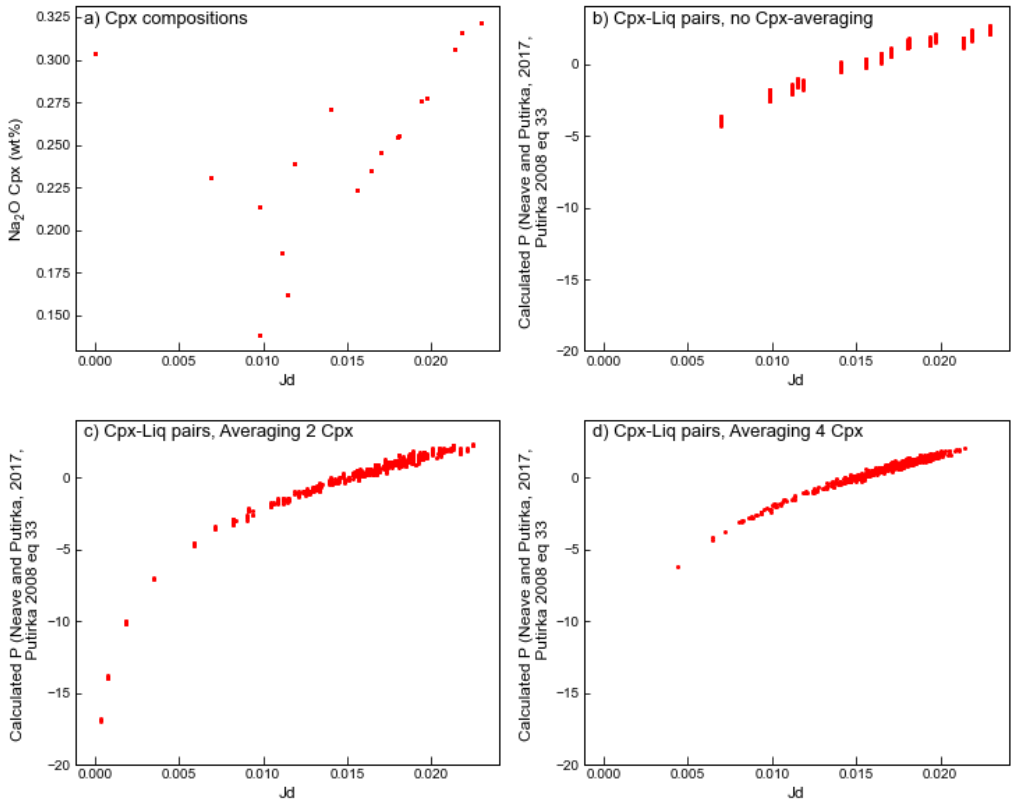

Supporting Fig. 24 –a) Cpx compositions from Experiment B1038 of Krawczynski et al. (2012). b) calculated Cpx-Liq pressures vs. Jd for measured Cpx matched with various liquid compositions. C-d) Cpx-Liq pressures averaging 2 and 4 Cpx. In c), a number of Cpx have very low, but non-zero Jd contents, resulting in strongly negative calculated pressures.

5. Investigating Na Migration in Pyroxene during EPMA analyses.

Analyses were performed on the SX100 at Oregon State at 15 kV with a beam size of 1 µm, using beam currents of 20, 40 and 100 nA. Na was analysed on the LTAP crystal, using Labradorite as a primary calibration standard (calibration performed at 20 nA).

We use three separate methods to track whether Na is migrating under the electron beam. First, we use the P-B-P-B "Subcounting" routine in the PeakSight software. The software splits the acquisition time of any given elements into 10 windows. Then, it measures the Peak counts, Background1 counts, Background 2 counts for each the first measurement. It then cycles through this for as many N as are specified. To validate this method, we first track the change in Na counts within a hydrous rhyolitic glass (3 wt% H_2O), which should show extensive migration. We plot the change in peak counts relative to the first measurement. Peak and P-B counts decline rapidly, to values only 0.4X the original after 50s of beam exposure, with a tail off to very low Na counts after 100s (Supporting Fig. 22).

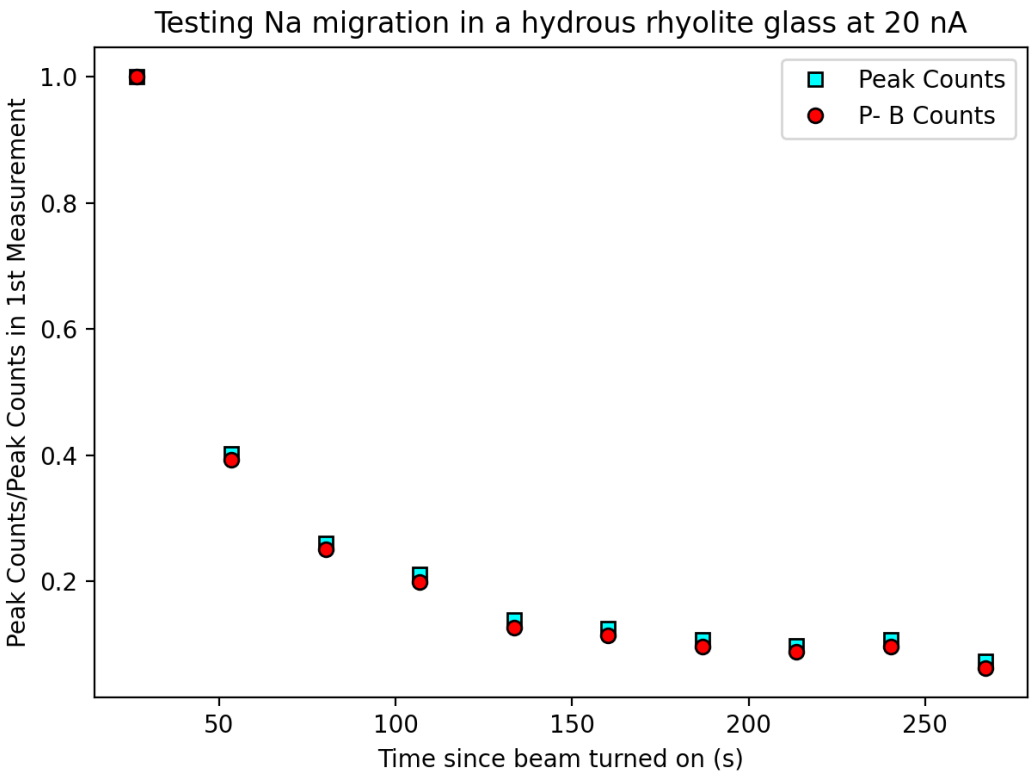

Supporting Figure 25 – Tracking Na counts in a hydrous rhyolite glass using the sub-counting P-B-P routine at 20 nA over >250 s.

In contrast, when we perform the same P-B-P routine on a Jadeite standard, counts only decline by ~4% over 250 s at 20 nA (Supporting Figure 23a), with a small r^2 value (compare to rhyolite in Supporting Figure 23b). At higher currents (40 and 100nA) counts decline by 15-20% over 250 s (Supporting Figure 24). In contrast, even at 100 nA, Na Peak counts, and Peak-Background counts show no noticeable change with time in natural augite (Kakanui Augite, 1.1 wt% Na, Supporting Figure 25). These subcounting routines demonstrate that while glasses are highly beam sensitive and undergone substantial beam loss, Jadeite is only very slightly beam sensitive at 20nA over prolonged count periods, and only shows strong correlations between peak counts and time at 40 nA and 100 nA. In contrast, even for prolonged count times (>250s) and very high probe currents (100 nA), natural pyroxenes undergo no noticeable migration of Na.

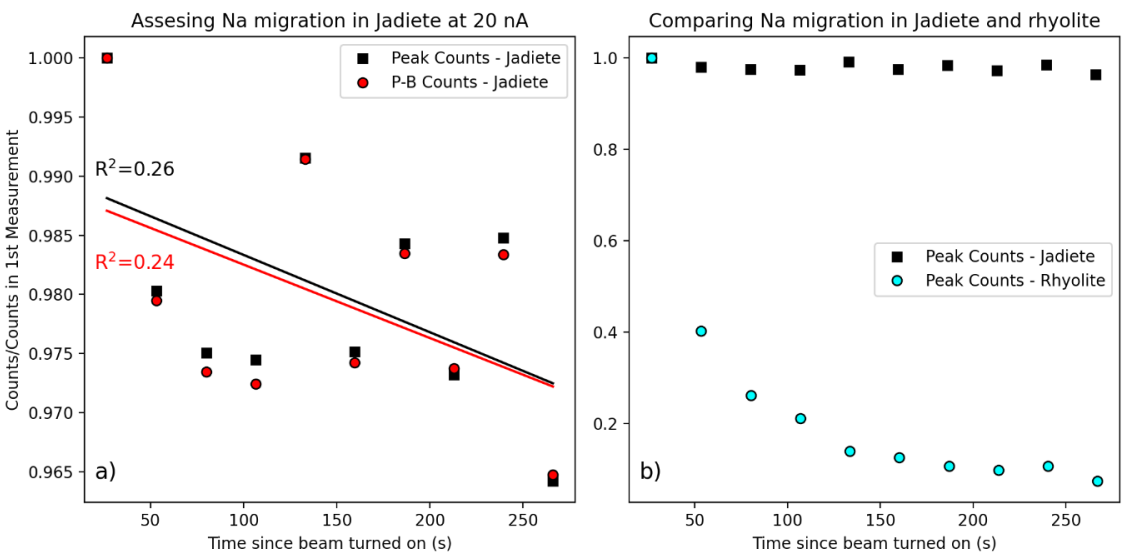

Supporting Figure 26 – a) Tracking peak and peak – background (P-B) counts in Jadeite vs. time at 20 nA. b) The changes are entirely overwhelmed by those seen in rhyolites.

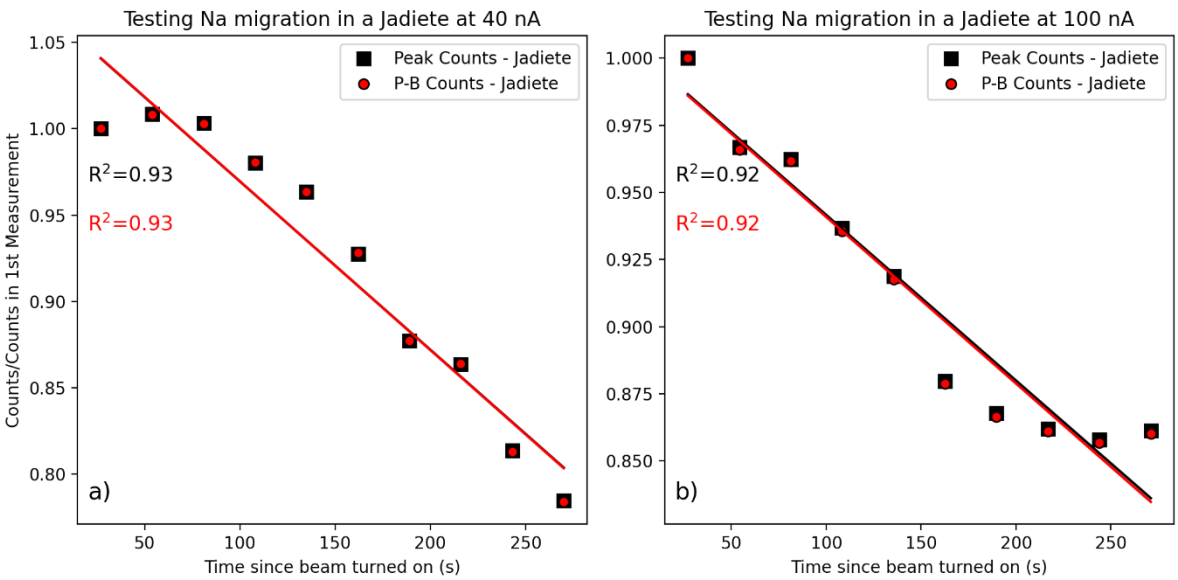

Supporting Figure 27 – Tracking peak and peak – background (P-B) counts in Jadeite vs. time at 40 nA (a) and 100 nA (b).

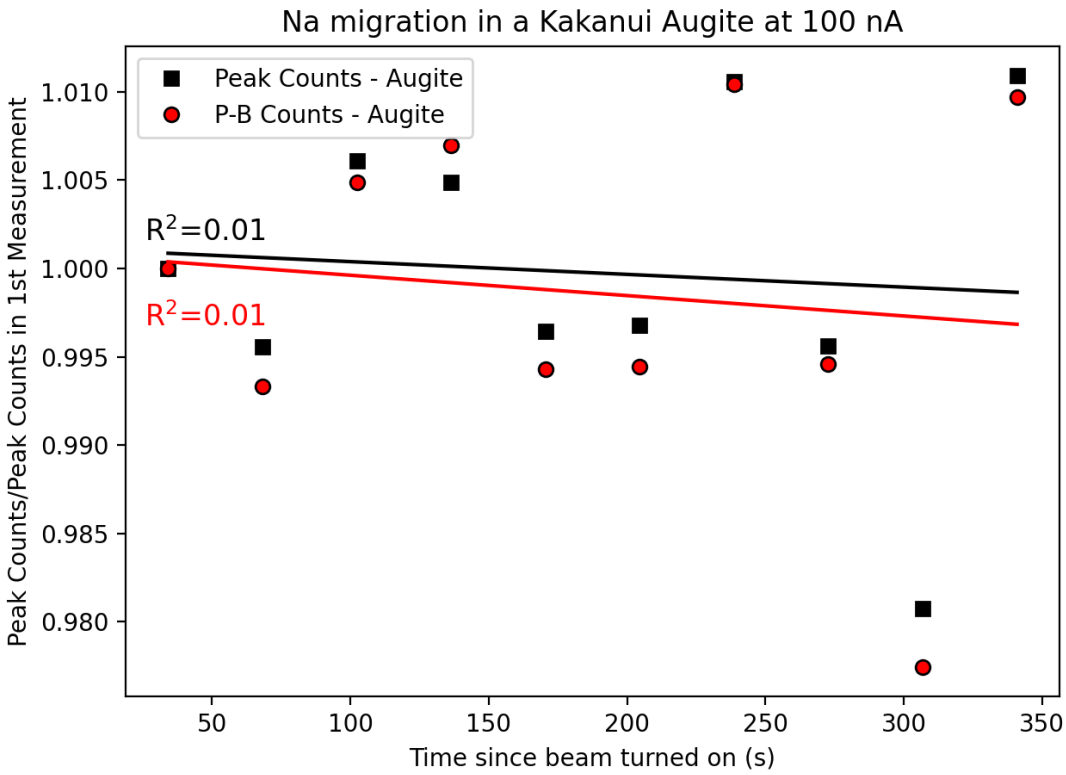

Supporting Figure 28 – Tracking changes in Na counts with time in Kakanui Augite at 100 nA.

Beam sensitivity of Jadeite is important in that it is often used as a primary calibration standard for Na in pyroxene. Given that P-B-P routines are missing gaps in time as the spectrometer position is constantly being adjusted, we also perform a routine where the Na peak is measured in short increments, without measuring backgrounds (as Supporting Figs. 22-25 show that Peak-counts and P-B counts show very similar trends). First, we count on the peak ten times for 1-second intervals and then count on the peak ten times over 15 s intervals (Supporting Figure 26). These graphs demonstrates that, even at 100 nA, Jadeite only begins to lose Na after 80s of beam exposure. This indicates that at common calibration conditions (e.g., 20-40 nA, 10-30s), Na migration in Jadeite is not a major problem.

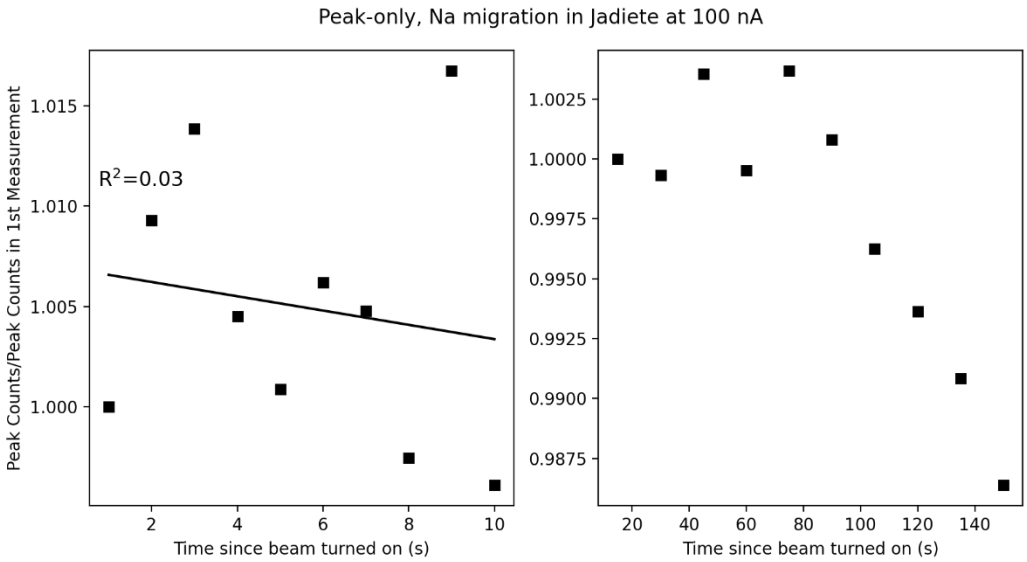

Supporting Figure 29 – Tracking Peak counts on Na over 10s and 150s (in 10 discrete measurement intervals).

We perform one additional set of tests at 100 nA to investigate changes in elemental concentrations where we perform a relatively short (1 minute total beam exposure) analytical routine for Na-Ca-Al-Si-Ti on a single point on Jadeite, and obtain a quantitative analysis for this point (in terms of wt%, Supporting Figure 27a). We then perform a repeat analysis without moving the stage. We compare element concentrations from 6 repeated measurements to those measured in the first spot. For Jadeite, the only element showing noticeable unidirectional changes is Na, declining by ~10 % relative after 6 minutes of beam exposure. For Kakanui augite, we use the same routine, but also split each measurement of the Na peak into 3 P-P-P subcount routines (3 seconds each), and apply the zero-time-intersection correction in the software. None of the 6 acquisitions show any coherent trends between Na counts and time (Supporting Figure 27c) so very similar results would have been achieved without using a zero time intercept.

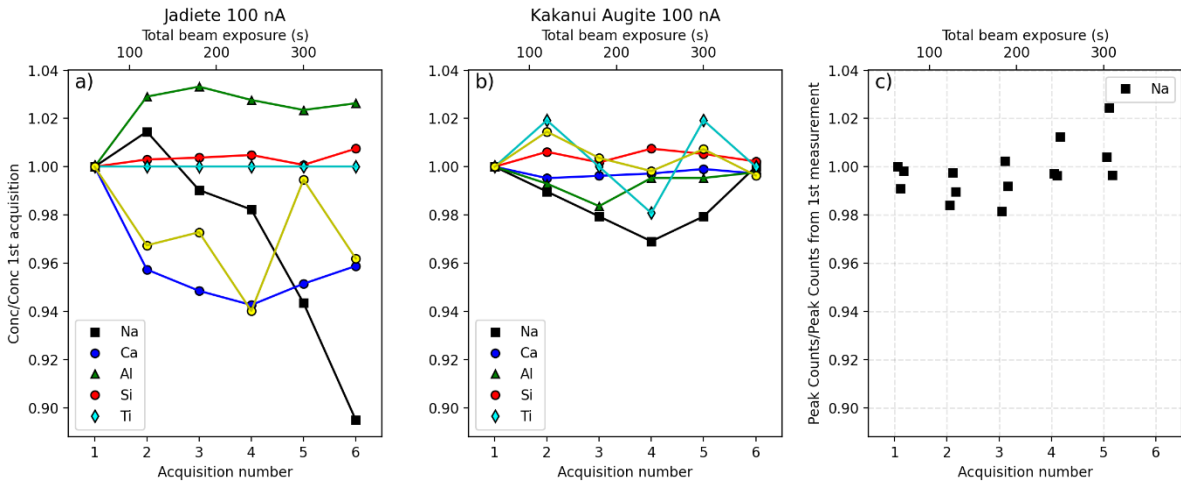

Supporting Figure 30 – a) Tracking changes in elemental concentrations during 6 repeated analyses (60s of beam exposure each) in the same stage position on Jadeite, with no zero-time-intercept correction. b) Same for Kakanui augite, but using a zero-time-intercept correction for Na

based on 3 subcounts on the Na Peak during each acquisition. In c), the counts for these are shown. There are no coherent changes with time above the noise of the measurement.

Additional References

Akella, J., 1976. Garnet pyroxene equilibria in the system CaSiOrMgSiOs-AlrOe and in a natural mineral mixture. American Mineralogist, V61, pp 589-598

Almeev, R.R., Holtz, F., Ariskin, A.A., Kimura, J.-I., 2013. Storage conditions of Bezymianny Volcano parental magmas: results of phase equilibria experiments at 100 and 700 MPa. Contrib Mineral Petrol 166, 1389–1414. https://doi.org/10.1007/s00410-013-0934-x

Alonso-Perez, R., Müntener, O., Ulmer, P., 2009. Igneous garnet and amphibole fractionation in the roots of island arcs: experimental constraints on andesitic liquids. Contrib Mineral Petrol 157, 541–558. https://doi.org/10.1007/s00410-008-0351-8

Andújar, J., Scaillet, B., Pichavant, M., Druitt, T.H., 2015. Differentiation Conditions of a Basaltic Magma from Santorini, and its Bearing on the Production of Andesite in Arc Settings. Journal of Petrology 56, 765–794. https://doi.org/10.1093/petrology/egv016

Baker, D.R., Eggler, D.H., 1987. Compositions of anhydrous and hydrous melts c
oexisting with plagioclase, augite, and olivine or low-Ca pyrxene from 1 atm to 8 kbar: Application to the Aleutian volcanic center of Atka. American Mineralogist 72.

Baker, M.B., Grove, T.L., Price, R., 1994. Primitive basalts and andesites from the Mt. Shasta region, N. California: products of varying melt fraction and water content. Contr. Mineral. and Petrol. 118, 111–129. https://doi.org/10.1007/BF01052863

Barclay, J., 2004. A Hornblende Basalt from Western Mexico: Water-saturated Phase Relations Constrain a Pressure-Temperature Window of Eruptibility. Journal of Petrology 45, 485–506. https://doi.org/10.1093/petrology/egg091

Berndt, J., 2004. An Experimental Investigation of the Influence of Water and Oxygen Fugacity on Differentiation of MORB at 200 MPa. Journal of Petrology 46, 135–167. https://doi.org/10.1093/petrology/egh066

Berndt, J., Holtz, F., Koepke, J., 2001. Experimental constraints on storage conditions in the chemically zoned phonolitic magma chamber of the Laacher See volcano. Contrib Mineral Petrol 140, 469–486. https://doi.org/10.1007/PL00007674

Blatter, D.L., Carmichael, I.S.E., 2001. Hydrous phase equilibria of a Mexican high-silica andesite:A candidate for a mantle origin? Geochimica et Cosmochimica Acta 65, 4043–4065. https://doi.org/10.1016/S0016-7037(01)00708-6

Blatter, D.L., Sisson, T.W., Hankins, W.B., 2013. Crystallization of oxidized, moderately hydrous arc basalt at mid- to lower-crustal pressures: implications for andesite genesis. Contrib Mineral Petrol 166, 861–886. https://doi.org/10.1007/s00410-013-0920-3

Blundy, J.D., Robinson, J.A.C., Wood, B.J., 1998. Heavy REE are compatible in clinopyroxene on the spinel lherzolite solidus. Earth and Planetary Science Letters 160, 493–504. https://doi.org/10.1016/S0012-821X(98)00106-X

Cadoux, A., Scaillet, B., Druitt, T.H., Deloule, E., 2014. Magma Storage Conditions of Large Plinian Eruptions of Santorini Volcano (Greece). Journal of Petrology 55, 1129–1171. https://doi.org/10.1093/petrology/egu021

Carroll, M.R., Wyllie, P.J., 1989. Experimental Phase Relations in the System Tonalite-Peridotite-H2O at 15 kb; Implications for Assimilation and Differentiation Processes near the Crust-Mantle Boundary. Journal of Petrology 30, 1351–1382. https://doi.org/10.1093/petrology/30.6.1351

Costa, F., 2004. Petrological and Experimental Constraints on the Pre-eruption Conditions of Holocene Dacite from Volcan San Pedro (36 S, Chilean Andes) and the Importance of Sulphur in Silicic Subduction-related Magmas. Journal of Petrology 45, 855–881. https://doi.org/10.1093/petrology/egg114

Di Carlo, I., 2006. Experimental Crystallization of a High-K Arc Basalt: the Golden Pumice, Stromboli Volcano (Italy). Journal of Petrology 47, 1317–1343. https://doi.org/10.1093/petrology/egl011

Draper, D.S., Green, T.H., 1999. P–T phase relations of silicic, alkaline, aluminous liquids: new results and applications to mantle melting and metasomatism. Earth and Planetary Science Letters 170, 255–268. https://doi.org/10.1016/S0012-821X(99)00111-9

Draper, D.S., Johnston, A.D., 1992. Anhydrous PT phase relations of an Aleutian high-MgO basalt: an investigation of the role of olivine-liquid reaction in the generation of arc high-alumina basalts. Contr. Mineral. and Petrol. 112, 501–519. https://doi.org/10.1007/BF00310781

Erdmann, S., Martel, C., Pichavant, M., Bourdier, J.-L., Champallier, R., Komorowski, J.-C., Cholik, N., 2016. Constraints from Phase Equilibrium Experiments on Pre-eruptive Storage Conditions in Mixed Magma Systems: a Case Study on Crystal-rich Basaltic Andesites from Mount Merapi, Indonesia. J. Petrology 57, 535–560. https://doi.org/10.1093/petrology/egw019

Feig, S.T., Koepke, J., Snow, J.E., 2010. Effect of oxygen fugacity and water on phase equilibria of a hydrous tholeiitic basalt. Contrib Mineral Petrol 160, 551–568. https://doi.org/10.1007/s00410-010-0493-3

Feig, S.T., Koepke, J., Snow, J.E., 2006. Effect of water on tholeiitic basalt phase equilibria: an experimental study under oxidizing conditions. Contrib Mineral Petrol 152, 611–638. https://doi.org/10.1007/s00410-006-0123-2

Firth, C., Adam, J., Turner, S., Rushmer, T., Brens, R., Green, T.H., Erdmann, S., O'Neill, H., 2019. Experimental constraints on the differentiation of low-alkali magmas beneath the Tonga arc: Implications for the origin of arc tholeiites. Lithos 344–345, 440–451. https://doi.org/10.1016/j.lithos.2019.07.008

Fram, M., Longhi, John, 1992. Phase equilibria of dikes associated with Proterozoic anorthosite complexes. American Mineralogist.v77, 605-616

Gee, L.L., Sack, R.O., 1988. Experimental Petrology of Melilite Nephelinites. Journal of Petrology 29, 1233–1255. https://doi.org/10.1093/petrology/29.6.1233

Hamada, M., Fujii, T., 2008. Experimental constraints on the effects of pressure and H2O on the fractional crystallization of high-Mg island arc basalt. Contrib Mineral Petrol 155, 767–790. https://doi.org/10.1007/s00410-007-0269-6

Husen, A., Almeev, R.R., Holtz, F., 2016. The Effect of H2O and Pressure on Multiple Saturation and Liquid Lines of Descent in Basalt from the Shatsky Rise. Journal of Petrology 57, 309–344. https://doi.org/10.1093/petrology/egw008

Kawamoto, T., 1996. Experimental constraints on differentiation and H2O abundance of calc-alkaline magmas. Earth and Planetary Science Letters 144, 577–589. https://doi.org/10.1016/S0012-821X(96)00182-3

Kennedy, A.K., Grove, T.L., Johnson, R.W., 1990. Experimental and major element constraints on the evolution of lavas from Lihir Island, Papua New Guinea. Contr. Mineral. and Petrol. 104, 722–734. https://doi.org/10.1007/BF01167289

Koepke, J., Botcharnikov, R.E., Natland, J.H., 2018. Crystallization of late-stage MORB under varying water activities and redox conditions: Implications for the formation of highly evolved lavas and oxide gabbro in the ocean crust. Lithos 323, 58–77. https://doi.org/10.1016/j.lithos.2018.10.001

Krawczynski, M.J., Grove, T.L., Behrens, H., 2012. Amphibole stability in primitive arc magmas: effects of temperature, H2O content, and oxygen fugacity. Contrib Mineral Petrol 164, 317–339. https://doi.org/10.1007/s00410-012-0740-x

Laporte, D., Toplis, M.J., Seyler, M., Devidal, J.-L., 2004. A new experimental technique for extracting liquids from peridotite at very low degrees of melting: application to partial melting of depleted peridotite. Contributions to Mineralogy and Petrology 146, 463–484. https://doi.org/10.1007/s00410-003-0509-3

Maal﹪e, S., 2004. The PT-phase relations of an MgO-rich Hawaiian tholeiite: the compositions of primary Hawaiian tholeiites. Contrib Mineral Petrol 148, 236–246. https://doi.org/10.1007/s00410-004-0601-3

Mandler, B.E., Donnelly-Nolan, J.M., Grove, T.L., 2014. Straddling the tholeiitic/calc-alkaline transition: the effects of modest amounts of water on magmatic differentiation at Newberry Volcano, Oregon. Contrib Mineral Petrol 168, 1066. https://doi.org/10.1007/s00410-014-1066-7

McCoy, T.J., Lofgren, G.E., 1999. Crystallization of the Zagami shergottite: an experimental study. Earth and Planetary Science Letters 173, 397–411. https://doi.org/10.1016/S0012-821X(99)00241-1

Melekhova, E., Blundy, J., Robertson, R., Humphreys, M.C.S., 2015. Experimental Evidence for Polybaric Differentiation of Primitive Arc Basalt beneath St. Vincent, Lesser Antilles. Journal of Petrology 56, 161–192. https://doi.org/10.1093/petrology/egu074

Métrich, N., Rutherford, M.J., 1998. Low Pressure Crystallization Paths of H2O-Saturated Basaltic-Hawaiitic Melts from Mt Etna: Implications for Open-System Degassing of Basaltic Volcanoes. Geochimica et Cosmochimica Acta 62, 1195–1205. https://doi.org/10.1016/S0016-7037(98)00048-9

Minitti, M.E., Rutherford, M.J., 2000. Genesis of the Mars Pathfinder ?sulfur-free? rock from SNC parental liquids. Geochimica et Cosmochimica Acta 64, 2535–2547. https://doi.org/10.1016/S0016-7037(00)00366-5

Nandedkar, R.H., Ulmer, P., Müntener, O., 2014. Fractional crystallization of primitive, hydrous arc magmas: an experimental study at 0.7 GPa. Contrib Mineral Petrol 167, 1015. https://doi.org/10.1007/s00410-014-1015-5

Neave, D.A., Bali, E., Guðfinnsson, G.H., Halldórsson, S.A., Kahl, M., Schmidt, A.-S., Holtz, F., 2019. Clinopyroxene–Liquid Equilibria and Geothermobarometry in Natural and Experimental Tholeiites: the 2014–2015 Holuhraun Eruption, Iceland. Journal of Petrology 60, 1653–1680. https://doi.org/10.1093/petrology/egz042

Nielsen, R.L., Gallahan, W.E., Newberger, F., 1992. Experimentally determined mineral-melt partition coefficients for Sc, Y and REE for olivine, orthopyroxene, pigeonite, magnetite and ilmenite. Contrib Mineral Petrol 110, 488–499. https://doi.org/10.1007/BF00344083

Parat, F., Streck, M., Holtz, F., Almeev, R.R., 2014. Experimental study into the petrogenesis of crystal-rich basaltic to andesitic magmas at Arenal volcano. Contributions to Mineralogy and Petrology, v168. https://doi.org/10.1007/s00410-014-1040-4

Pertermann, M., 2003. Anhydrous Partial Melting Experiments on MORB-like Eclogite: Phase Relations, Phase Compositions and Mineral-Melt Partitioning of Major Elements at 2-3 GPa. Journal of Petrology 44, 2173–2201. https://doi.org/10.1093/petrology/egg074

Pertermann, M., Lundstrom, C.C., 2006. Phase equilibrium experiments at 0.5 GPa and 1100–1300 °C on a basaltic andesite from Arenal volcano, Costa Rica. Journal of Volcanology and Geothermal Research 157, 222–235. https://doi.org/10.1016/j.jvolgeores.2006.03.043

Pichavant, M., Macdonald, R., 2007. Crystallization of primitive basaltic magmas at crustal pressures and genesis of the calc-alkaline igneous suite: experimental evidence from St Vincent, Lesser Antilles arc. Contrib Mineral Petrol 154, 535–558. https://doi.org/10.1007/s00410-007-0208-6

Prouteau, G., 2003. Experimental Constraints on the Origin of the 1991 Pinatubo Dacite. Journal of Petrology 44, 2203–2241. https://doi.org/10.1093/petrology/egg075

Rader, E.L., Larsen, J.F., 2013. Experimental phase relations of a low MgO Aleutian basaltic andesite at XH2O = 0.7–1. Contrib Mineral Petrol 166, 1593–1611. https://doi.org/10.1007/s00410-013-0944-8

Rushmer, T., 1993. Experimental high-pressure granulites: Some applications to natural mafic xenolith suites and Archean granulite terranes. Geol 21, 411. https://doi.org/10.1130/0091-7613(1993)021<0411:EHPGSA>2.3.CO;2

Scaillet, B., 2003. Experimental Constraints on the Relationships between Peralkaline Rhyolites of the Kenya Rift Valley. Journal of Petrology 44, 1867–1894. https://doi.org/10.1093/petrology/egg062

Scoates, J.S., Lo Cascio, M., Weis, D., Lindsley, D.H., 2006. Experimental constraints on the origin and evolution of mildly alkalic basalts from the Kerguelen Archipelago, Southeast Indian Ocean. Contrib Mineral Petrol 151, 582–599. https://doi.org/10.1007/s00410-006-0070-y

Springer, W., Seck, H.A., 1997. Partial fusion of basic granulites at 5 to 15 kbar: implications for the origin of TTG magmas. Contributions to Mineralogy and Petrology 127, 30–45. https://doi.org/10.1007/s004100050263

Toplis, M.J., Corgne, A., 2002. An experimental study of element partitioning between magnetite, clinopyroxene and iron-bearing silicate liquids with particular emphasis on vanadium. Contrib Mineral Petrol 144, 22–37. https://doi.org/10.1007/s00410-002-0382-5

Tsuruta, K., Takahashi, E., 1998. Melting study of an alkali basalt JB-1 up to 12.5 GPa: behavior of potassium in the deep mantle. Physics of the Earth and Planetary Interiors 107, 119–130. https://doi.org/10.1016/S0031-9201(97)00130-1

Ubide, T., Mollo, S., Zhao, J., Nazzari, M., Scarlato, P., 2019. Sector-zoned clinopyroxene as a recorder of magma history, eruption triggers, and ascent rates. Geochimica et Cosmochimica Acta 251, 265–283. https://doi.org/10.1016/j.gca.2019.02.021

Ulmer, P., Kaegi, R., Müntener, O., 2018. Experimentally Derived Intermediate to Silica-rich Arc Magmas by Fractional and Equilibrium Crystallization at 1·0 GPa: an Evaluation of Phase Relationships, Compositions, Liquid Lines of Descent and Oxygen Fugacity. Journal of Petrology 59, 11–58. https://doi.org/10.1093/petrology/egy017

Wang, W., Takahashi, E., 1999. Subsolidus and melting experiments of a K-rich basaltic composition to 27 GPa; implication for the behavior of potassium in the mantle. American Mineralogist 84, 357–361. https://doi.org/10.2138/am-1999-0319

Wasylenki, L.E., 2003. Near-solidus Melting of the Shallow Upper Mantle: Partial Melting Experiments on Depleted Peridotite. Journal of Petrology 44, 1163–1191. https://doi.org/10.1093/petrology/44.7.1163

Waters, L.E., Cottrell, E., Coombs, M.L., Kelley, K.A., 2021. Generation of Calc-Alkaline Magmas during Crystallization at High Oxygen Fugacity: An Experimental and Petrologic Study of Tephras from Buldir Volcano, Western Aleutian Arc, Alaska, USA. Journal of Petrology 62, egaa104. https://doi.org/10.1093/petrology/egaa104

Wood, B.J., Trigila, R., 2001. Experimental determination of aluminous clinopyroxene–melt partition coefficients for potassic liquids, with application to the evolution of the Roman province potassic magmas. Chemical Geology 172, 213–223. https://doi.org/10.1016/S0009-2541(00)00259-X